Nonlinear Doppler Warp Correction for Acoustic OFDM

Avik Dayal

Thesis submitted to the Faculty of the

Virginia Polytechnic Institute and State University

in partial fulfillment of the requirements for the degree of

Master of Science

in

Electrical Engineering

A. A. (Louis) Beex, Chair

A. Lynn Abbott

Daniel J. Stilwell

August 17th, 2016

Blacksburg, Virginia

Keywords: Orthogonal Frequency Division Multiplexing, Underwater Acoustic Communication, Wideband Doppler Correction, Time Warp

Nonlinear Doppler Warp Correction for Acoustic OFDM

Avik Dayal

ABSTRACT

The Underwater Acoustic (UWA) channel has been an area of interest for many researchers and engineers, but also a very challenging area. Compared to the over-the-air radio frequency (RF) channel, the underwater acoustic channel causes multiple distortions – due to multipath, frequency selectivity, noise, and Doppler – some of which are more severe. The increased distortion causes many techniques and assumptions made for typical RF communication systems to break down.

One of the assumptions that breaks down is that the Doppler effect that the signal undergoes can be modelled with a simple shift in frequency, since the signals used to communicate in a UWA channel are effectively wideband. In this work the Doppler Effect that a signal undergoes is modelled as a nonlinear time warp. A procedure is developed to estimate the parameters of the time warp from the observed signal. These time warp parameters are then used to reverse the effect of the time warp. Two different methods for estimating the time warp parameters and correcting the Doppler are compared.

The first technique uses sinusoids placed at the beginning and end of the signal to estimate the parameters of the warp that the signal undergoes. The second technique uses sinusoids that are present during the signal to estimate and correct for the warp. The frequencies of the sinusoids are outside of the frequency range used for the transmitted data signal, so there is no interference with the information that is being sent.

The transmitted data signal uses Orthogonal Frequency Division Multiplexing (OFDM) to encode the data symbols, but the Doppler Correction technique will in principle work for other kinds of wideband signals as well. The results, which include MATLAB based simulations and over-the-air experiments, show that performance improvements can be realized using the time warp correction model.

Table of Contents

List of Abbreviations

ACI – Adjacent Channel Interference

AUV – Autonomous Underwater Vehicle

BER – Bit Error Rate

BPSK – Binary Phase Shift Keying

CCDF – Complementary Cumulative Distribution Function

CDF – Cumulative Distribution Function

CFO – Carrier Frequency Offset

CIR – Channel Impulse Response

CP – Cyclic Prefix

CS – Cyclic Suffix

DFT – Discrete Fourier Transform

DMT – Discrete Multi-Tone

DSWC – Double Sliding Window Correlation

FDM – Frequency Division Multiplexing

FFT – Fast Fourier Transform

FM.# – Packet # from Far Moving Experiment

FOSE – Fraction of Sinusoidal Energy

FS.# – Packet # from Far Stationary Experiment

ICI – Inter Carrier Interference

IFO – Integer Frequency Offset

ISI – Inter Symbol Interference

LFM – Linear Frequency Modulated

MF – Matched Filter

NAM – Normalized Absolute Magnitude

NM.# – Packet # from Near Moving Experiment

NS.# – Packet # from Near Stationary Experiment

OFDM – Orthogonal Frequency Division Multiplexing

PAPR – Peak to Average Power Ratio

PRC – Peak Reduction Carriers

SNR – Signal to Noise Ratio

SONAR – Sound Navigation and Ranging

STO – Symbol Timing Offset

TL – Transmission Loss

TR – Tone Reservation

T_s – Inverse of Sampling Frequency

UWA – Underwater Acoustic

UWB – Ultra Wide Band

UWSN – Underwater Wireless Sensor Network

ZP – Zero Padded

List of Figures

List of Tables

1 Introduction

1.1 Background and Problem Statement

In the last century, underwater wireless communication has made advances in research and engineering. There is a lot of interest in military and commercial applications, particularly in building underwater wireless sensor networks that give performance enhancement for underwater applications, such as pollution control, climate monitoring, deep sea exploration, etc. The underwater channel has several characteristics that make it challenging to communicate over compared to an over the air radio channel. The power loss with RF transmission is much higher for underwater channels, leaving acoustic communication as a much more viable transmission mode. However, underwater acoustic channels come with a set of engineering difficulties. One of these difficulties is that the delay spread, caused by the reverberation or multipath effect, is much larger in underwater acoustic (UWA) channels and leads to strong frequency selectivity. Another challenge is that because of the low carrier frequency with respect to the bandwidth of the signal, underwater acoustic signals are generally wideband in nature.

Most of the previous research in UWA channels involved a single carrier modulation scheme with decision feedback equalization. However there has been a push recently to using multicarrier modulation, particularly Orthogonal Frequency Division Multiplexing (OFDM) [1]. The benefit of multicarrier modulation is that it can convert a frequency selective channel into multiple flat fading channels. Having a flat fading channel simplifies the equalization process at the receiver and, as a result, is a good candidate for use in UWA channels.

Amongst multicarrier modulation schemes, OFDM is a popular technique in which orthogonal subcarriers are used to carry data. The transmitted bit stream is divided into multiple parallel bit streams and sent over separate overlapping sub-carriers. To achieve orthogonality between subcarriers, each subcarrier is placed at a spacing equal to the reciprocal of the OFDM symbol period. A cyclic prefix is inserted before the OFDM symbol, and typically has the length of at least the delay spread of the channel. The use of a cyclic prefix helps to cancel out ISI due to multipath. The combination of being able to combat frequency selective fading and multipath makes OFDM an attractive modulation scheme for UWA channels.

There are many problems in dealing with OFDM or any multicarrier modulation scheme in a UWA channel as opposed to its RF over the air counterpart for which much research has been done. Because the UWA carrier frequency is so low, the transmitted signal tends to be wideband in nature as the bandwidth of operation equals a major fraction of the carrier frequency. As a result, relative movement between the transmitter and receiver creates different frequency offsets for different subcarrier frequencies. For this reason, typical RF Doppler correction techniques, such as applying the same frequency shift across all frequencies, do not work for the UWA channel.

First, modeling of the Doppler correction as a nonlinear scaling in time is discussed. The benefit of this method is that the relative velocity between the receiver and transmitter does not need to be constant. This model for a Doppler warp and subsequent Doppler correction can be simulated in MATLAB, which is treated in Chapter 3 using reasonable parameters for the movement of a typical transmitter and receiver.

1.2 Description of Experiments

Four acoustic experiment scenarios were used to validate the Doppler correction techniques. All of these experiments involved the transmission of an OFDM signal over the air in a room at the Digital Signal Processing Research Laboratory at Virginia Tech. The four experimental scenarios were conducted with two computers acting as the transmitter and receiver respectively. The transmitted signal used OFDM as the modulation scheme in the acoustic band of 3-5 kHz. The transmitted acoustic signal was played out of a speaker connected to one computer. A microphone attached to the second computer recorded the sound waves in each experiment. In the first set of experiment scenarios, the transmitter and receiver were placed "near" to each other, about one foot apart. The sound waves were recorded with a stationary microphone, while a simultaneous recording was done with a second microphone moving in a semicircular arc, i.e. the second recording was subject to the Doppler effect. In the second set of experiments, the receiver was placed "far" away, at a distance of approximately 5 feet from the transmitter. Again, one of the receivers recorded the sound waves with a stationary microphone while the second receiver recorded the sound waves while moving. The movement of the microphone, while the OFDM packet transmission was in progress, introduced a wideband Doppler effect.

1.3 Specific Contributions

In this work there were three major contributions. The first contribution was an improvement in the method for finding the Doppler warp model parameters. Instead of using the exact length of the transmitted signal, the new method accounted for the expansion or contraction of the signal, providing flexibility in selecting the time interval over which the Doppler is modeled and corrected. The second contribution was a detection scheme for the packets, based on identifying

the fraction of sinusoidal energy present in a signal. The third contribution was a method of estimating the parameters for the warp during the burst, as opposed to using preamble and postamble signals to estimate the warp. Using simultaneous estimates provided multiple Doppler models over time, and mitigated violating the applicability of a quadratic Doppler model.

This thesis consists of six chapters. The second chapter provides the background of the features, problems, and history of communication over a UWA channel. The third chapter contains an explanation of the proposed wideband Doppler model and an illustration of the generation and subsequent correction of a sinusoid using the model. In the fourth chapter the design parameters of the OFDM burst are described and the results based on the stationary experiment scenarios (for both the near and far cases) are shown. In the fifth chapter the results of the OFDM experiments with movement and multipath are shown for the near and far cases. The results are discussed, as are possible solutions to dealing with severe multipath with Doppler warping. Chapter six concludes the thesis.

2 Background

2.1 Introduction to Underwater Communications

With over two thirds of the Earth's surface covered by water, the lakes, seas, and oceans contain a great amount of information, yet are largely unexplored. One of the key technologies that can enable exploration is the transmission of information underwater. However, underwater communications pose many challenges not present in over the air communications. There are three primary communication mediums used in underwater wireless communications: acoustic waves, electromagnetic waves, and optical waves.

a. Acoustic

Acoustic communication is the most widely used technique for underwater environments due to the low attenuation of sound in water. However, acoustic waves have low propagation speed (about 1520 m/s) and a very limited frequency band, a major limiting factor for efficient communication. The use of acoustic waves can also be adversely affected by temperature gradients, surface noise, and multipath propagation due to reflection and refraction [2].

b. Electromagnetic waves

Electromagnetic (EM) waves have several advantages over acoustic waves, including a higher velocity and higher carrier frequency. However, EM propagation in seawater has two main challenges, the large absorption loss underwater and the size of the antenna needed. The Absorptive loss (P_{AL}) [3] is defined as:

$$P_{AL} = e^{\alpha(f)d} \tag{2.1}$$

where $\alpha(f)$ is the absorption coefficient at frequency f and d is the propagation distance.

The absorption loss coefficient α in seawater can be expressed as:

$$\alpha \approx \sqrt{\pi f \mu \sigma} \tag{2.2}$$

where μ is the magnetic permeability, σ is the electric conductivity, and f is the frequency of transmission. With a high frequency of transmission which is required for lower antenna complexity, this absorption coefficient limits the transmission distance to tens of meters. Using a frequency such as 50 MHz, would require an antenna of a couple meters. This is impractical for underwater sensor networks [4]. Current modems that operate using RF propagation support 100 bps over tens of meters and over a frequency range of 1 to 20 MHz.

c. Optical waves

Optical waves for communication have an advantage of a large data rate that can exceed 1Gbps. However, optical signals can be rapidly absorbed in water and the optical scatter caused by suspended particles is significant. Ambient light present near the surface of oceans and lakes can add significant noise to the received signal. The intensity of the received signal I_d is presented as [3]

$$I_d = I_0 e^{-\varsigma d} \tag{2.3}$$

where I_0 is the transmitted intensity of the light, d is the distance, and ς is the turbidity, which is similar to the absorption coefficient for EM waves. However, turbidity depends on the scattering of the wave while absorption is the power loss due to energy conversion. Scattering is more prevalent in optical communications as compared to absorption. The turbidity is a measure of the clarity of the water and is measured in nephelometric turbidity units (NTU). Since seawater often

has a large turbidity, in the tens to thousands of NTU, this limits the range of optical communications underwater.

The characteristics of these channels are summarized in Table 2.1 [4].

Table 2.1: Characteristics of channels.

	Acoustic	Radio	Optical
Speed of Propagation	1500 m/s	$3_{10}8$ m/s	$3_{10}8$ m/s
Power Loss	>0.1dB/m/Hz	~28 dB/km/100MHz	Depends on scattering of water
Data Rate	Up to 100 kbps	Up to 10Mbps	Up to 1Gbps
Bandwidth	~kHz	~MHz	~10-150MHz
Frequency band	~kHz	~MHz	~1014-1015 Hz
Transmission Range	~50m-5km	~1m-100m	1m-100m

Because of the limited range of EM and optical techniques, acoustic signals are generally used for long range communication underwater. Underwater Acoustic (UWA) Communication has three major limitations including the slow speed of sound underwater, time varying multipath propagation, and limited bandwidth. This has led to a lot of research in finding techniques to communicate over channels of poor quality and with high latency.

2.2 Underwater Acoustic Channel Characteristics

The underwater acoustic channel has several challenging properties that cause it to be difficult to communicate over. Two of these properties are the limited bandwidth available on the channel and the wideband nature of the signals used. The delay spreads can easily be in excess of hundreds of milliseconds, creating frequency selective distortion, and any relative motion between the transmitter and receiver creates a non-uniform Doppler warp. In addition to transmission loss, the background noise is not always Gaussian or white, which makes the noise difficult to model. The characteristics of Underwater Acoustic channels are investigated in more detail.

2.2.1 Sound Velocity

An important difference between acoustic channels and electromagnetic channels is the slow propagation speed through seawater. The speed of sound in water is highly variable and dependent on several water properties including temperature, salinity, and pressure. The average speed of sound near the surface of the ocean is 1520 m/s, but this grows with increasing water temperature, salinity, and depth. Because the speed of sound varies depending on the depth of the ocean, the speed profile is divided into four layers:

- Surface Layer: The surface layer is restricted to tens of meters. Since the salinity is low and the temperature is high, these factors create a constant sound velocity, at approximately 1520 m/s.
- Seasonal and permanent thermocline layers: The water temperature decreases in the thermocline layer, which leads to a lower speed for sound. In the permanent thermocline layers, the speed of sound decreases further, to about 1475 m/s at a depth of 1000 meters.
- Deep isothermal layer: At this layer, the temperature is constant at 4˚ C. Since the water pressure increases, the speed of sound increases linearly.

The temperature T is denoted in degrees Celsius, the salinity S in parts per thousand, and the depth D in meters. The speed of sound in water, c, can be estimated using [4]

$$c = 1449 + 4.6T + 0.055T^2 + 1.39(S - 35) + 0.016D \tag{2.4}$$

For purposes of simulation, the speed of sound in water is considered to be 1520 m/s, though a change in velocity could be solved with a time varying Doppler correction model.

2.2.2 Time-varying Multipath

Any type of wave, whether it is acoustic or electromagnetic, can reach a certain receiver location via multiple paths. In shallow water environments, wave reflections off the surface and bottom interfaces of the channel can generate multiple arrivals (echoes) due to the same signal. In addition, the underwater channel varies with time. The variation can be caused by inherent changes in the channel or a change in the velocity between the transmitter and receiver, making the multipath much more severe. This multipath may be less for deeper water. The number of propagation paths depends on the reflection and refraction properties of the channel.

Since the received signal is a sum of the various paths along which the transmitted wave travels the impulse response of the channel can be modeled as

$$h(t) = \sum_i h_i(t - \tau_i) \tag{2.5}$$

where $h_i(t)$ represents the impulse response and τ_i the path delay of the i^{th} path.

The acoustic channel is particularly susceptible to multipath and is characterized by a large delay spread and a large Doppler spread. The channel delay spread is defined as the maximum difference between the times of arrival of the channel paths, or the length of the longest path delay. This is expressed as [5]

$$D_\tau = \max(|\tau_p - \tau_q|) \tag{2.6}$$

where τ_p and are the p^{th} and q^{th} times in the path of arrival, respectively.

In underwater environments this can be as large as 100 ms. The channel Doppler spread is defined as the maximal difference between the Doppler rates of the channel paths. The Doppler spread D_d is expressed as [6]

$$D_d = \max\left\{\frac{|v_p - v_q|}{c}\right\} \tag{2.7}$$

where v_p and v_r are the p^{th} and q^{th} velocities in the path of arrival, respectively. The Doppler frequency spreads are typically large, especially compared to optical or electromagnetic mediums.

2.2.3 Propagation Loss.

There is a great deal of path loss in acoustic channels that can be characterized as absorptive loss, and geometrical spreading.

Absorptive Loss is the energy that is absorbed by the medium. This energy loss is different for the different modes of propagation. For example, electromagnetic and optical waves have a comparatively much high absorptive loss than acoustical signals. Absorptive energy loss depends on the frequency that is used, which is why electromagnetic waves have a higher absorptive loss. Earlier, the absorptive loss for EM waves was defined in (2.1). Equation (2.1) holds for acoustic waves with a different absorption coefficient [1].

For low frequencies (below 50 kHz), the absorption coefficient is calculated as [7]:

$$\alpha(f) = \frac{0.11 f^2}{1+f^2} + \frac{44 f^2}{4100+f^2} + 2.75\times10^{-4} f^2 + 0.003 \tag{2.8}$$

where f denotes frequency in kHz.

Geometric spreading is the power loss due to the increased surface area that the wave occupies over larger and longer distances. The wave energy in each unit surface becomes less over distance, decreasing by the inverse square of the distance. This type of spreading loss is frequency independent, as opposed to absorption loss. Different types of geometrical spreading loss are considered by assuming that a point source generates either spherical or cylindrical waves. For a point source generating spherical waves, the power loss caused by spreading is proportional to the square of the distance away from the source. A point source generating cylindrical waves has a power loss proportional to the distance away from the source. For an underwater setting, the geometric spreading loss as assumed proportional to d^{β}, where d is the distance from the point source to the receiver and β depends on the type of spreading loss. In cases where the propagation is not usually classified as purely cylindrical or spherical, β can be taken to be 1.5 [5]. The spreading factor (SF) can also be expressed logarithmically as:

$$SF = 10\beta \log_{10} d \tag{2.9}$$

Though these are the common expressions for the spreading loss and the absorption loss, there are several different definitions for the total transmission loss (TL). [8] expresses the total transmission loss as

$$TL = SS + \alpha(f) d \times 10^{-3} \tag{2.10}$$

However, Stojanovic and Reisig [9] define the overall transmission loss as

$$TL(d, f) = \left(\frac{d}{d_r}\right)^{\beta} \alpha(f)^{d-\beta} \tag{2.11}$$

where d is the transmission distance taken with reference to some point d_r. Again, β depends on the type of spreading and can be assumed to be 1.5.

2.2.4 Noise

The noise in any acoustic channel consists of ambient and site specific noise. Ambient noise is background noise which can come from a variety of different sources. Some of the common sources of ambient noise include volcanic and seismic activities, turbulence, weather processes, and thermal noise. Generally ambient noise is prevalent over a larger area compared to site specific noise. Site specific noise is an interfering signal which is recognizable in the received signal. An example of site specific noise would include marine animal sounds or the sounds of ice cracking. These noises are non Gaussian, though they can be modeled using Gaussian mixture or stable distributions [10].

Ambient noise can be measured as Gaussian, not white, and has a power spectral density (PSD) that changes with time. The power spectral density of ambient noise decays with frequency, which results in a signal to noise ratio (SNR) that varies over the signal bandwidth. The SNR of a band of frequency Δf around some frequency f is represented as [10]

$$SNR(l, f) = \frac{S_l(f)}{A(l, f)N(f)} \tag{2.12}$$

where $N(f)$ is the combination of ambient and site specific noise in the environment and $S_l(f)$ is the power of the signal. Ambient noise is normally classified into four categories, turbulence (N_t), shipping (N_s), wind (N_w), and thermal (N_{th}), which are each modeled as [10]:

$$
\begin{aligned}
10\log N_t(f) &= 17 - 30\log f \\
10\log N_s(f) &= 40 + 20(s - 0.5) + 26\log f - 60\log(f + 0.03) \\
10\log N_w(f) &= 50 + 7.5\sqrt{w} + 20\log f - 40\log(f + 0.4) \\
10\log N_{th}(f) &= -15 + 20\log f
\end{aligned}
\tag{2.13}
$$

This model shows that the SNR is a function of frequency, limiting the bandwidth for large distances. Thus, bandwidth efficient schemes are necessary for acoustic channels.

2.2.5 Doppler

Another factor in underwater communications is the non-uniform Doppler shift/spread that is more severe compared to in a radio or optical channel. In communications, relative movement between the receiver and transmitter causes the signal to undergo a Doppler warp. In radio channels, this warp can be modeled as a simple shift across all frequencies, but because the speed of sound is low compared to electromagnetic waves, this may not apply. Models for estimating and correcting a more severe underwater Doppler Warp are explored in Chapter 3. In the case of narrow band signals, where the entire spectrum can be translated by the same shift as the carrier frequency, the magnitude of the Doppler Effect is defined, called the Doppler rate a as $a = \frac{v}{c}$, where v is the velocity between the transmitter and receiver and c is the speed of sound. This effect can be present even with no deliberate movement between the transmitter and receiver, as they can drift with the waves and tides. The Doppler effect for a single shifted frequency ω_r is represented as

$$\omega_r = \omega_n(1 + a) \tag{2.14}$$

where ω_n is the original frequency.

This assumption often works for narrow band signals in which the entire spectrum is assumed to be translated by the same frequency as the carrier. The Doppler shift in such cases can

be negated by carrier synchronization, which is equivalent to adjusting the local carrier frequency [11].

In wideband signals, Doppler translates each frequency component by a different amount. Hence the Doppler Effect is more accurately modeled as a time scaling (expansion or contraction) of the signal waveform. The discretized received signal can be represented as having a period T_s and the received signal $r(nT_s)$ as:

$$r(nT_s) = s((1+a)nT_s) \tag{2.15}$$

To recover the original signal $s(nT_s)$, an inverse time scaling is applied, which is equivalent to resampling the received signal by $1+a$

$$s(nT_s) = r\left(\left(\frac{n}{1+a}\right)T_s\right) \tag{2.16}$$

This effect can be represented as a scaling of the sampling frequency f_s:

$$\tilde{f}_s = (1+a)\, f_s \tag{2.17}$$

2.3 Modulation Techniques for Underwater Communications

Here are the main techniques that are used in underwater acoustic communications: Frequency Hopped Frequency Shift Keying (FSK) modulation, Direct Sequence Spread Spectrum (DSSS) modulation, Single Carrier transmission, and multicarrier modulation.

2.3.1 Frequency Hopped FSK

In Frequency Shift Keying (FSK) modulation, information bits are used to select the carrier frequencies of the transmitted signal and the receiver compares the measured power at different

frequencies to infer the transmitted bits. This method does not require channel estimation, although guard bands are required to avoid interference from frequency spreading. The transmitted FSK signal can be represented as

$$\tilde{x}(t) = 2\Re \sum_{i=-\infty}^{\infty} e^{j2\pi f(i;s[i])(t-iT)} g(t-iT) \tag{2.18}$$

where T is the time duration of each tone spaced by $1/T$, $f(i;s[i])$ is a function that determines the tone of the i^{th} symbol, $s[i]$ is the data symbol, and $g(t)$ is the pulse shaping function. Within any bandwidth B, the total number of tones that can be used is BT. In underwater channels, FSK often falls prey to the severe multipath in the system, making it less efficient than other modulation schemes.

2.3.2 Direct Sequence Spread Spectrum

In Direct Sequence Spread Spectrum (DSSS) modulation, a narrowband waveform of bandwidth W is spread to a large bandwidth before transmission. Each symbol is multiplied by a spreading code of length $N = B/W$ chips. The baseband signal is represented as:

$$x(t) = \sum_{i=-\infty}^{\infty} s[i] \sum_{n=0}^{N-1} c[i,n] g(t-(iN+n)T_c) \tag{2.19}$$

where $c[i;n]$ is the chip sequence for the i^{th} symbol, and T_c is the chip duration. The passband signal can be represented as

$$\tilde{x}(t) = 2\Re\{x(t)\, e^{j2\pi f_c t}\} \tag{2.20}$$

The despreading operation at the receiver side suppresses time spreading induced interference. Channel estimation and tracking is required unless noncoherent DSSS is used with multiple spreading codes.

2.3.3 Single Carrier Modulation

Single Carrier transmission is the direct transmission of phase coherent modulations such as phase shift keying (PSK) and quadrature amplitude modulation (QAM). However, the multipath propagation introduces a lot of inter-symbol interference into the channel. The transmitted signal is represented as

$$x(t) = \sum_{i=-\infty}^{\infty} s[i]\,\mathrm{g}(t - iT) \tag{2.21}$$

Advanced signal processing is needed for channel equalization. Previous work has used second order phase locked loops to track phase variations and an adaptive decision feedback equalizer that suppresses the ISI.

2.3.4 Multicarrier Modulation

In multicarrier modulation such as frequency division multiplexing (FDM) or Orthogonal Frequency Division Multiplexing (OFDM), the bandwidth is divided into a large number of overlapping subbands. The waveform duration is designed to be long compared to the multipath spread of the channel. Guard bands are used between neighboring subbands, and bandpass filtering is used to separate the signals from different subbands. OFDM is described in more detail in Section 2.4.

2.4 Orthogonal Frequency Division Multiplexing

With severe multipath present in underwater communications, Orthogonal Frequency-Division Multiplexing (OFDM) is considered a way to combat the large delay spreads underwater. OFDM is a form of multicarrier modulation with overlapping subcarriers. While typical single carrier transmission systems are built serially, OFDM is a block transmission method. The transmitted

information is partitioned into blocks, with guard intervals in between blocks to prevent overlap. The guard intervals can be either padded zeros at the end of an OFDM symbol or a cyclic prefix at the front of an OFDM symbol.

The main advantage of OFDM over other schemes is its ability to cope with severe channel conditions. Because the signal is split up over several orthogonal frequencies, each symbol period is longer than in a single carrier system. This gives the data more resiliency to multipath, since the delay spread must be large to cause intersymbol interference. OFDM does not require a guard band between the subcarriers in the frequency domain, which results in saving spectrum.

When considering OFDM, it is assumed that the channel $h(t)$ is invariant, expressed in spectral terms as

$$H(f) = \int_0^{T_{ch}} h(t) e^{-j2\pi ft} dt \tag{2.22}$$

where T_{ch} is the non zero interval over which the channel is defined. The received passband signal after transmission is denoted as:

$$\begin{aligned} \tilde{y} &= h(t) * \tilde{x}(t) + \tilde{n}(t) \\ &= \int_0^{T_{ch}} h(\tau)\tilde{x}(t-\tau) d\tau + \tilde{n}(t) \end{aligned} \tag{2.23}$$

where $\tilde{n}(t)$ is the noise in the system.

In OFDM, bits are divided into several parallel bit streams and then sent over several overlapping carriers. Each subcarrier is separated by a multiple of $\frac{1}{T}$, where T is the OFDM symbol period, and each carrier has an integer number of cycles over the symbol period. Multiple modulation schemes such as quadrature amplitude modulation (QAM) or Phase Shift Keying

(PSK) can be used on each symbol. A comparison between the subcarriers in Frequency Division Multiplexing and Orthogonal Frequency Division Multiplexing is illustrated in Figure 2.1.

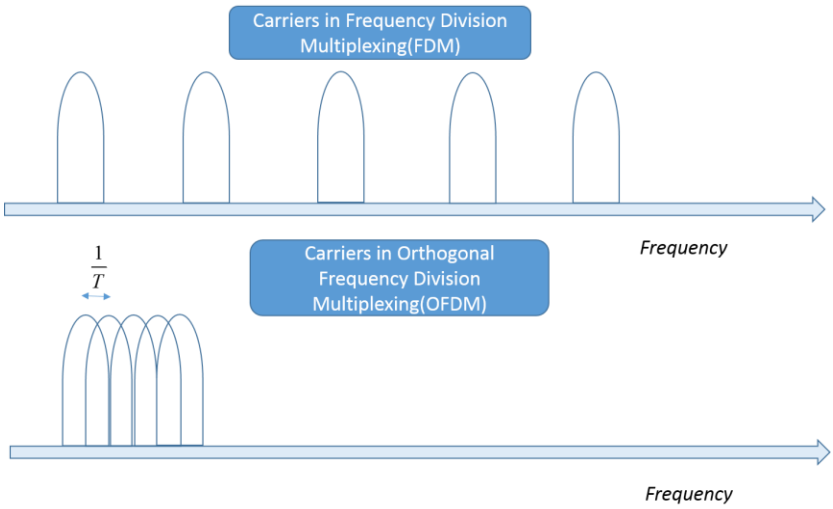

Figure 2.1: Subcarriers in FDM as compared to OFDM.

There are many variables that go into OFDM design and many potential obstacles that need to be addressed in OFDM. This discussion of OFDM is split into three parts, the transceiver design, different techniques in designing the guard interval, and techniques in the synchronization of OFDM. These are the most relevant issues when dealing with Underwater Channels, although there are other performance aspects related to OFDM, such as Peak to Average Power (PAPR).

2.4.1 Transceiver Design

Weinstein and Ebert [12] used the Discrete Fourier Transform to modulate and demodulate the OFDM symbol. This technique has been the standard for OFDM transmission. To improve the time in processing, the FFT can be used in place of the Discrete Fourier Transform. Allow f_s to be the sampling rate, which is at least twice the highest frequency of any signal component. For example if the highest frequency used is 8 kHz, then the sampling frequency would be 16 kHz. Each subcarrier is considered to be of the form

$$\phi_k(t) = \mathrm{e}^{j2\pi f_k t}; 0 < t < NT \tag{2.24}$$

where N is the number of subcarriers and $f_k = \frac{k}{NT}$ refers to the k^{th} subcarrier frequency. The time domain representation of the OFDM symbol is as follows

$$s(t) = \frac{1}{\sqrt{N}} \sum_{k=0}^{N-1} I_k \phi_k(t) \tag{2.25}$$

where I_k is the bit/symbol modulated onto the subcarrier. The discrete time representation with a sampling period of T is:

$$s_n = \frac{1}{\sqrt{N}} \sum_{k=0}^{N-1} I_k e^{\frac{j2\pi nk}{N}} \tag{2.26}$$

This representation shows that the DFT, and subsequently, the FFT, can be used to generate an OFDM symbol.

The performance of an OFDM transceiver is optimized by considering the bandwidth, bit/symbol rate, and delay spread of the system. The guard time has to be larger than the delay spread of the channel to avoid ISI. The underlying assumption for OFDM equalization is that the channel is time invariant. The symbol duration is generally larger than the guard time to include more information, i.e. to increase the number of bits per second. However, larger symbol durations result in a larger number of subcarriers with a smaller subcarrier spacing, and more sensitivity to phase noise and frequency offsets.

A simplified OFDM transceiver is illustrated in Figure 2.2. The data bits are first mapped to symbols and converted into parallel. An IFFT is performed on these symbols after inserting

zeros or a cyclic prefix. This is followed by receiver operations aimed at reversing the transmitter operations.

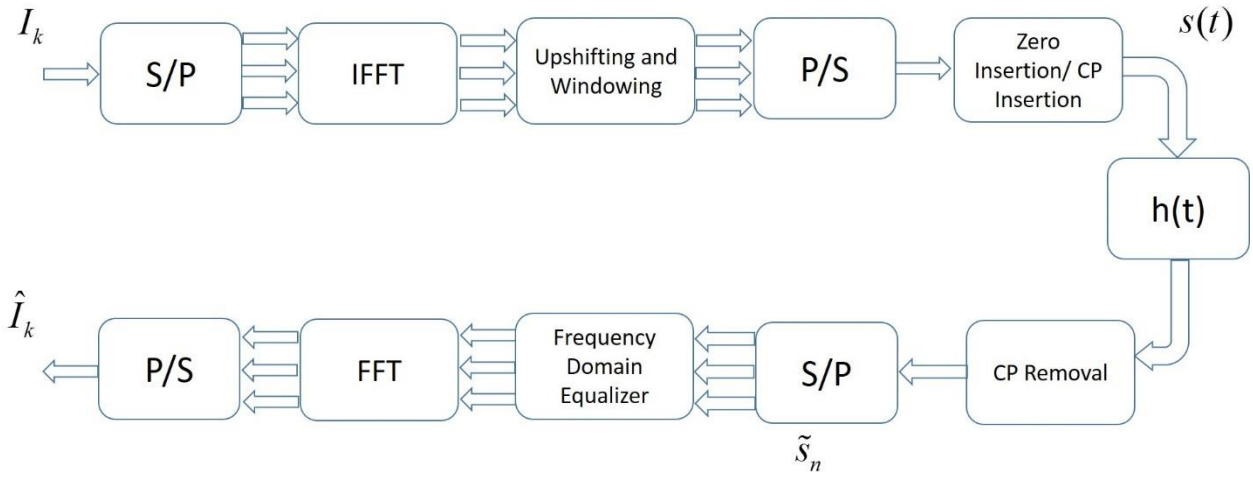

Figure 2.2: OFDM Transceiver Structure.

2.4.2 Guard Interval

Once the signal goes through a multipath channel, there could be Inter-Symbol Interference (ISI) caused by a loss of orthogonality of the subcarriers. Guard intervals are used in the time domain to prevent ISI to a certain extent. The guard interval can either be a Cyclic Prefix/Suffix, or a Zero Pad.

a. Cyclic prefix/suffix

A cyclic prefix and/or suffix are/is created by appending copies of the first and last part of the OFDM symbol to the beginning and/or end of the transmitted symbol as shown in Figure 2.3. The length of the prefix/suffix is at least as long as the delay spread of the channel. The prefix/suffix acts as a guard interval between consecutive OFDM symbols and allows for cyclic convolution between the OFDM symbol and the Channel Impulse Response. Because cyclic convolution is multiplication in the frequency domain, each subcarrier remains orthogonal. The cyclic

prefix/suffix can also be used for timing synchronization and carrier frequency offset correction, as will be shown later [13].

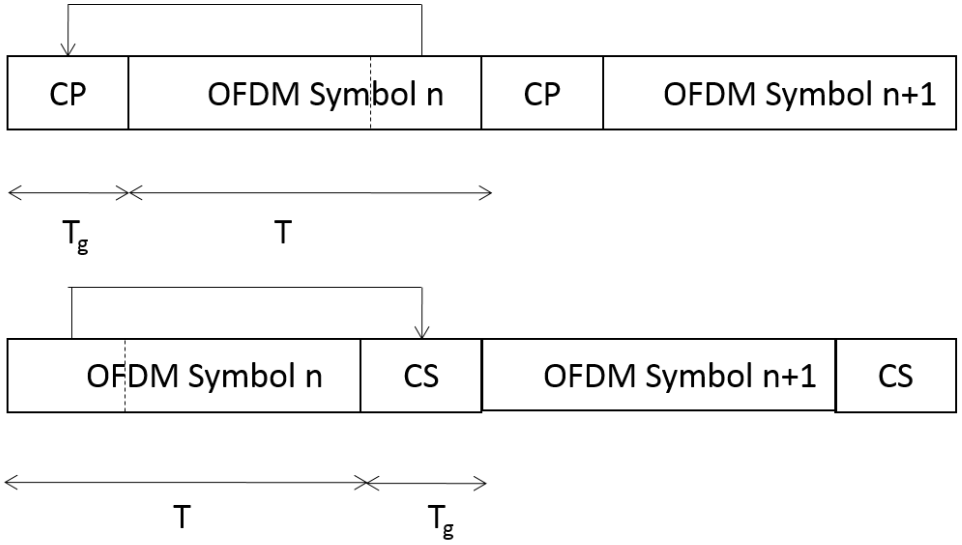

Figure 2.3: Illustration of Cyclic Prefix and Cyclic Suffix in the Time Domain.

b. Zero padded OFDM

An alternative to cyclic prefix/suffix as a guard interval is padding each OFDM symbol with zeros at the transmitter. The receiver would add the samples corresponding to the guard interval (no longer containing zeros, but noise and multipath) to the beginning of the OFDM symbol. Adding the samples to the beginning of the symbol will turn the linear convolution between the OFDM symbol and the channel impulse response into a circular convolution [13].

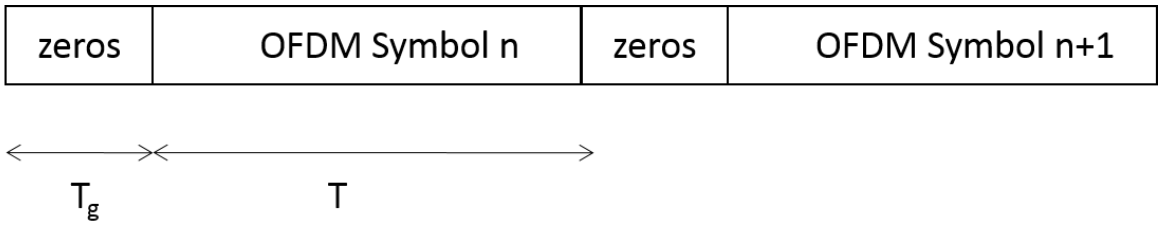

Figure 2.4: Illustration of Zero-padded OFDM Symbol in the Time Domain.

2.4.3 Synchronization

Synchronization is one of the most important and challenging issues in an OFDM system. While OFDM is useful in combating multipath, it requires that the transmitter and receiver are synchronized in time and frequency. Without synchronization, either ISI or ICI can degrade the performance of an OFDM system.

Synchronization is divided into two parts: synchronization in time and synchronization in frequency. A receiver has to deal with the effects of symbol timing offset (STO) and carrier frequency offset (CFO). Normalized CFO and STO is represented as ε and δ, respectively. The received signal $r[n]$ can be represented as

$$\begin{aligned} r[n] &= IDFT\{R(k)\} = IDFT\{H(k)X(k) + Z(k)\} \\ &= \frac{1}{N}\sum_{k=0}^{N-1} H(k)X(k)e^{j2\pi(n+\partial)(k+\varepsilon)/N} + z[n] \end{aligned} \tag{2.27}$$

where $X(k)$ and $H(k)$ refer to the Fourier transform of the input and the frequency response of the channel respectively, and $z[n]$ refers to $IDFT\{Z(k)\}$.

Time domain synchronization is done in two steps, by first performing packet detection and symbol synchronization. Packet detection involves techniques to find the beginning and end points of the symbols. Symbol synchronization follows packet detection and is the process used to obtain estimates of the beginning and end of the symbols at sample level precision.

Here are some of the popular techniques that can be used to perform packet detection:

a. Energy Detection

In energy detection, the received signal is divided into windows of length L, and a decision is made on whether the packet exists or not based on the energy in that window. The decision metric on whether to accept a packet is represented as m_n. In the presence of a packet the energy in the window would be high, leading to acceptance of that packet. The decision metric can be written as:

$$m_n = \sum_{k=0}^{L-1} \left| r[n-k] \right|^2 \tag{2.28}$$

However, the received energy can vary in the presence of noise and multipath in the signal. For this reason, setting a threshold to accept packets can be difficult and lead to many false alarms.

b. Double Sliding Window

Instead of using the energy in a single window for deciding whether the signal exists, this method uses the energy of two consecutive windows to form the decision metric. Consider two consecutive windows A and B, of which window A contains the received signal. The decision metric first increases, when the packet is present only in window A, and then decreases, when the packet enters window B.

The decision metric is defined as:

$$\begin{aligned} a_n &= \sum_{m=0}^{M-1} \left| r[n-m] \right|^2 \\ b_n &= \sum_{m=M}^{2M-1} \left| r[n-m] \right|^2 \\ m_n &= \frac{a_n}{b_n} \end{aligned} \tag{2.29}$$

where a_n and b_n refer to the energy in windows A and B respectively. Using the double sliding window, the decision metric is not dependent on the energy of the received signal.

c. Double Sliding Window Correlation

If the packet in question has a repetitive structure, a more accurate packet detection method can be developed. One technique for packet detection is similar to the algorithm developed by Schmidl and Cox [10] for estimating symbol timing and CFO. In this method, the preamble would consist of two identical OFDM training symbols, or a single OFDM symbol with a repetitive structure. The decision metric would use two consecutive windows to produce a correlation. The correlation will be high when the two windows contain the same repetitive parts of the preamble. The cyclic prefix of an OFDM symbol can be used in this method. However, this method is susceptible to ISI if the guard time is shorter than the delay spread of the channel. The correlator is represented as c_n and the decision metric is represented as:

$$\begin{aligned} c_n &= \sum_{k=0}^{L-1} y[n+k]y^*[n+k+D] \\ p_n &= \sum_{k=0}^{L-1} \left| y[n+k+D] \right|^2 \\ m_n &= \frac{c_n}{p_n} \end{aligned} \tag{2.30}$$

The output of the correlator will have a flat interval consisting of multiple points that one can use as the packet synchronization point. This technique can also be used for symbol synchronization, though a common problem is that the output does not produce a distinct peak in the correlation output. However, an average of the correlation values can help produce a better peak [11].

After packet detection, another technique determines where a packet begins and ends; symbol synchronization estimates the beginning and end of the symbol with sample level precision. Two of the most common methods in symbol synchronization are matched filtering and a correlator developed by Schmidl and Cox [14] utilizing the cyclic prefix.

a. Matched Filter

The matched filter uses a preamble $t[n]$ known to the transmitter and receiver. The receiver calculates the cross correlation of the received signal and $t[n]$. The sample that maximizes the absolute value of the cross correlation gives the timing estimate of the symbol. The cross correlation is calculated as follows:

$$\hat{t}_s = \arg\max_n \left| \sum_{k=0}^{L-1} r[n+k] t_k^* \right| \tag{2.31}$$

This approach can fail when the received signal has undergone a lot of distortion, typically from Doppler, or when there is a CFO between the transmitter and receiver. However, the performance of the matched filter correlator is in general considered to be better than the double sliding window correlator when there is no CFO between the transmitter and the receiver [13].

b. Using Cyclic Prefix

Consider an OFDM symbol with a cyclic prefix of N_G samples and data of N_{sub} samples. Recall that the CP is a copy of the last N_G samples of the OFDM symbol. This feature can be used to estimate the STO. Consider two sliding windows W1 and W2 which are spaced N_{sub} samples apart. The similarity between W1 and W2 is maximized when the CP of an OFDM symbol falls into W1. The similarity between W1 and W2 can be found by either finding the point where the

difference between the two windows is minimized or the correlation between the windows is maximized [15] as shown in the following equations:

$$\hat{\partial} = \arg\min_{\partial} \left\{ \sum_{i=\partial}^{N_G - 1 - \partial} \left| y[n+i] - y[n+N_{sub}+i] \right| \right\}$$
$$\widehat{\partial} = \arg\min_{\partial} \left\{ \sum_{i=\partial}^{N_G - 1 - \partial} \left| y[n+i] y^*[n+N_{sub}+i] \right| \right\} \quad (2.32)$$

This technique may not work when the delay spread of the channel is comparable to the length of the CP, as the cyclic prefix would have undergone too much distortion for the correlator to produce a distinct peak.

While these are some of the most common timing synchronization techniques, they do not always work in underwater environments. Frequency domain approaches can also be used to obtain timing synchronization [16]. Some of these frequency domain approaches provide better timing synchronization, as discussed in Chapter 4.

A major type of distortion in OFDM systems results from the Doppler warp that occurs due to relative motion between the transmitter and the receiver. If the carrier frequency is large compared to the bandwidth of the system, the Doppler warp can be modelled as a simple Doppler shift, which is then denoted as a CFO. In (2.27), the CFO is represented as the parameter ε. This ε refers to the normalized CFO, which is the difference in carrier frequencies between the transmitter and receiver. The CFO can be broken down into a sum of ε_i and ε_f, which refers to the integer and fractional part of the normalized CFO respectively. Suppose the transmitted signal is represented in the frequency domain as $X[k]$. If the carrier frequency offset is an integer, then any cyclical shift ε_i would produce an $X[k-\varepsilon_i]$ in the k^{th} subcarrier, causing all of the carriers to be shifted over by a integer number of frequency bins. This would cause a severe increase in

the bit error rate. Fractional frequency offsets would also negatively affect the BER by causing the destruction of the orthogonality of the subcarriers [17].

A major difficulty with OFDM is the sensitivity to CFO. CFO can cause the OFDM symbol to lose its orthogonality, creating ICI and causing the BER to increase. In order to preserve the orthogonality of the subcarriers in the frequency domain, several algorithms can be used to estimate and correct for the CFO.

a. Repeated Training Symbols

This method involves consecutive training symbols that are part of the OFDM structure. There are at least two consecutive repeated training symbols and the received signal is assumed to be demodulated using a carrier frequency that is slightly different from the carrier frequency that generated the transmitted signal. $s[n]$ and $x[n]$ represent the transmitted signal in baseband and passband respectively. f_{tx} and f_{rx} refer to the carrier frequencies generated locally at the transmitter and receiver respectively [14]. Thus the received signal at baseband is represented as:

$$y[n] = s[n]e^{j2\pi f_{tx}nT_s}e^{-j2\pi f_{rx}nT_s} = s[n]e^{j2\pi(f_{tx}-f_{rx})nT_s} \tag{2.33}$$

The frequency offset estimator is based on:

$$\begin{aligned} m_n &= \sum_{n=0}^{L-1} y[n]y^*[n+D] \\ &= \sum_{n=0}^{L-1} s[n]s^*[n+D]e^{j2\pi\Delta fnT_s}e^{-j2\pi\Delta f(n+D)T_s} \\ &= e^{-j2\pi\Delta fDT_s}\sum_{n=0}^{L-1}|s_n|^2 \end{aligned} \tag{2.34}$$

where D is the length of the training symbol.

The CFO estimate is then expressed as:

$$\hat{\Delta f} = \frac{-1}{2\pi D T_s} \angle m_n \tag{2.35}$$

This estimator is limited in the frequency range by the length of the training symbol and the sampling period:

$$|\Delta f| \leq \frac{1}{2DT_s} \tag{2.36}$$

This type of estimator cannot estimate CFOs outside this range. A major problem with using this type of estimator for underwater channels is that the added training symbols make the symbol longer, making the Doppler estimation more difficult and less accurate.

b. Using the CP

Since the repeated training symbols can add unnecessary overhead, the CP can be used instead to estimate the CFO. Since the CP is identical to the last part of the OFDM symbol, this inbuilt repetition can be used to estimate the CFO. The CFO estimate is represented as:

$$\Delta \hat{f} = \frac{1}{2\pi N_{sub} T_s} \arg\left\{ \sum_{n=0}^{N_G - 1} y[n] y^*[n + N_{sub}] \right\} \tag{2.37}$$

where N_G refers to the number of samples in the CP and N_{sub} refers to the effective data length in each OFDM symbol. However, this method will also not work when the delay spread of the channel is comparable to the length of the CP, because the CP would have undergone too much distortion to produce a good estimate. For this reason, a new model is needed to estimate the Doppler warp that affected the transmitted signal.

3 Doppler Estimation

3.1 Introduction

In communication systems, OFDM signals often need a Doppler Correction in order to correct for the average Doppler shift over a packet. Since the speed of sound in water is low compared to that of electromagnetic waves in water (1.484 km/s for sound as opposed to 225,000 km/s for electromagnetic), acoustic signals have a much larger propagation delay and the Doppler warp that affects the received signal is much more severe. As a result of the propagation delay and the Doppler warp, the received signal in an underwater environment is harder to decode compared to the same signal in an RF environment. In order to correct for the distortion arising from the Doppler warp, a uniform Doppler correction that expands and/or contracts the received signal in time is introduced. This uniform Doppler expansion/contraction assumes that the relative velocity between the transmitter and receiver is constant over the duration of the packet. The Doppler shift/spread can be measured by the ratio $a = \frac{v}{c}$, where c is the speed of sound in water and v is the relative velocity between the transmitter and the receiver.

This uniform Doppler expansion/contraction is measured as a change in time scale by a constant factor. The relationship between the old and new time axes can be modeled as:

$$t_{doppler} = (1+\alpha)t_{original} \tag{3.1}$$

where $t_{doppler}$ and $t_{original}$ refer to the Doppler affected time scale and the original time scale respectively. α refers to the relative Doppler expansion or contraction. In the model represented by (3.1), negative values of α reflect a contraction (in time) while positive values reflect an

expansion. To simulate the Doppler effect on a uniformly sampled signal, the signal can be uniformly resampled. The time warp is illustrated in Figure 3.1.

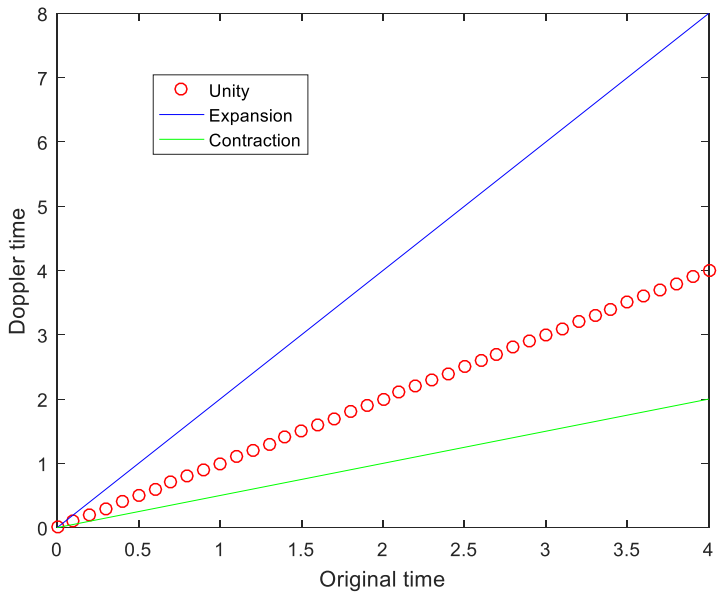

Figure 3.1: Time Warp for Uniform Expansion/Contraction.

In Figure 3.1, values for α of 0.5 (expansion) and -0.5 (contraction) are used. These values represent an expansion and contraction in time, respectively, and the time scales can be represented as $t_{Doppler} = 1.5t_{original}$ and $t_{Doppler} = 0.5t_{original}$, for α values of 0.5 and -0.5, respectively. In the frequency domain, α of -0.5 corresponds to a doubling of frequency, while an α of 0.5 corresponds to an expansion in time and a two thirds decrease in frequency relative to the original frequency.

Figure 3.1 visually demonstrates the linear Doppler time warp model, but such values are not an accurate representation of values found in experimentation. In practical scenarios, the value of α is not very high, even in underwater scenarios, where the maximum speed of the vehicle can go up to 65 km/hour or 18 m/s. The values of α using acoustic signals are expected to be large

compared to RF situations, since the frequency change relative to the carrier frequency is higher in acoustic situations (since the carrier frequency is in the MHz range in RF scenarios and in the kHz range in acoustic scenarios). To calculate practical values of α, assume maximum speeds of up to 65 km/hour, or 18 m/s. This is close to typical for submarines. Such a speed can correspond to an α value of 0.012. This is calculated by using $\alpha = \frac{v}{c}$, assuming a positive 18 m/s range rate (negative closing rate) and the speed of sound in water as 1484 m/s. In simulation experiments, realistic speeds of underwater vehicles are assumed, and thus corresponding α values are used.

The Doppler effect is corrected by finding the Doppler warp that has affected the received signal, and then inverting the time scale that represents the Doppler warped time scale.

$$\hat{t}_{original} = \frac{t_{Doppler}}{1+\alpha} \tag{3.2}$$

For uniformly sampled sequences, inverting the uniform Doppler time warp corresponds to uniform resampling, i.e. changing the sampling rate by a factor of $(1+\alpha)^{-1}$.

The expansion and contraction effects can be illustrated through simulation with a 5 kHz sinusoid, using α values of 0.5 and -0.5. The spectrogram of a 5 kHz sinusoid, before contraction or expansion in time, is shown in Figure 3.2.

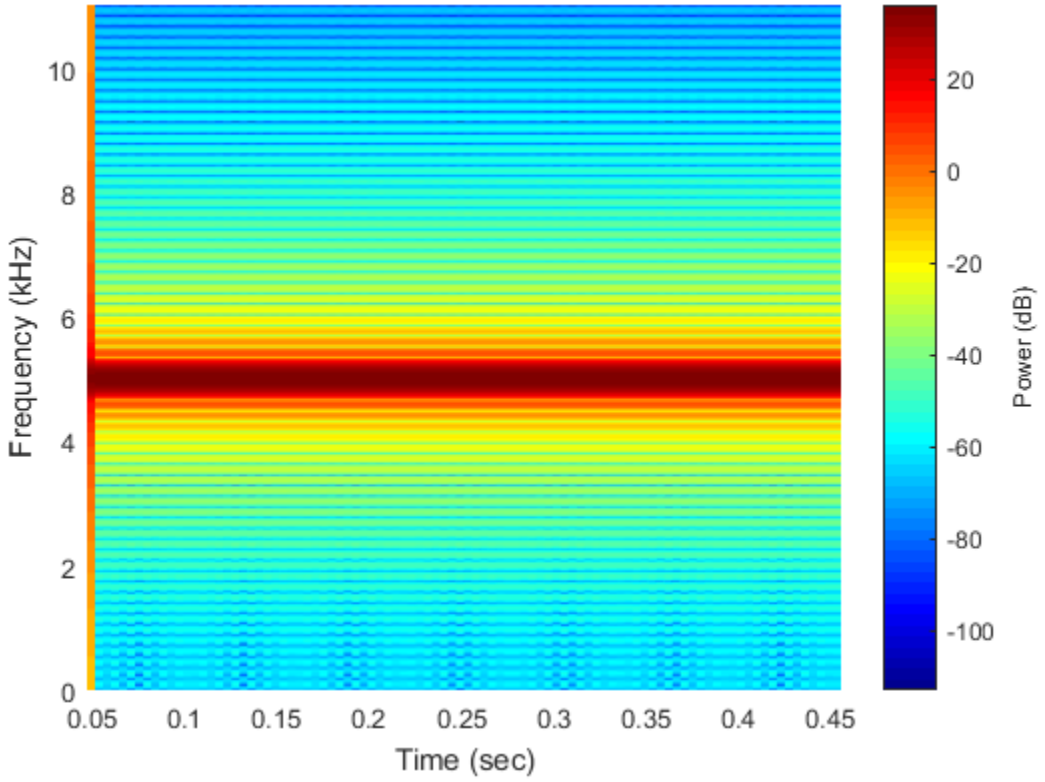

Figure 3.2: Spectrogram of Original 5 kHz Sinusoid.

Using an α value of -0.5, the relationship between the time scales becomes $t_{Doppler} = 0.5 t_{original}$. This results in contraction (halving) of the signal in time duration, and therefore a corresponding doubling of frequency. This change in frequency is evident in the spectrogram shown in Figure 3.3. Similarly, when the value of α is 0.5 the relationship between the time scales becomes $t_{Doppler} = 1.5 t_{original}$. This is equivalent to an expansion in time and a corresponding decrease in frequency (to two thirds of the actual frequency). This change in frequency is observed in the spectrogram shown in Figure 3.4 where the measured frequency of the sinusoid after the Doppler warp is now equal to 3333.33 Hz (two thirds of 5 kHz).

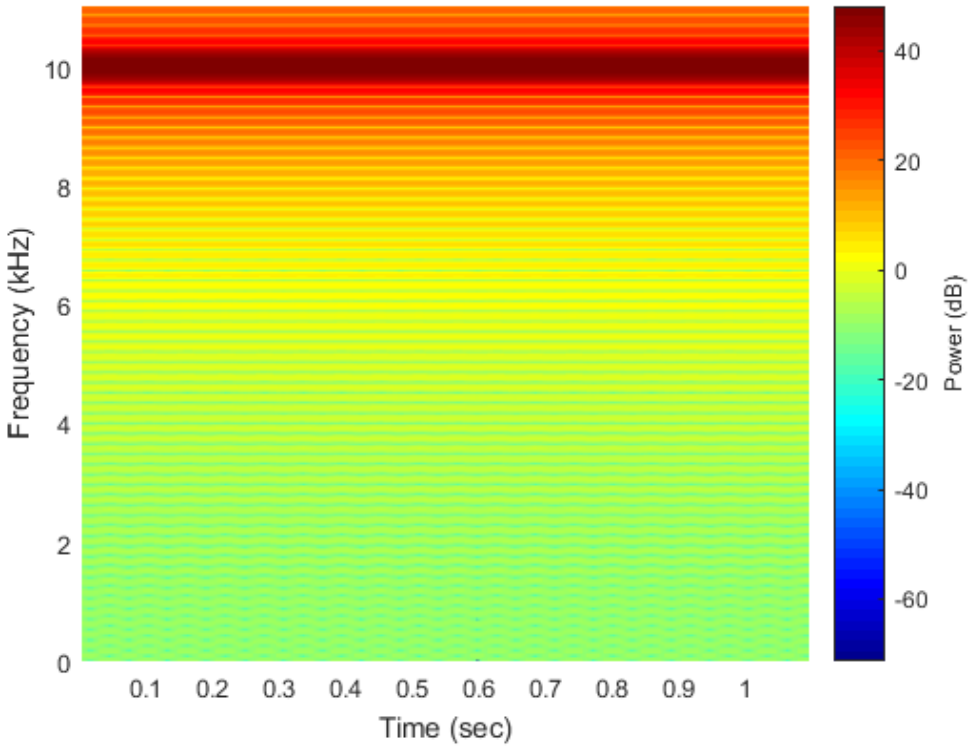

Figure 3.3: Spectrogram of Time Warped Sinusoid with α of 0.5.

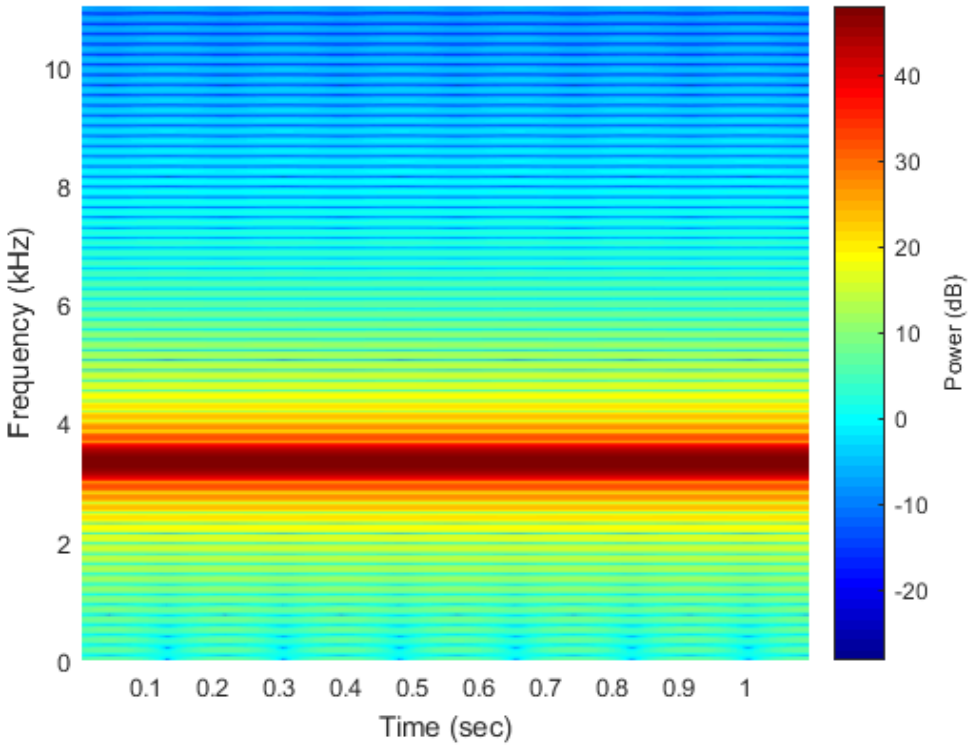

Figure 3.4: Spectrogram of Time Warped Sinusoid with α of -0.5.

3.2 Non Linear Doppler Warp Model

In very wideband systems, signals undergo non-linear Doppler warps that cannot be corrected using the uniform expansion/contraction model represented by (3.1). For this reason, an improved method of finding and estimating the non-linear warp that a time warped signal undergoes is used.

Instead of using a model of the time warped signal as a uniform expansion or contraction a polynomial can be used to map the time from the original unwarped signal to the time warped signal. The simplest example of such a polynomial is a quadratic equation which can approximate a linear change in frequency over a short enough time period. The quadratic equation for the time on the Doppler scale is approximated by

$$t_{Doppler} = \left(1 + \alpha + \beta t_{original}\right) t_{original} \tag{3.3}$$

where $t_{doppler}$ and $t_{original}$ are the Doppler and original time scales and α, β are the parameters for the Doppler warp model in (3.3). This method assumes that a non-linear Doppler warp can be modeled as a quadratic equation between the Doppler affected time and the original non warped time. This is illustrated in Figure 3.5.

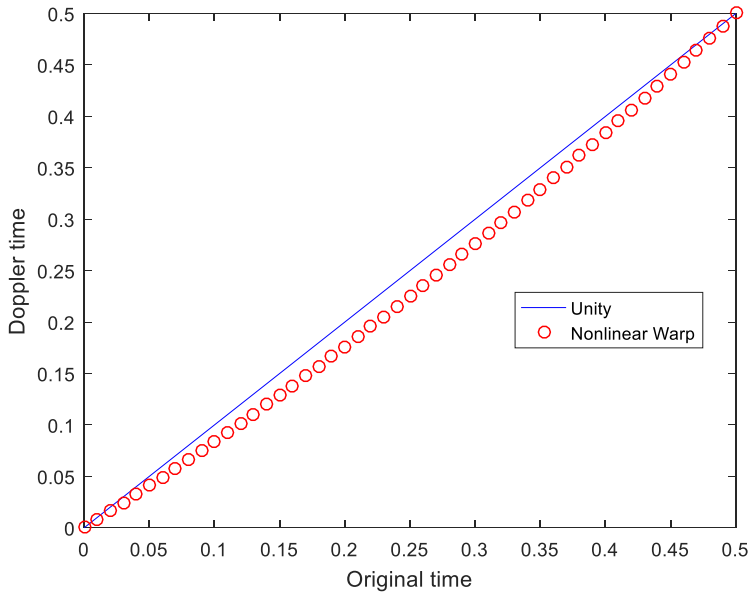

Figure 3.5: Nonlinear Doppler Warp Model with α of -0.2 and β of 0.4.

Observe in Figure 3.5 that the warp model includes periods of compression and expansion over the given time interval. From 0 to 0.25 seconds, the signal undergoes compression while from 0.25 to 0.5 seconds the signal undergoes expansion.

In order to undo a Doppler warp as in (3.3), the parameters α and β are needed, so that the received signal can be appropriately resampled and an estimate of the original unwarped signal recovered. Assuming that $r(t)$ is the received uniformly sampled signal that was subject to the Doppler effect, then after applying the (inverting) Doppler warp correction the samples will be non-uniformly spaced. These non-uniformly spaced samples are resampled, or converted, to uniformly spaced samples spaced at T_s (or inverse of the sampling frequency F_s) through a linear interpolation of the non-uniformly spaced sample values straddling the desired uniformly spaced time points. Methods of resampling other than linear interpolation can prove useful, such as a

quadratic or sinusoidal interpolation, though what is best will depend on the characteristics of the received signal. The linearly interpolated resampled signal is represented as:

$$r\left\{t_{uniform}\left(n\right)\right\} = r\left\{t_{doppler}\left(k\right)\right\} + \gamma\left[r\left\{t_{doppler}\left(k+1\right)\right\} - r\left\{t_{doppler}\left(k\right)\right\}\right] \tag{3.4}$$

where

$$\gamma = \frac{t_{uniform}\left(n\right) - t_{doppler}\left(k\right)}{t_{doppler}\left(k+1\right) - t_{doppler}\left(k\right)} \tag{3.5}$$

In the above, $r\{t_{uniform}(n)\}$ represents the uniformly spaced output, k represents the k^{th} sample of the Doppler-corrected non-uniformly spaced time axis, n represents the n^{th} sample of the uniform time axis, and $t_{doppler}\left(k\right) \le t_{uniform}\left(n\right) \le t_{doppler}\left(k+1\right)$.

Similar to the uniform expansion/contraction, the nonlinear warp can be applied to a sinusoid. In this case a sinusoid at 5 kHz was passed through a time warp (with an α value of -0.2 and β value of 0.4) and then non-uniformly resampled to uniformly spaced samples. Figure 3.6 shows the spectrogram of the simulated Doppler affected burst.

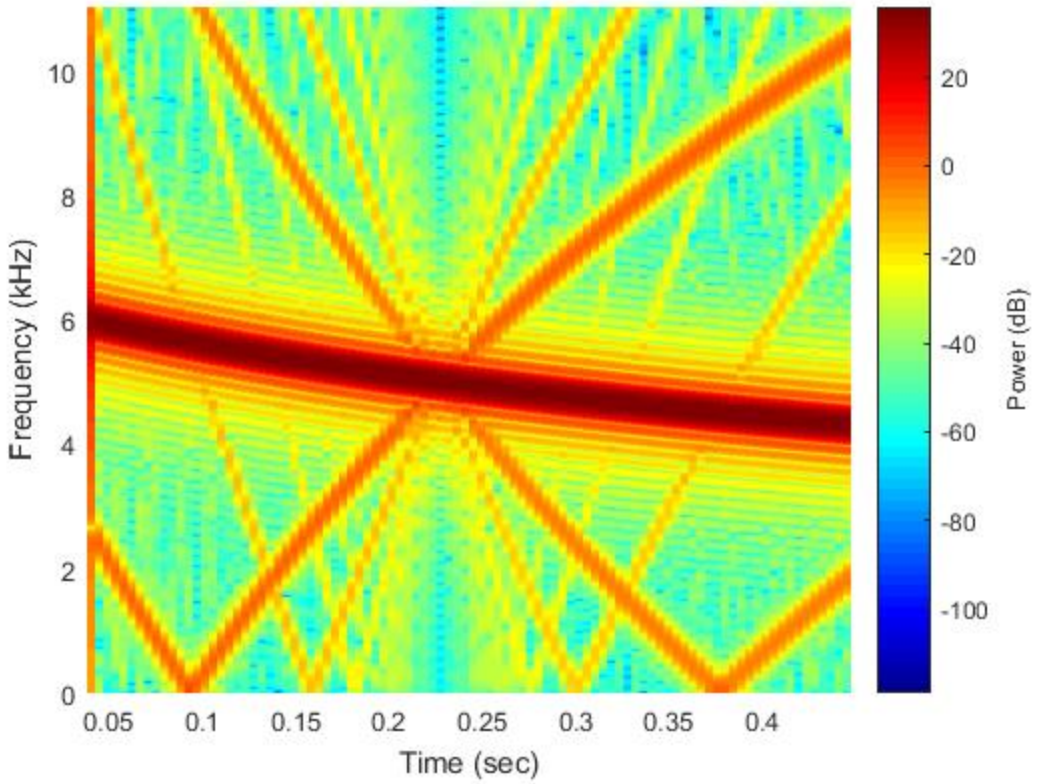

Figure 3.6: Spectrogram of Doppler Affected Burst.

Observe that frequency changes non-linearly with time for the chosen α and β warp parameter values. Note that the simulation process uses linear interpolation of non-uniformly spaced samples and that this process generates some distortion components, which are approximately 30 dB or more below the level of the main frequency component. While a more refined interpolation process would likely mitigate the distortion components such approaches are not the focus of this work and thus not pursued here.

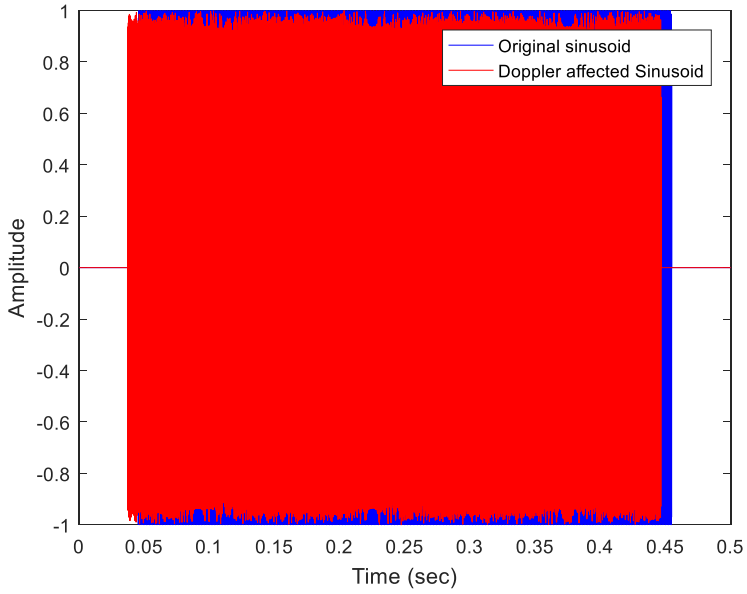

Figure 3.7: The Doppler Affected Burst in the Time Domain.

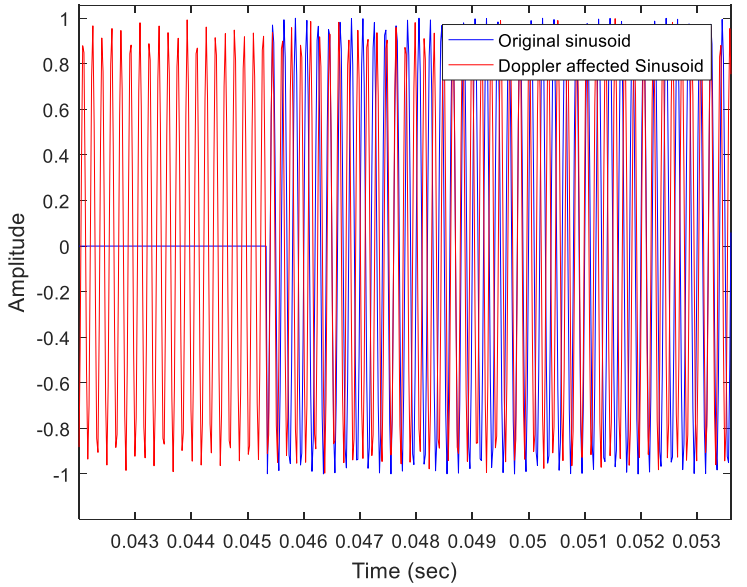

Figure 3.8: Beginning of the Doppler Affected Burst in the Time Domain.

As Figure 3.6 shows, the Doppler warp causes a time-varying (nearly linear) shift in frequency – due to β being relatively large. Figure 3.7 and Figure 3.8 show how the Doppler warp affects the burst in the time domain, with the Doppler affected signal occurring at an earlier

point in time due to the time compression. The time expansion during the second half of the Doppler warp model causes the length of the Doppler affected signal to end up being nearly the same as of the original sinusoid. The time warp can be inverted by mapping the Doppler time axis back to the original time axis. This would mean using the (estimated) α and β parameters to generate (an estimate of) the time warp which (presumably) caused the observed Doppler effect (so as to facilitate the inverse mapping of the time axis). The next section describes the technique that can be used to estimate α and β based on the received burst.

3.3 Derivation of Estimate for α and β.

In order to undo the nonlinear warp shown in Figure 3.5, an estimate of α and β is needed. The period of a signal that undergoes a Doppler warp can be used to derive estimates for α and β. First denote T as a time interval $[t, t+T]$ during the undistorted signal, i.e. prior to its undergoing a Doppler warp. After undergoing a Doppler warp described by (3.3), the time interval after the warp, denoted by $\tilde{T}$, can be expressed as:

$$\begin{aligned}\tilde{T} &= \{1+\alpha+\beta(t+T)\}(t+T)-(1+\alpha+\beta t)t \\ &= (1+\alpha+\beta T)T+\beta Tt+(1+\alpha+\beta t)t+\beta Tt-(1+\alpha+\beta t)t \\ &= (1+\alpha+\beta T)T+2\beta Tt\end{aligned} \tag{3.6}$$

Equation (3.6) expresses the length of the time interval of the warped signal in terms of α and β. Accurate estimates for α and β can be derived by comparing the length of the time interval $\tilde{T}$, after the warp, to the length of the time interval T, before the warp. The detailed explanation of this derivation is given below.

To estimate the parameters α and β, two time instants are used to represent points at the beginning and end of the original unwarped burst, denoted t_0 and t_1 respectively. The interval length estimates, at t_0 and t_1 respectively, are denoted as T_0 and T_1. In the case of a sinusoidal burst, or any burst considered, T_0 and T_1 are chosen to be the same, and thus denoted as T. Furthermore, t_0 and t_1 correspond to $\tilde{t}_0$ and $\tilde{t}_1$ in the Doppler affected burst, and the estimated interval lengths for the time warped burst are $\tilde{T}_0$ and $\tilde{T}_1$. Previous work [18] relied on finding a fixed time interval between $\tilde{t}_0$ and $\tilde{t}_1$, but in this work, since the Doppler warp affects the length of the time warped signal, this assumption is not held to be true. Substituting t_0 and t_1 into (3.6) yields

$$\tilde{T}_0 = (1+\alpha+\beta T)T + 2\beta T t_0 \tag{3.7}$$

and

$$\tilde{T}_1 = (1+\alpha+\beta T)T + 2\beta T t_1 \tag{3.8}$$

Equations (3.7) and (3.8) give a relation between the time warped period of the signal and the original time instants of the unwarped signal. An expression for t_0 is found from (3.3):

$$\tilde{t}_0 = (1+\alpha+\beta t_0)t_0 \tag{3.9}$$

Solving this quadratic equation for t_0 yields:

$$t_0 = \frac{-(1+\alpha)+\sqrt{(1+\alpha)^2+4\beta\tilde{t}_0}}{2\beta} \tag{3.10}$$

Similarly, an expression for t_1 is found as:

$$t_1 = \frac{-(1+\alpha)+\sqrt{(1+\alpha)^2+4\beta\tilde{t}_1}}{2\beta} \tag{3.11}$$

Inserting (3.10) into (3.7) yields

$$\tilde{T}_0 = (1+\alpha+\beta T)T + T\left\{\sqrt{(1+\alpha)^2+4\beta\tilde{t}_0}-(1+\alpha)\right\} \tag{3.12}$$

Inserting (3.11) into (3.8) yields

$$\tilde{T}_1 = (1+\alpha+\beta T)T + T\left\{\sqrt{(1+\alpha)^2+4\beta\tilde{t}_1}-(1+\alpha)\right\} \tag{3.13}$$

Dividing (3.12) and (3.13) by T and cancelling terms yields:

$$\frac{\tilde{T}_0}{T} = \beta T + \sqrt{(1+\alpha)^2+4\beta\tilde{t}_0} \tag{3.14}$$

$$\frac{\tilde{T}_1}{T} = \beta T + \sqrt{(1+\alpha)^2+4\beta\tilde{t}_1} \tag{3.15}$$

To approximate the set of nonlinear equations (3.14) and (3.15), a two dimensional Taylor series expansion is used to generate a set of linear equations.

$$\frac{\tilde{T}_0}{T} = \beta T + f_0(\alpha_0,\beta_0) + (\alpha-\alpha_0)\frac{\partial f_0(\alpha_0,\beta_0)}{\partial\alpha} + (\beta-\beta_0)\frac{\partial f_0(\alpha_0,\beta_0)}{\partial\beta} \tag{3.16}$$

$$\frac{\tilde{T}_1}{T} = \beta T + f_1(\alpha_0,\beta_0) + (\alpha-\alpha_0)\frac{\partial f_1(\alpha_0,\beta_0)}{\partial\alpha} + (\beta-\beta_0)\frac{\partial f_1(\alpha_0,\beta_0)}{\partial\beta} \tag{3.17}$$

where the following were defined

$$f_0(\alpha,\beta) \triangleq \sqrt{(1+\alpha)^2+4\beta\tilde{t}_0} \tag{3.18}$$

$$f_1(\alpha,\beta) \triangleq \sqrt{(1+\alpha)^2+4\beta\tilde{t}_1} \tag{3.19}$$

Now (3.16) and (3.17) are used to obtain an estimate of β, denoted $\hat{\beta}$. First α is eliminated by multiplying (3.16) and (3.17) by $\frac{\partial f_1}{\partial \alpha}$ and $\frac{\partial f_0}{\partial \alpha}$ and subtracting (3.16) from (3.17). Solving for $\hat{\beta}$ yields:

$$\hat{\beta}_i = \frac{\left(\frac{\tilde{T}_1}{T}\frac{\partial f_0}{\partial \alpha} - \frac{\tilde{T}_0}{T}\frac{\partial f_1}{\partial \alpha} + \hat{\beta}_{i-1}\frac{\partial f_1}{\partial \beta}\frac{\partial f_0}{\partial \alpha} - \hat{\beta}_{i-1}\frac{\partial f_0}{\partial \beta}\frac{\partial f_1}{\partial \alpha}\right) - \left(f_1\frac{\partial f_0}{\partial \alpha} - f_0\frac{\partial f_1}{\partial \alpha}\right)}{T\left(\frac{\partial f_0}{\partial \alpha} - \frac{\partial f_1}{\partial \alpha}\right) + \frac{\partial f_1}{\partial \beta}\frac{\partial f_0}{\partial \alpha} - \frac{\partial f_0}{\partial \beta}\frac{\partial f_1}{\partial \alpha}} \tag{3.20}$$

where $f_0 = f_0(\alpha_0, \beta_0)$ and $f_1 = f_1(\alpha_0, \beta_0)$, and i is the iteration index. This value of $\hat{\beta}_i$ is then substituted in (3.17) to generate an estimate $\hat{\alpha}_i$:

$$\hat{\alpha}_i = \frac{\left(\frac{T_1}{T} - \hat{\beta}_i T + \hat{\alpha}_{i-1}\frac{\partial f_1}{\partial \alpha} - f_1 - \left(\hat{\beta}_i - \hat{\beta}_{i-1}\right)\frac{\partial f_1}{\partial \beta}\right)}{\frac{\partial}{\partial \alpha} f_1} \tag{3.21}$$

The results of alternating updates between the latter two iterations are compared to the results that use an approximation method, such as *fsolve* in Matlab. However, the observation was that the results of (3.20) and (3.21) do not solve for α and β estimates exactly, as their solution hovers/circles around the true solution instead. Consequently, α and β have to be iteratively solved for simultaneously. Such estimates for α and β are found by solving (3.16) and (3.17) as a matrix equation. This matrix equation is set up as follows:

$$\begin{bmatrix} \hat{\alpha}_{i+1} \\ \hat{\beta}_{i+1} \end{bmatrix} = \begin{bmatrix} \frac{\partial f_0(\alpha_i, \beta_i)}{\partial \alpha} & T + \frac{\partial f_0(\alpha_i, \beta_i)}{\partial \beta} \\ \frac{\partial f_1(\alpha_i, \beta_i)}{\partial \alpha} & T + \frac{\partial f_1(\alpha_i, \beta_i)}{\partial \beta} \end{bmatrix}^{-1} \begin{bmatrix} \frac{\tilde{T}_0}{T} - f_0(\alpha_i, \beta_i) + \frac{\alpha_{i-1}\partial f_0(\alpha_i, \beta_i)}{\partial \alpha} + \frac{\beta_i \partial f_0(\alpha_i, \beta_i)}{\partial \beta} \\ \frac{\tilde{T}_1}{T} - f_1(\alpha_i, \beta_i) + \frac{\alpha_{i-1}\partial f_1(\alpha_i, \beta_i)}{\partial \alpha} + \frac{\beta_i \partial f_1(\alpha_i, \beta_i)}{\partial \beta} \end{bmatrix} \tag{3.22}$$

where i is the iteration number of the equation. Equation (3.22) shows the iterative process for estimation of the α_i and β_i values that depend on, and are valid for, the time interval associated which the interval between the sinusoidal frequency estimates. A simulation using α and β values to create and subsequently correct a Doppler warp according to the model in (3.3) is shown below. Notice how (3.22) is an iterative solution. The initial values α_0 and β_0 were both taken to be 0. Since α and β are typically quite small, this is not an unreasonable assumption.

3.4 Estimating Doppler Warp

Equation (3.22) shows a way to estimate the parameters describing the Doppler time warp model in (3.3) from a received signal that was subject to Doppler. To illustrate, an example is shown. As shown in the Doppler warp generation, the Doppler warp model is applied to a signal and the α and β values are estimated using (3.22). For consistency of illustration, this example aims to undo the warp shown in Figure 3.6 and 3.7. In that warp, a 5 kHz sinusoidal pulse is used as the input.

The goal of this section is to show that the Doppler warp process works on the 5 kHz sinusoid shown in Figure 3.5 by using (3.3) and (3.22). Equation (3.3) is used to warp two time instants, t_0 and t_1, corresponding to an unwarped signal, into two time instants $\tilde{t}_0$ and $\tilde{t}_1$ using an α and β. Equation (3.22) is then used to find an $\hat{\alpha}$ and $\hat{\beta}$ that approximate the original α and β. The Doppler warp model is shown in Figure 3.6 and Figure 3.7, which have α and β values of -0.2 and 0.4, respectively, generating Doppler warped time instances $\tilde{t}_0$ and $\tilde{t}_1$. Equations (3.7) and (3.8) are used to compute $\tilde{T}_0$ and $\tilde{T}_1$. Finally, (3.22) is used to compute estimates for $\hat{\alpha}$ and $\hat{\beta}$, and those estimates are compared to the original values. In this scenario, T is 0.0002 s, since the frequency of the sinusoid used for approximation is 5 kHz. The time instants t_0 and t_1 are

chosen to be $0.1000s$ and $0.4000s$ which, as seen in Figure 3.7, are time instants that fall within the unwarped sinusoidal burst. Matching the Doppler warp example illustrated in Figure 3.6, the ideal values for α as well as β are 0.1. Using the above values for α, β, t_0, and t_1 yield $\tilde{T}_0$ as $1.7602\times10^{-4}s$, $\tilde{T}_1$ as $2.2402\times10^{-4}s$, $\tilde{t}_0$ as $0.0840s$, and $\tilde{t}_1$ as $0.3840s$. Table 3.1 provides all of the values used to create the Doppler warped sinusoid. The values α_0 and β_0 were both taken to be 0.

Using these values for T_0, T_1, $\tilde{t}_0$, and $\tilde{t}_1$, (3.22) is used to compute estimates $\hat{\alpha}$ and $\hat{\beta}$ using 50 iterations. 25 iterations were experimentally observed as the minimum number of iterations required to reach a steady state solution. The result of this approximation is shown for $\hat{\alpha}$ in Figure 3.9 and for $\hat{\beta}$ in Figure 3.10.

Table 3.1: Summary of values used in Doppler warp simulation.

α	–0.2
β	0.4
T	$2.0000\times10^{-4}s$
$\tilde{T}_0$	$1.7602\times10^{-4}s$
$\tilde{T}_1$	$2.2402\times10^{-4}s$
t_0	$0.1000s$
t_1	$0.4000s$
$\tilde{t}_0$	$0.0840s$
$\tilde{t}_1$	$0.3840s$

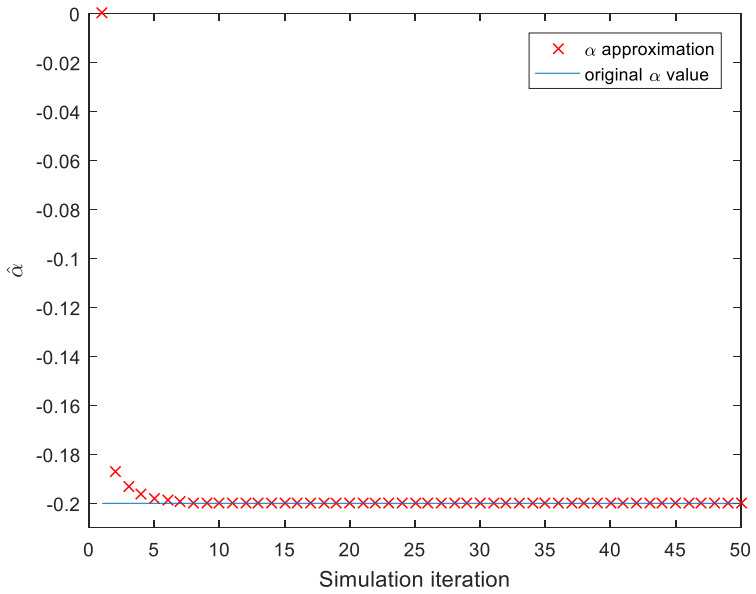

Figure 3.9: α found using matrix solution, as described in (3.22).

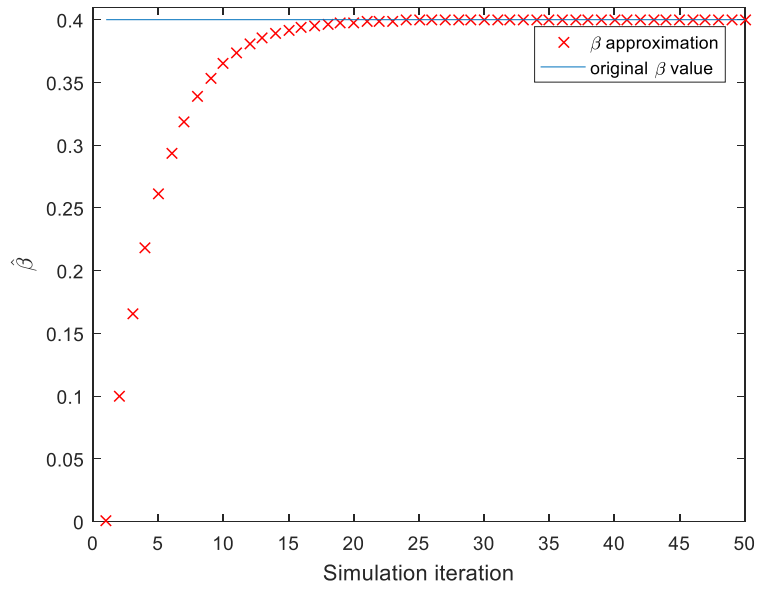

Figure 3.10: β found using matrix solution, as described in (3.22).

As Figures 3.9 and 3.10 show, the result of the approximation iteration process converges to the true value of α and β, within 30 iterations.

Having illustrated that, given an $\tilde{T}_0$, $\tilde{T}_1$, $\tilde{t}_0$, and $\tilde{t}_1$, the original α and β can be approximated well by solving (3.22), the remaining task is to demonstrate the unwarping procedure on an actual signal, using estimates. Although any signal can be used, for the purposes of illustration, a 5 kHz sinusoid is used to correspond with the example in Table 3.1. $\tilde{T}_0$, $\tilde{T}_1$ must be estimated from the time warped sinusoid and (3.4) must be used to resample the warped signal and recover/estimate the original signal. To illustrate the latter process, the time warped sinusoid generated in Figure 3.6 is used. The sinusoid used is a pure sinusoid with zeros before and after the sinusoid showing where the sinusoid occurs in time. In this case, no noise is added. In addition to verifying that the method for approximation/estimation of α and β converges to the correct solution, the frequency estimation method and Doppler warp correction method will be illustrated as well. This is done by estimating the frequency (and equivalently the sinusoidal period) over time intervals centered at time instants $\tilde{t}_0$ and $\tilde{t}_1$. $\tilde{t}_0$ and $\tilde{t}_1$ are taken as $0.0840s$ and $0.3840s$, consistent with the values in Table 3.1. The windows used for evaluating the frequency are shown in Figure 3.11, where the black rectangles indicate the time frames over which frequency is estimated in order to determine $\tilde{T}_0$ and $\tilde{T}_1$.

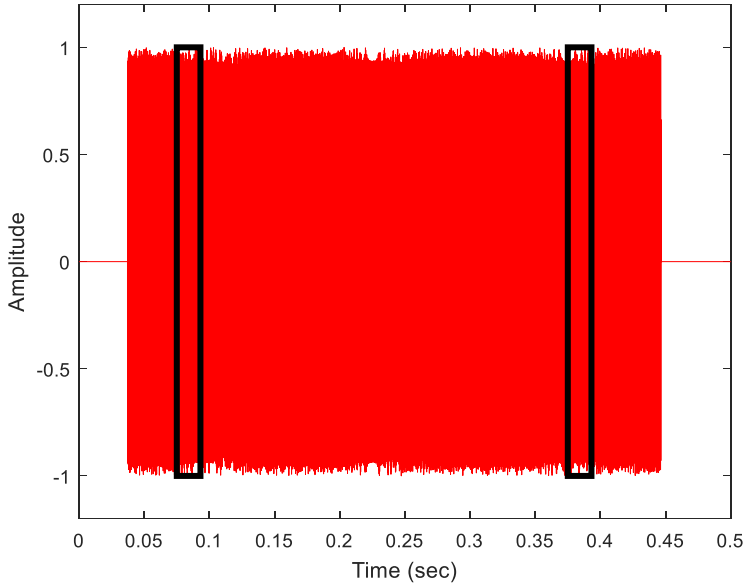

Figure 3.11: Doppler Warped Sinusoid with rectangles centered at $\tilde{t}_0$ and $\tilde{t}_1$ showing the time intervals used to estimate frequencies to correct for the Doppler.

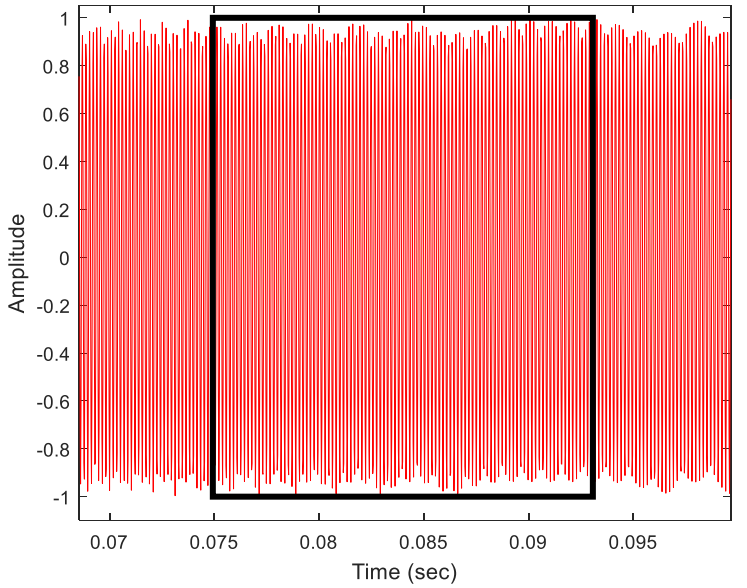

Figure 3.12: Doppler Warped Sinusoid with 800 sample time interval centered at $\tilde{t}_0$ that is used for the first Frequency Estimate.

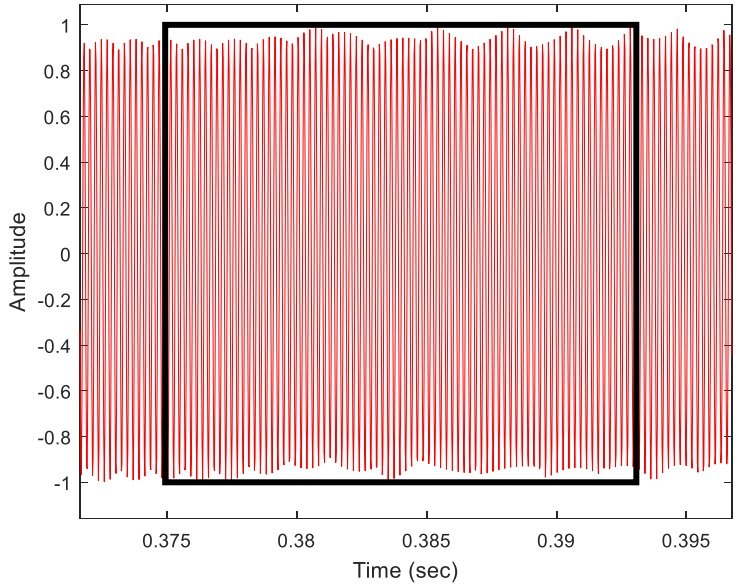

Figure 3.13: Doppler Warped Sinusoid with 800 sample time interval centered at $\tilde{t}_1$ that is used for the second Frequency Estimate.

In order to determine accurate frequency estimates, a Blackman window is first applied to the observed frame of samples to reduce out of band leakage. The frequencies are estimated by taking 800 sample data records centered around $\tilde{t}_0$ and $\tilde{t}_1$. 4096 point FFTs with a sampling rate of 44.1 kHz of these data samples are then taken. The frequency estimate was taken to be the frequency corresponding to the point at which the FFT magnitude spectrum was the largest. For example, Figure 3.14 shows the FFT magnitude spectrum of the data over the observation window centered at $\tilde{t}_0$ (shown in Figure 3.12). The point at which the FFT magnitude spectrum is the greatest is at 5.6813 kHz, which corresponds to a $\hat{T}_0$ of $2.220\times10^{-4}s$. Figure 3.13 shows the FFT magnitude for the windowed data centered at $\tilde{t}_1$ showing the frequency estimate of the Doppler warped sinusoid at 4.464 kHz, which corresponds to a $\hat{T}_1$ of $2.3520\times10^{-4}s$. The values found for the preamble and postamble frequencies match with the expected $\tilde{T}_0$ and $\tilde{T}_1$ shown in Table 3.1.

The preamble and postamble refer to the time intervals around $\tilde{t}_0$ and $\tilde{t}_1$ used to generate the first and second frequency estimates, respectively.

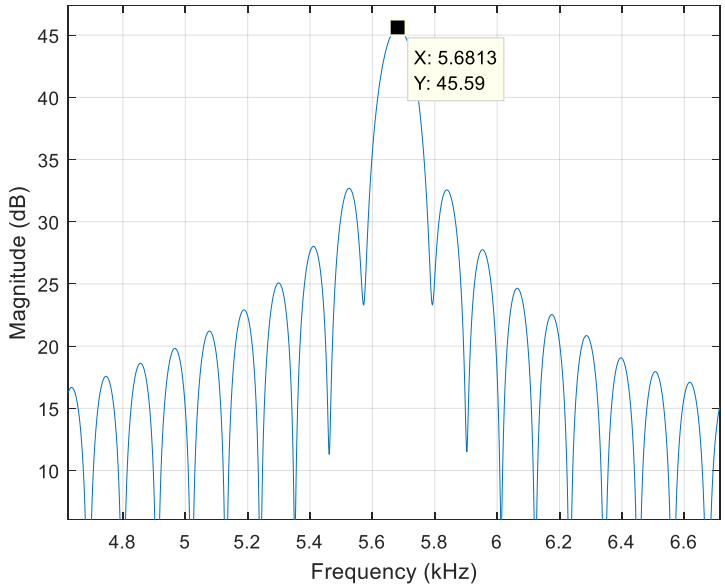

Figure 3.14: Magnitude spectrum of Doppler Warped Sinusoid at $\tilde{t}_0$.

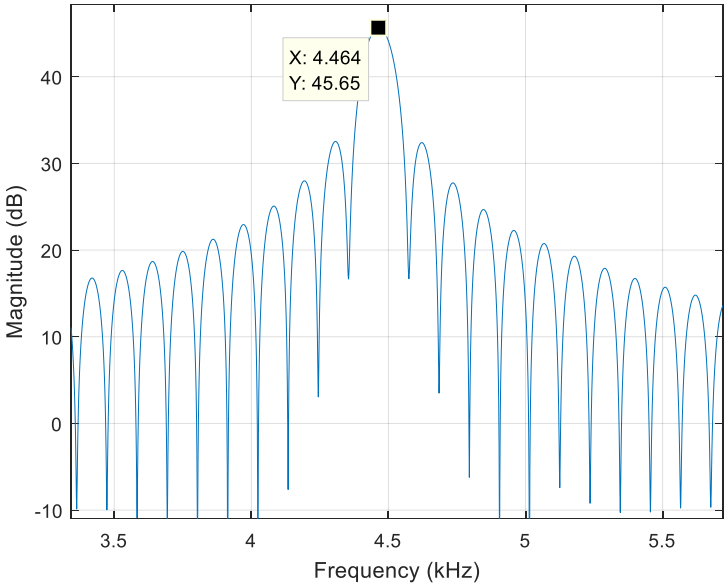

Figure 3.15: Magnitude spectrum of Doppler Warped Sinusoid at $\tilde{t}_1$.

As Figures 3.14 and 3.15 show, the estimated parameters T_0 and T_1 for the warp match with the original $\tilde{T}_0$ and $\tilde{T}_1$ used to generate the Doppler warped sinusoid. Now to correct for this Doppler warped signal, (3.22) is used to obtain $\hat{\alpha}$ and $\hat{\beta}$ and (3.4) is used to resample the Doppler warped signal in order to obtain the (Doppler un-warped) recovered sinusoid. The spectrogram of the recovered sinusoid is given in Figure 3.16. As Figure 3.16 shows, the Doppler warp corrected sinusoid is now a sinusoid at 5 kHz, which was the frequency of the original signal before the Doppler warp was applied.

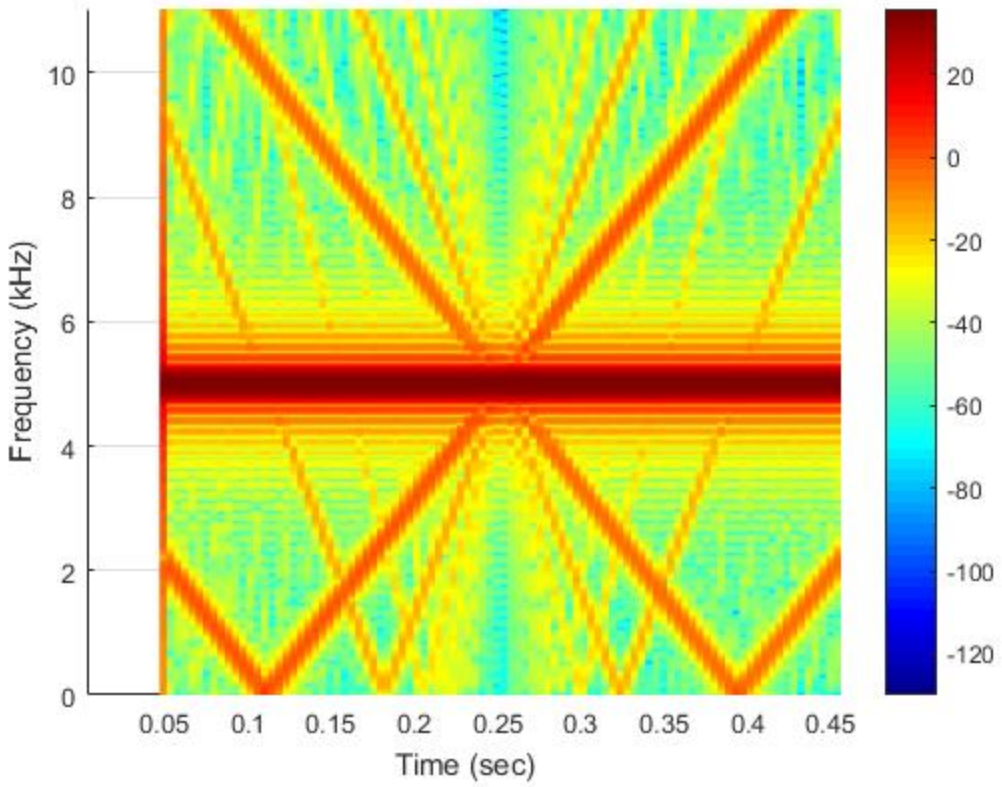

Figure 3.16: Spectrogram of Recovered Sinusoid.

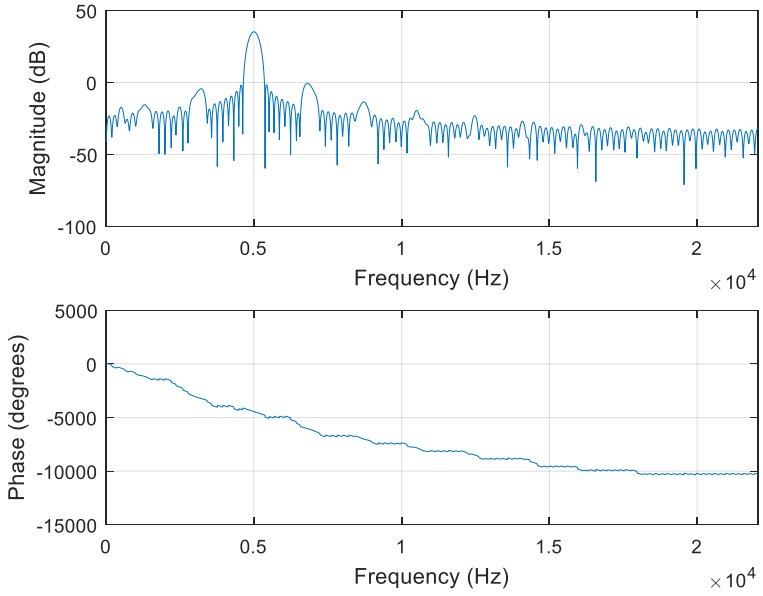

Figure 3.17: Magnitude and Phase of Recovered Sinusoid between 0.3 s and 0.301 s.

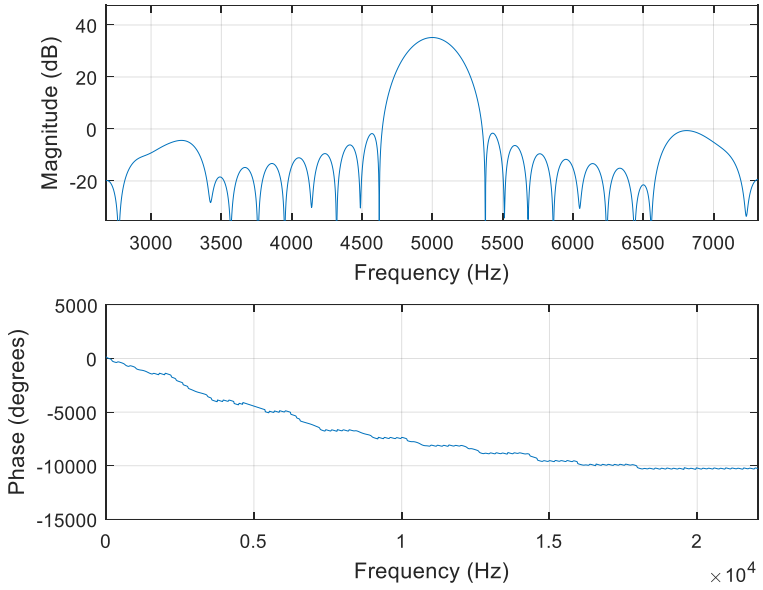

Figure 3.18: Zoomed in Magnitude and Phase of Recovered Sinusoid between 0.3 s and 0.301 s.

The recovered sinusoid shows that the Doppler unwarping procedure works for a sinusoid with no noise added. Notice from Figure 3.16, there are distortions in the spectrum of the recovered sinusoid. Figure 3.17 and Figure 3.18 show the magnitude and phase of the recovered sinusoid

between 0.30 s and 0.301 s. Note the distortions in the magnitude at approximately 3 and 7 kHz, which correspond to the distortions in Figure 3.16. These distortions arise from the linear interpolation in the resampling process. However, these distortions are small compared to the peak of the sinusoid, being 35 dB below the main lobe. As mentioned earlier, different types of interpolation can reduce the effect of these distortions. In the next chapter, characteristics of the multipath channel are introduced and measured with adjustments in the Doppler unwarping procedure. The characteristics of the multipath channel are used in the design of the OFDM burst, which is used in place of the signal presented in Figure 3.6.

4 Acoustic Experiment

4.1 Experiment Introduction

This chapter describes the implementation of an OFDM transceiver over an acoustic channel. The experiment was designed to simultaneously correct for the Doppler warp caused by the non-constant (closing/range) rate between the transmitter and receiver and the multipath present in the room. While the problem is ultimately to address underwater communications, this experiment was conducted over the air, as a proxy for the underwater environment. A diagram of this setup is shown in Figure 4.1. This chapter is organized by first describing the structure of the experiment, using a signal composed of several sinusoids to determine characteristics of the acoustic channel, and then designing/creating the OFDM burst structure that takes these characteristics into account.

Figure 4.1: The Over The Air experiment.

As discussed in Chapter 3, the speed of sound is about 5 times slower in air than in water. Because the speed of sound in air is slower than in water, there is a much larger propagation delay and the Doppler warp that affects the wideband received signal is much more severe. This makes the received signal harder to decode compared to the same signal in an underwater environment. OFDM modulation is used to deal with the multipath, with additional sinusoids to facilitate the estimation of Doppler frequencies. These frequencies, used with the Doppler warp model discussed in Chapter 3, facilitate correction of the Doppler. Once the signal has been resampled

and corrected according to the Doppler warp model, the OFDM demodulation will account for the multipath in the system.

4.2 Description of Acoustic Experiment

This section describes the four acoustic experiments conducted to evaluate the performance of the OFDM transceiver. Each experiment consisted of the acoustic transmission of four identical OFDM bursts from a speaker to a microphone. In two of the experiments, the microphone was stationary while in the other two experiments the microphone was moving at a varying speed. The placement (if the microphone was stationary) and path (if the microphone was moving) of the microphone during each experiment is depicted in Figure 4.2.

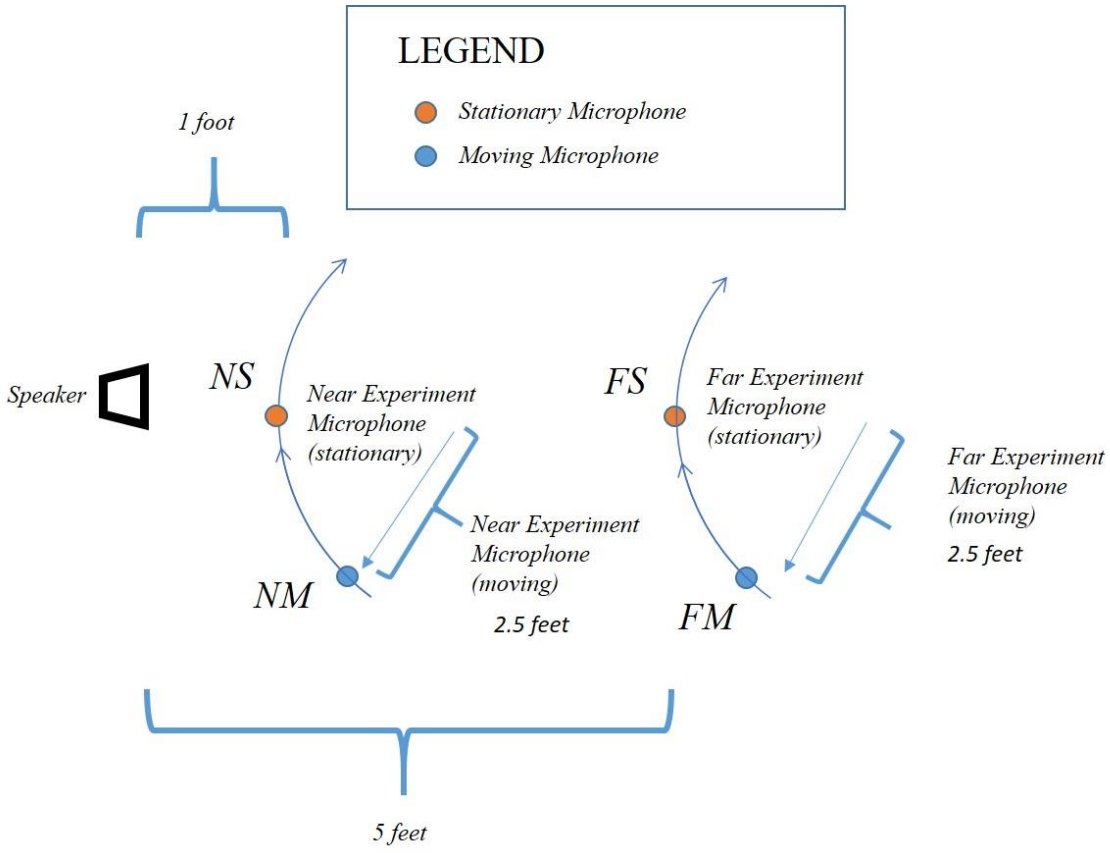

Figure 4.2: Illustration of Four Acoustic Experiments.

The terms used to refer to the four experiments are the near stationary (NS) experiment, the near moving (NM) experiment, the far stationary (FS) experiment, and the far moving (FM) experiment. The two near experiments, the NS and NM experiments, are meant to show the effects of the Doppler warp on the OFDM burst at a point close to the transmitter (1 foot between the transmitter and the receiver), i.e. with less multipath affecting the received signal. The FS and FM experiments were conducted at a distance of 5 feet between transmitter and microphone. The FS and FM experiments are aimed at showing the effect of severe multipath on the received signal, and the performance of the Doppler model in the presence of severe multipath and signal deterioration. In the NM and FM experiments, the movement of the microphone was caused by the radial sweep of a human arm. The length of the human arm including the microphone, consequently the radius of the arc, was approximately 2.5 feet.

The setup of the four experiments is important in testing the limitations of the Doppler warp model. The positions of the near and far stationary (NS and FS) experiments are meant to give a best case scenario for comparison with the near and far moving (NM and FM) experiments. The OFDM burst was generated in MATLAB with data modulated onto carriers over the range 3-5 kHz. The resultant signal was transmitted using a speaker connected to the soundcard of the computer. The design of the OFDM burst is discussed in Section 4.4. A separate instance of MATLAB on the same computer acted as the OFDM receiver that demodulated the received signal. The receiver had to account for several issues discussed in Chapter 2, such as timing synchronization, carrier frequency offset estimation, Doppler Warp correction, and channel equalization. A rough estimation of the multipath in the room is needed to properly design the OFDM signal used for transmission. In the next section, the estimation of the multipath is done using a signal composed of several sinusoids in the frequency band of interest.

4.3 Delay Spread Estimation

The previous section described the four experiments that are used in the development of the OFDM transceiver. To determine the design considerations for the OFDM transmitter, several channel characteristics need to be determined. One such channel characteristic is the delay spread of the channel. The OFDM transceiver needs to compensate for the delay spread of the channel by using a cyclic prefix, which should be at least as long as the delay spread. To estimate this delay spread a signal composed of four sinusoids, at 2, 3, 5 and 6 kHz, was transmitted. The transmitted signal is shown in Figure 4.3.

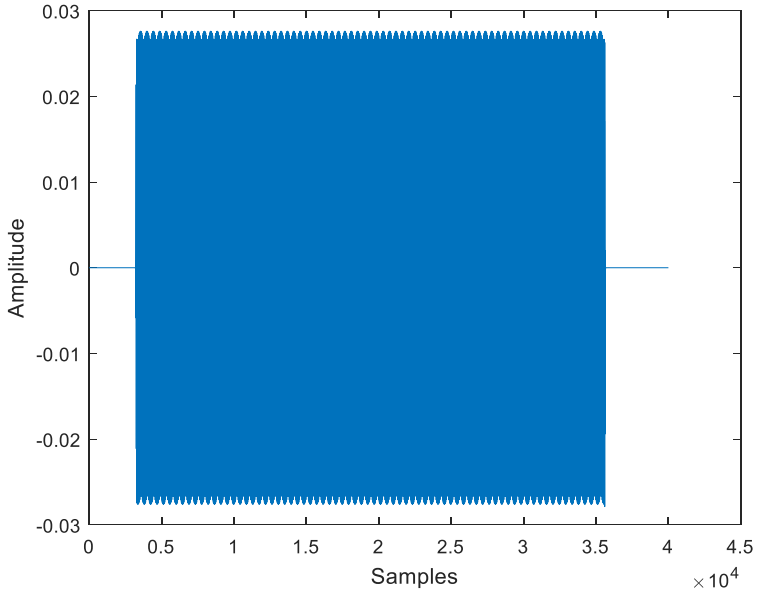

Figure 4.3: Transmitted Signal used for Delay Spread Estimation.

The transmitted signal is 32384 samples in length, which at a sampling frequency of 44.1 kHz corresponds to 734 ms. For consistency, the placement of the microphone used in the stationary experiments, or the NS and FS experiments described in Section 4.2, is used to estimate the acoustic channel. This means that the transmitted signal in Figure 4.3 is transmitted to a

microphone placed at a distance of 1 foot away in one test, and again transmitted to a microphone placed at a distance of 5 feet away in another test.

The signal received by the stationary receiver is used to estimate the delay spread of the channel. Figures 4.4 and 4.5 show the received signal and the spectrogram of the received signal with the microphone placed at the location for the NS Experiment.

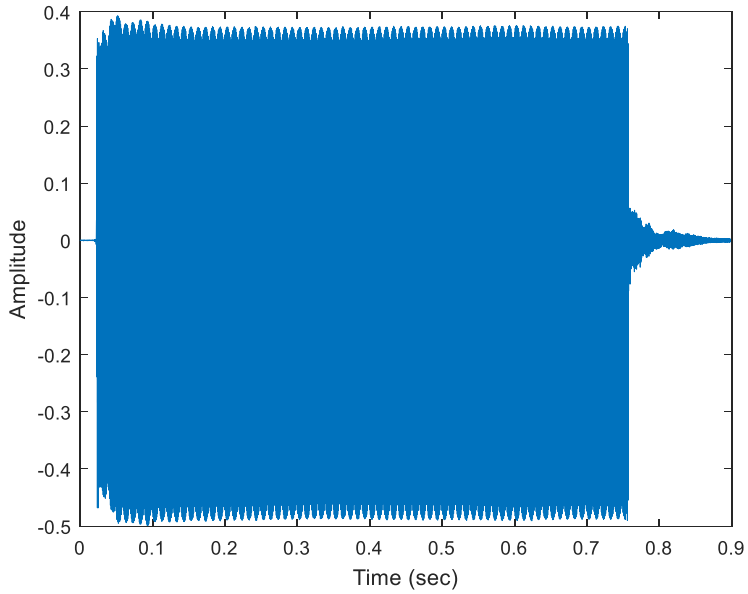

Figure 4.4: Received signal with multipath at the NS experiment location.

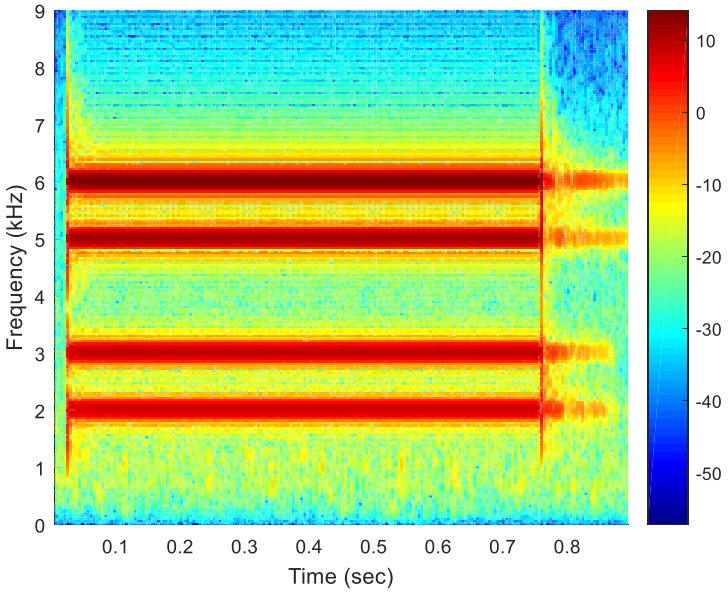

Figure 4.5: Spectrogram of received signal with multipath at the NS experiment location.

Observe from Figures 4.4 and 4.5 that the major delay spread for the NS experiment exists from approximately 0.76 s to 0.85 s. In order to combat this multipath, a guard interval of at least 90 ms needs to be used. Such a guard interval requires 4000 samples, or the last half of the OFDM symbol when the sampling rate is 44.1 kHz.

Figures 4.6 and 4.7 show the received signal and the spectrogram of the received signal with the microphone placed at the location for the FS experiment.

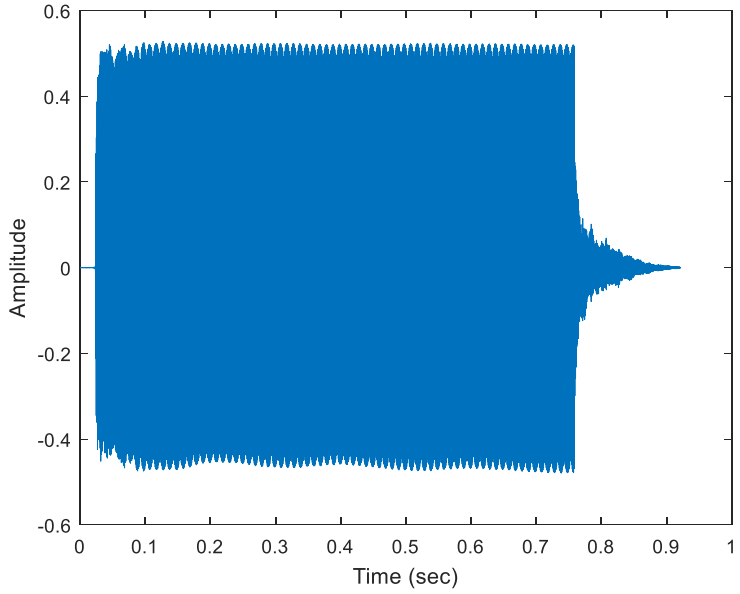

Figure 4.6. Received signal with multipath at the FS experiment location.

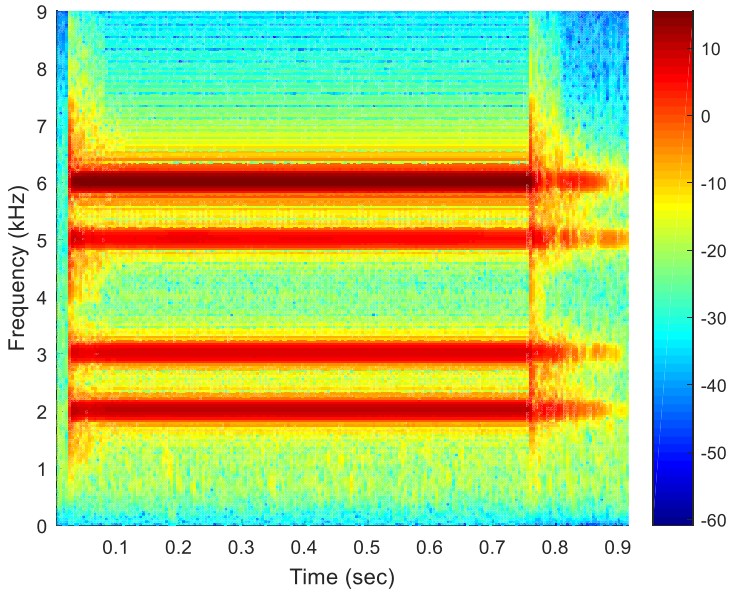

Figure 4.7: Spectrogram of received signal with multipath at the FS experiment location.

Observe from Figure 4.6 that the major delay spread for the FS experiment exists from approximately 0.76 s to 0.9 s. In order to combat this multipath, a guard interval of at least 150 ms needs to be used. Such a guard interval requires 7000 samples, or the last two-thirds of the OFDM

symbol when the sampling rate is 44.1 kHz. A 7000 sample interval corresponds to 158 ms at 44.1 kHz, which is roughly equivalent to the delay spread of the channel. To account for the delay spread, a cyclic prefix of 8192 samples is used, which happens to be the length of the OFDM symbol itself. The reason for using this long cyclic prefix is so that the performance of the overall Doppler correction scheme for the near experiments can be compared to the performance for the far experiments. However, if the transmitter is close to the receiver, this long cyclic prefix is not needed. Since there is only one symbol, there is no multipath that can spread from successive symbols, and the cyclic prefix is used for synchronization only.

Having seen the effects of multipath on a signal made up of several sinusoids, the length of the cyclic prefix is determined and used across all acoustic experiments. Now, a model for the transmitted OFDM symbols can be created.

In Chapter 2, the benefits of both ZP-OFDM and CP-OFDM were discussed. Ultimately, CP-OFDM was used to see if the cyclic prefix could be exploited for synchronization. The 3-5 kHz band was used because the low range speaker used at the transmitter did not transmit signals with frequency content over 7 kHz.

4.4 OFDM Transmitter Design

The structure of the entire transmitted signal is shown in Figure 4.8.

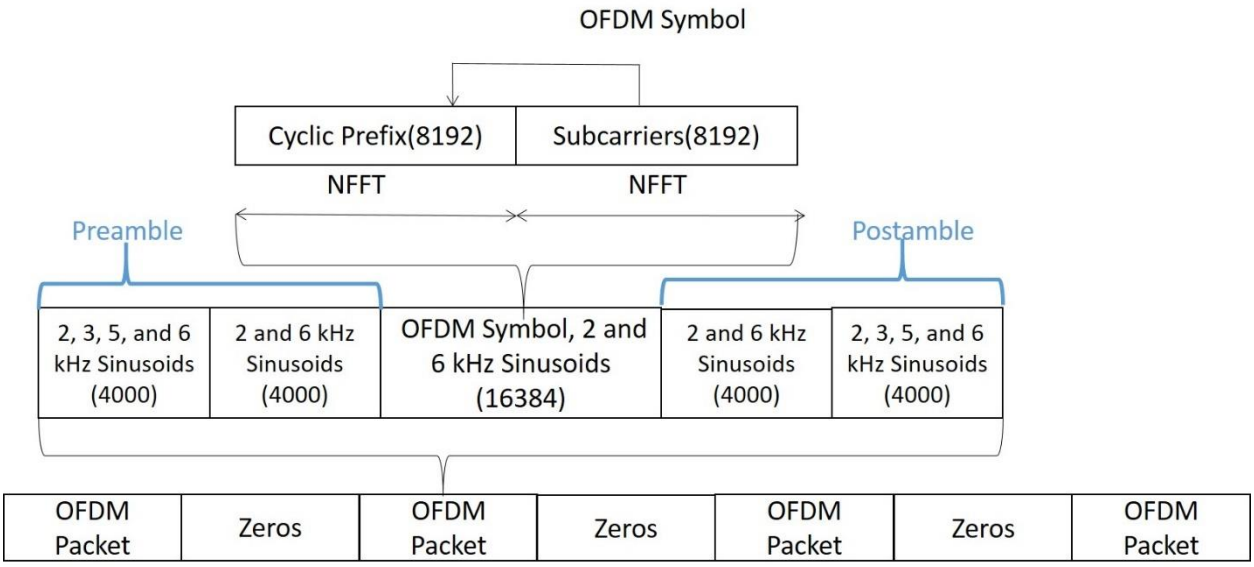

Figure 4.8: OFDM packet structure in time.

The transmitted signal consists of four packets. Each packet contains a Cyclic Prefix (CP), an OFDM symbol, a preamble, and a postamble. Ultimately one symbol was used in a packet. The reason for this is that as a packet grows in size, it takes more time to transmit the packet. If the packet takes too long to transmit, the nonlinear warp model shown in Chapter 3 may no longer apply. In this experiment, 4 successive bursts are sent, with each OFDM symbol containing the same data. The bandwidth of the OFDM signal was in the 3-5 kHz range to use the low-end speaker on the transmitter. The preamble and postamble consisted of 4 sinusoids, at 2, 3, 5, and 6 kHz. The sinusoids at 2 and 6 kHz were present during the CP-OFDM signal as well as immediately before and after the CP-OFDM signal. The placement of the sinusoids with respect to the OFDM symbol is shown in Figure 4.8.

The sinusoids at 2 and 6 kHz are used to facilitate the derivation of alpha and beta estimates during the OFDM burst, which are then used to correct the Doppler warp. The preamble/postamble structure is discussed in greater detail later in this section.

Before creating the OFDM burst, it was necessary to make a choice for the number of data bits and pilot bits. The total number of bits is dictated by the number of subcarriers allowed in the OFDM burst. The OFDM burst was created using an 8192 point IFFT at a 44.1 kHz sampling frequency to create a symbol between 3 and 5 kHz. A 8192 point IFFT at a 44.1 kHz sampling rate yields 368 sub-carriers to be used in the band between 3 and 5 kHz. 184 of those subcarriers were chosen to hold data bits and the remaining 184 subcarriers were used as pilots. Although fewer pilots could be used, a one to one ratio was chosen to help with equalization. More pilot bits help give a better channel estimate. Although this is not the most efficient scheme, it is able to provide a best case scenario that can be improved on for various environments. The pilots were all chosen to be 1 bits, as from observation over multiple experiments the specific value of the pilot symbols did not make a difference in the performance.

The Matlab command *randi* was used to generate the data bits modulated onto the OFDM symbol. Though other designs are possible, the choice was made to insert a pilot bit after every data bit, resulting in uniform spacing between pilots. The data and pilot bits were mapped to BPSK symbols, which yielded a 1 for a bit 1 and -1 for a bit 0. This symbol stream was used to create the conjugate symmetric input to the IFFT block. To create the conjugate symmetric input, the symbol stream was reversed in time and appended to the beginning of the symbol stream. The IFFT was applied to the resultant conjugate symmetric input, creating the real samples that made up the OFDM symbol. The real output from the IFFT operation was concatenated with the Cyclic Prefix and this OFDM burst was used to create packets.

Since the modulation scheme was BPSK, the data was binary, composed of 0s and 1s. Transmitting this real output of the IFFT at a sampling rate of 44.1 kHz yields an OFDM symbol

with subcarriers between 3 and 5 kHz. The pilot subcarriers were used at the receiver to estimate the frequency response of the channel.

Another major design consideration is the type of insertion used for the pilot subcarriers. As discussed in Chapter 2, there are two major types of pilot insertion, comb type pilot insertion, and block type pilot insertion. In comb type pilot insertion, pilots are inserted in the frequency domain, while block pilot insertion injects pilots in the time domain. Pilots are known bits that are used for equalizing and correcting the channel. While comb type pilot insertion works well in channels with little frequency variation, block type channels work well in channels that do not vary rapidly in time. The underwater acoustic channel is referred to in literature as being time varying, which makes comb type pilot insertion a better candidate. Comb type pilot insertion was therefore used in this experiment, with the pilot frequencies modulated directly onto specific subcarriers. Figure 4.9 illustrates comb type carrier insertion. Note how the pilot symbols are inserted at particular frequencies, and that they remain there for consecutive symbols.

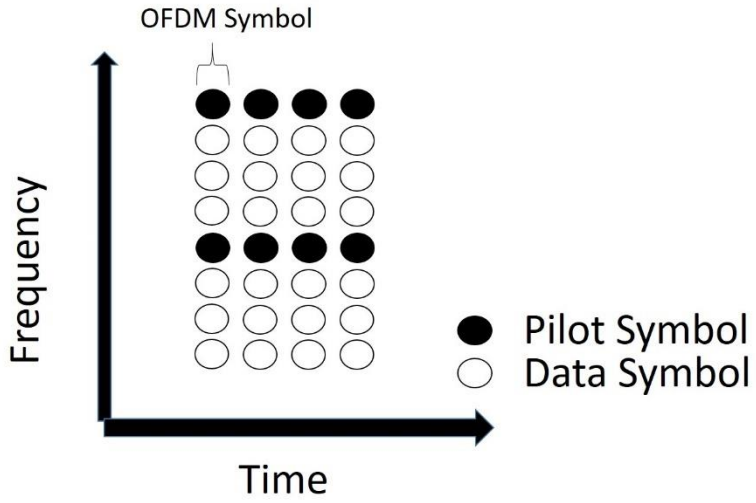

Figure 4.9: Time Frequency diagram showing comb type pilot insertion.

The overall transmitter structure is shown in Figure 4.10.

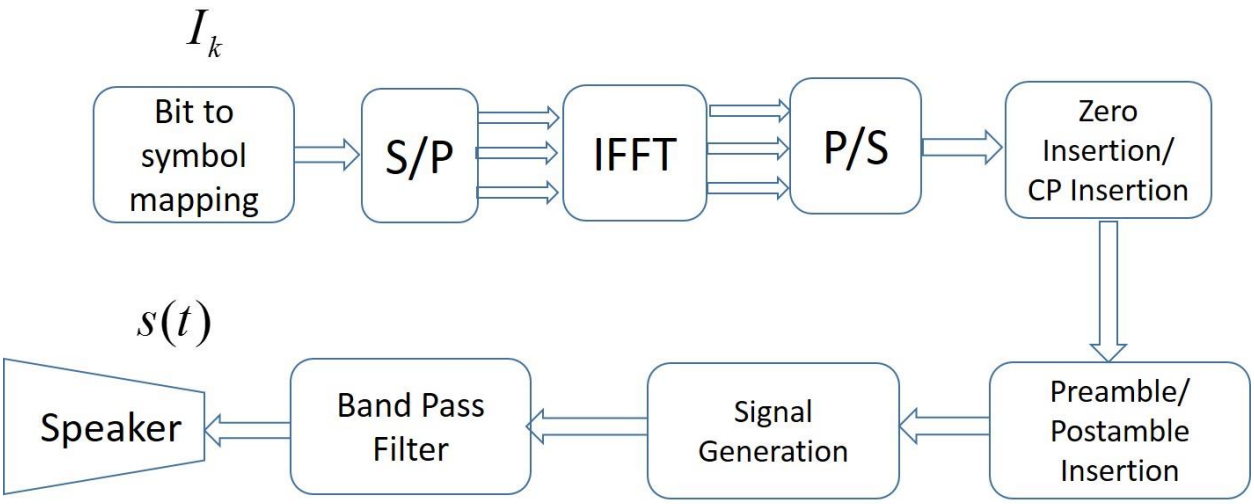

Figure 4.10: Transmitter Block Diagram.

Figure 4.11 shows the resultant OFDM burst after the cyclic prefix has been inserted. The OFDM burst is defined as the combination of the cyclic prefix with the OFDM symbol. Note that the length of the burst is 16384 samples while the symbol length is 8192 samples.

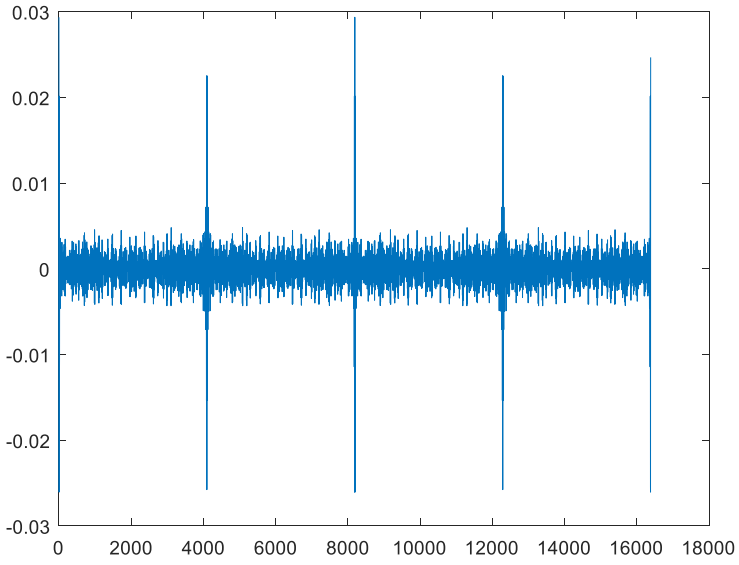

Figure 4.11: One OFDM burst in time.

Now the preamble/postamble is discussed in further detail. The preamble/postamble was designed to have a repetitive structure. The preamble was a signal that consisted of four sinusoids, one each at 2 kHz, 3 kHz, 5 kHz, and 6 kHz followed by sinusoids at 2 and 6 kHz. The postamble was a signal that consisted of four sinusoids, one at 2 kHz, 3 kHz, 5 kHz, and 6 kHz preceded by sinusoids at 2 and 6 kHz. All sinusoids are continuous in amplitude and phase for entire packet including the OFDM burst. The reason for selecting this type of a waveform and preamble/postamble structure was for packet detection as well as Doppler warp estimation. The 2 kHz and 6 kHz sinusoids were also present during the OFDM burst and immediately after and before the OFDM burst. The reason for 2 kHz and 6 kHz sinusoid insertion was to be able to update and/or track the alpha and beta estimates during the OFDM burst and also to compare the alpha and beta estimates taken during the OFDM burst to the alpha and beta estimates found from the preamble/postamble sinusoids. This comparison will be discussed in further detail in Chapter 5. The resultant packet with the preamble/postamble insertion is shown in Figure 4.12.

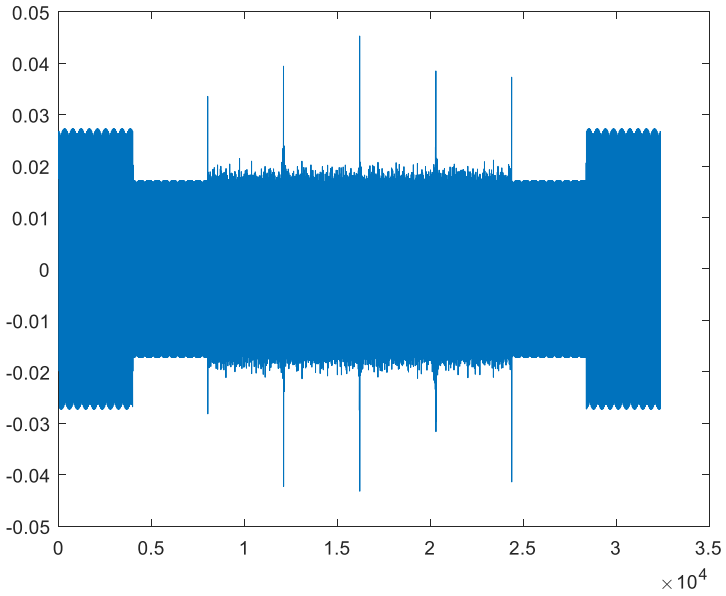

Figure 4.12: One packet containing preamble, OFDM burst, and postamble.

The overall transmitted burst contained 4 consecutive packets, each identical to the packet shown in Figure 4.12. Successive packets were separated by 53000 zeros, which corresponded to about 1.2 seconds between packets. This was to prevent multipath from leaking from one packet to the next, and also to give the experimenter time to move the microphone back to the initial starting position in the case of the experiments involving a moving microphone. The overall transmitted burst with all 4 packets is shown in Figure 4.13.

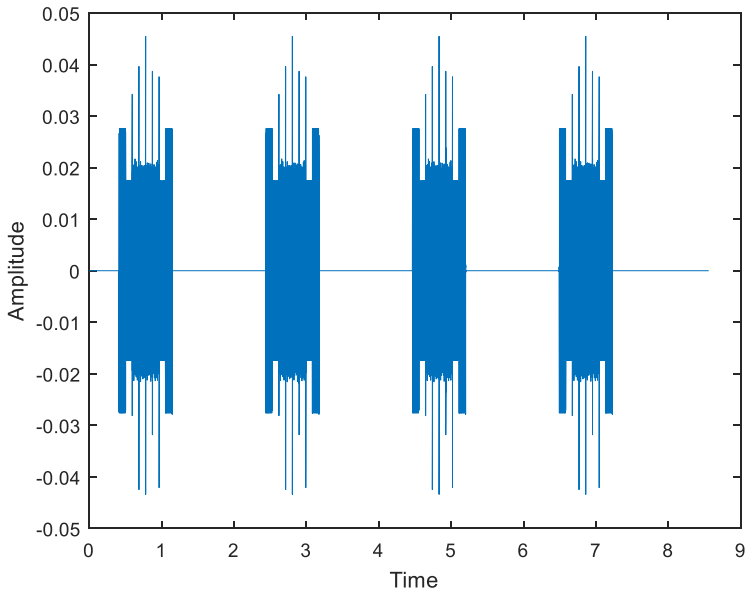

Figure 4.13: Total transmitted burst with 4 OFDM packets.

Now that the structure of the transmitted burst has been defined, the actual transmission of OFDM packets is described. The transmitted bursts shown in Figure 4.13 are bandpass filtered before being sent to the speaker. The bandpass filter was a FIR bandpass filter designed using the Parks-McClellan equiripple design technique (*firpm* command in MATLAB). The frequency response of the band pass filter is shown in Figure 4.14.

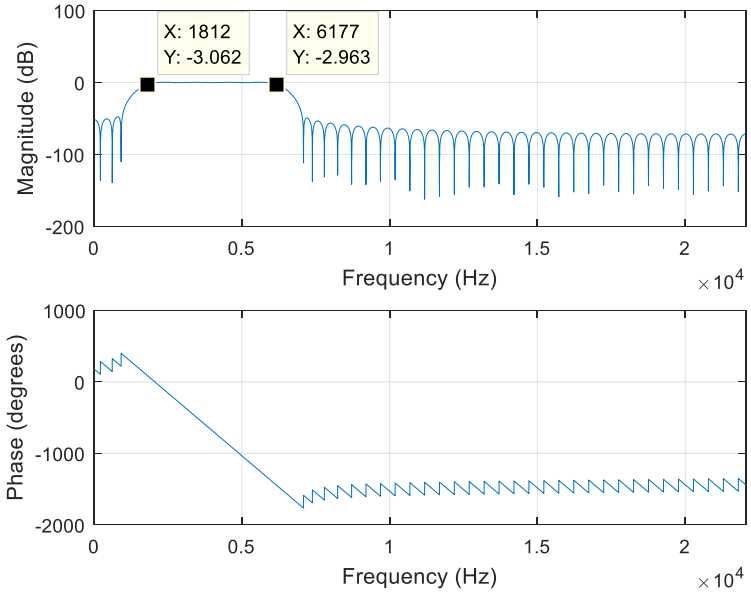

Figure 4.14: Frequency Response of the band pass filter used in transmission.

This is the same filter that is used in the receiver to filter the out of band noise present in the channel. The filter was designed to have a lower 3dB cutoff frequency at 1800 Hz, and an upper 3dB cutoff frequency at approximately 6200 Hz. The transmitted signal was in the band from 2 kHz to 6 kHz, so this filter captures the frequencies that are transmitted. The bandpass filtered signal was then played through the speaker using the soundcard of the computer. Figure 4.15 shows the spectrogram of the bandpass filtered OFDM burst.

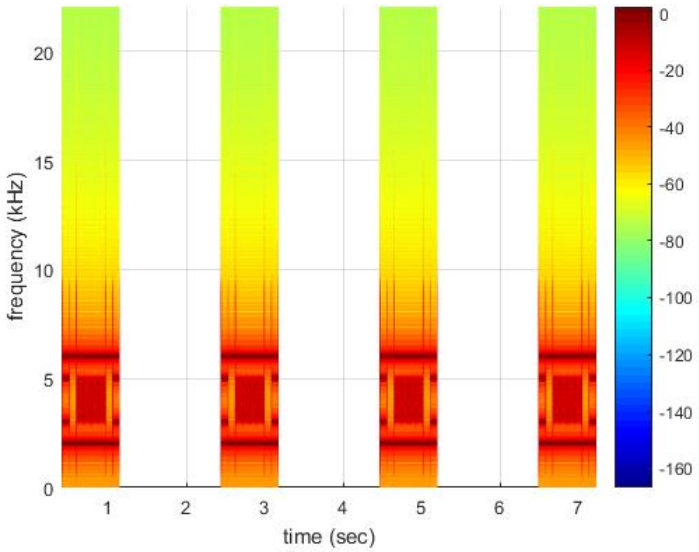

Figure 4.15. Spectrogram of transmitted signal with 4 packets.

The preamble, OFDM, and postamble segments are readily recognizable in the spectral domain.

Table 4.1 summarizes the parameters that are used in the OFDM transmitter.

Table 4.1: OFDM Transmitter Parameters.

Parameter	Values of Structure 1
FFT/IFFT Size	8192
Active Carriers	186
Pilot Carriers	186
Sampling rate	44.1 kHz
CP length	8192 samples (=185.8 ms)
Number of OFDM symbols per packet	1
Modulation	BPSK
Pre-amble/Post-amble	Sinusoids at 2, 3, 5, and 6 kHz

In this section the parameters and structure of the transmitted OFDM signal were defined. In the next section the basic structure of the OFDM receiver is described.

4.5 OFDM Receiver

The structure of the ideal OFDM receiver is shown in Figure 4.16.

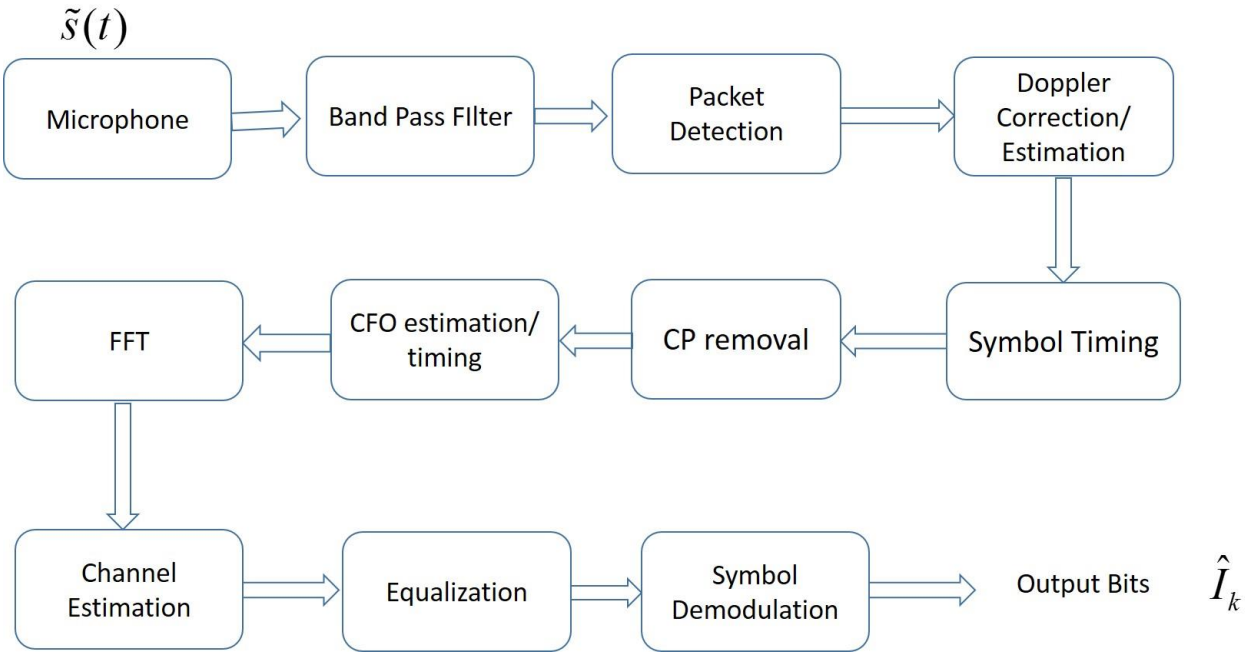

Figure 4.16: OFDM Receiver Structure.

In this section, each of the receiver blocks will be examined in more detail with the exception of the Doppler Estimation and Doppler Correction/Resampling. The Doppler warp model was discussed in Chapter 3, while the Doppler Estimation of a signal subjected to multipath and Doppler is discussed in Chapter 5. This chapter focuses on the channel estimation, equalization, and symbol demodulation for an ideal OFDM symbol (with no noise) and the demodulation of the signal received by a stationary receiver kept at the locations used for the NS and FS experiments.

Since this section is only considering transmitted bursts with multipath, the first packets of 3 different OFDM bursts are analyzed and demodulated. The signal shown in Figure 4.17 consists of the 4 transmitted OFDM packets, before the effects of noise and/or multipath. The signal is the

ideal burst, with no noise, no channel effect and bandpass filtered with the filter used at the receiver.

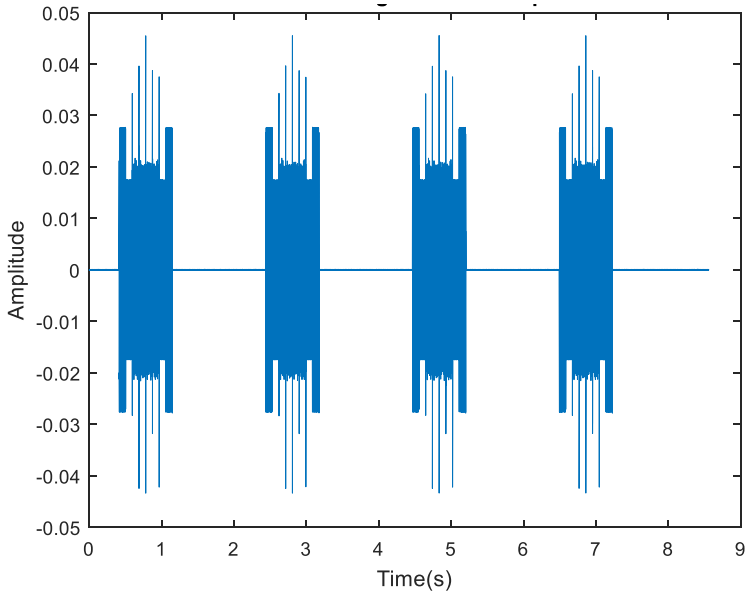

Figure 4.17: Ideal OFDM burst with no noise added.

The signal shown in Figure 4.18 is the signal captured by the stationary microphone kept at the location about one foot away from the transmitter, referred to as the NS experiment.

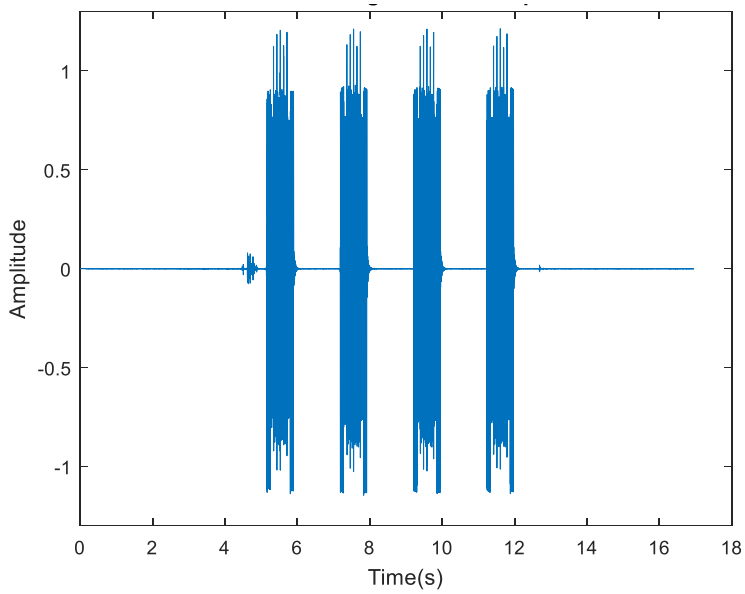

Figure 4.18: The received OFDM burst of NS Experiment (~ 1 foot).

The signal shown in Figure 4.19 is the signal captured by the stationary microphone kept at the location about five feet away from the transmitter, referred to as the FS experiment. Each signal was captured using the sound card of the computer, at a sampling rate of 44.1 kHz.

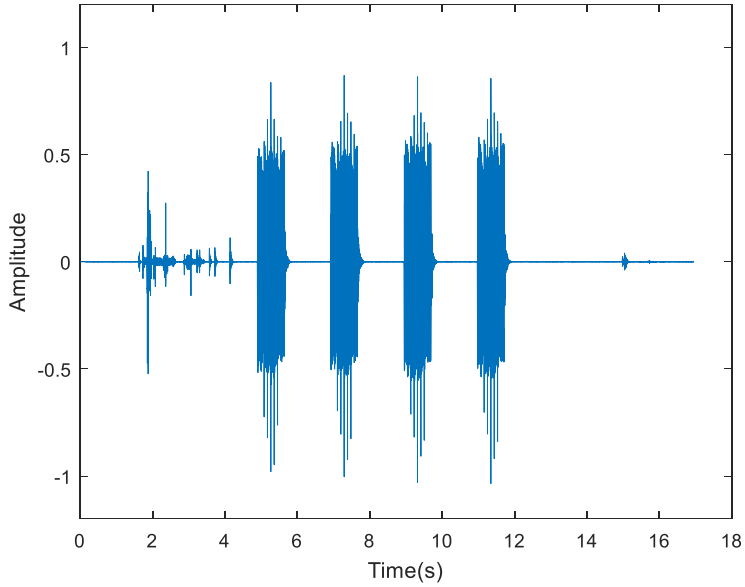

Figure 4.19: The received OFDM burst of FS Experiment (~5 feet).

In the progression from Fig. 4.18 to Fig. 4.19, an increase in reverberation (seen at the trailing edge of each packet) and in distortion is observable as the direct signal component becomes weaker relative to the multipath and noise components.

4.5.1 Bandpass Filtering

The first step in the OFDM receiver is applying a bandpass filter to the received signal. In order to extract the original signal, the bandpass filter is designed with a lower frequency cutoff of 1.8 kHz and a higher frequency 3 dB cutoff of 6.2 kHz. Since the same filter was used in transmission, the Magnitude and Phase spectrum of the designed FIR filter are those shown in Figure 4.14. The filter in Figure 4.14 was applied to the received signal shown in Figures 4.17, 4.18, and 4.19. Packets

were identified from the resultant signal using a robust energy detection method detailed in the next section.

4.5.2 Packet Detection

After filtering the received signal, to remove any out of band components, the next step is identifying packets. The packets are identified using the energy of the sinusoids present in the preamble and postamble of the packet. The locations of the preamble and postamble were found by calculating the Fraction of Sinusoidal Energy (*FOSE*) across the received signal. The *FOSE* was found by dividing the received signal into overlapping frames and calculating – for each frame – the ratio of the energy in the (pre- or post-amble) sinusoids to the energy across all spectral content. The Fraction of Sinusoidal Energy, for frame *k*, was defined as

$$FOSE(k) = \frac{\sum_{f_i=-f_t}^{f_t} \left(\left|H_k(f_1 - f_i)\right|^2 + \left|H_k(f_2 - f_i)\right|^2 + \left|H_k(f_3 - f_i)\right|^2 + \left|H_k(f_4 - f_i)\right|^2 \right)}{\sum_{f_i=0}^{f_n} \left|H_k(f_i)\right|^2} \quad (4.1)$$

In (4.1), f_1, f_2, f_3, and f_4 denote the frequencies of interest in the preamble and postamble, or 2, 3, 5 and 6 kHz, respectively, f_t denotes the frequency range around the frequency of interest, in this case 0.1 kHz, and f_n denotes the maximum frequency in the signal. $|H_k|$ is the spectrum magnitude for the particular frame *k* of samples. Since the signal was sampled at 44.1 kHz, f_n was 22.1 kHz, half of the sampling rate. The *FOSE* was calculated for the received signal on a frame-by-frame basis, with the 400 sample frames overlapping by 50%. Figure 4.20, 4.21, and 4.22 show *FOSE* for the three received signals shown in Figure 4.17, 4.18, and 4.19.

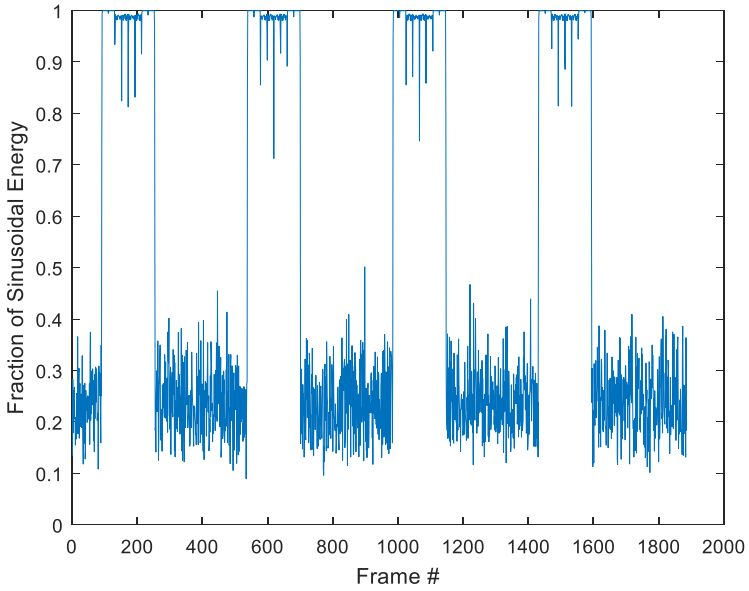

Figure 4.20: *FOSE* for the Ideal Received Signal.

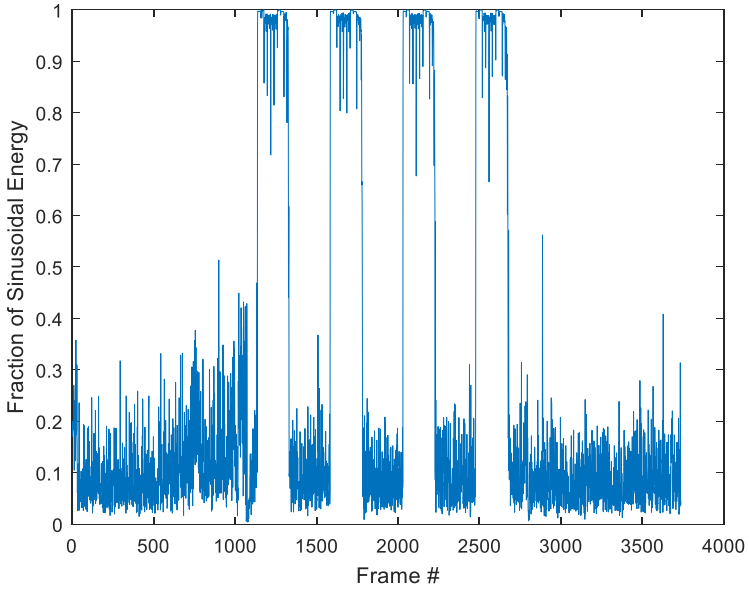

Figure 4.21: *FOSE* for the received OFDM packets in NS Experiment.

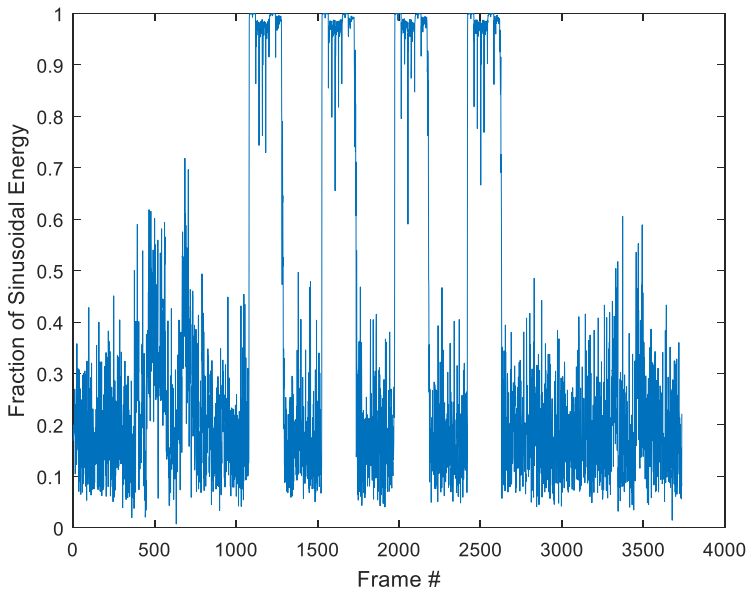

Figure 4.22: *FOSE* for the received OFDM packets in FS Experiment.

Observe that *FOSE* appears to provide visual clues that can be used to delineate the individual packets, even when there is severe multipath. To examine this issue a bit closer, the first packet itself and the *FOSE* for the first packet in the received OFDM burst in the FS experiment are shown in Figure 4.23 after zooming in.

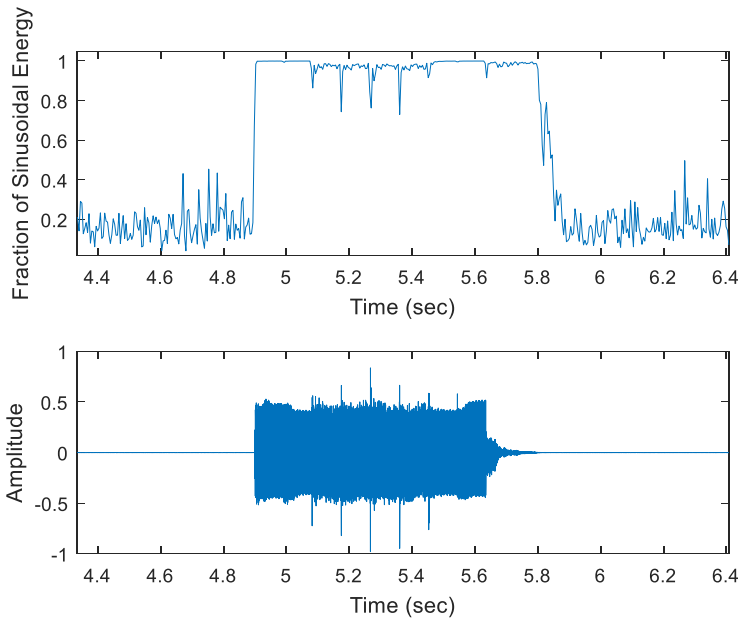

Figure 4.23: *FOSE* for packet #1 of FS Experiment (top) and packet #1 of FS Experiment (bottom).

As observed from Figure 4.23, the *FOSE* measurement is close to 1 for the majority of the OFDM packet. The packet is considered identified when the average *FOSE* of any 6 consecutive frames is greater than 0.99 and the average *FOSE* of 6 consecutive frames 141 frames ahead in time is also greater than 0.99. The 141 frame difference is used because this is the length of the OFDM symbol measured in (overlapping) frames. The results of the corresponding detection of the first packet for the 3 signals above are shown in Figure 4.24, Figure 4.25, and Figure 4.26.

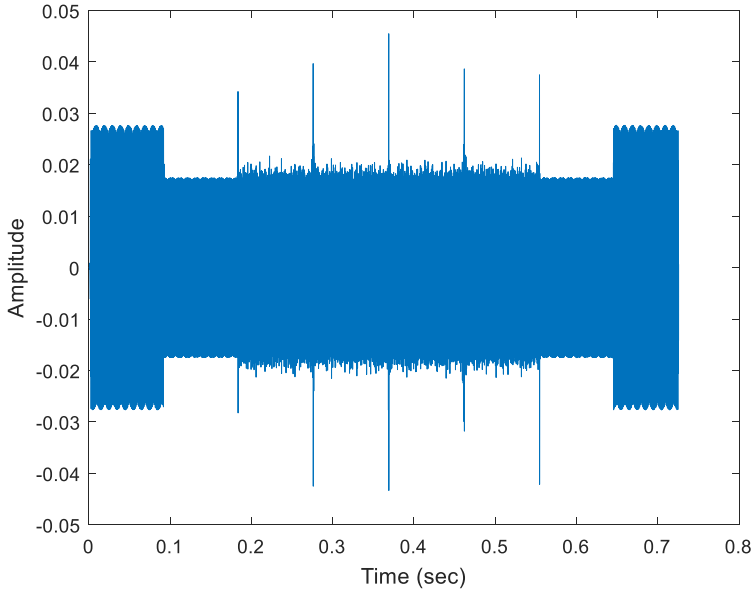

Figure 4.24: *FOSE* packet detection for packet #1 of the Ideal Received Signal.

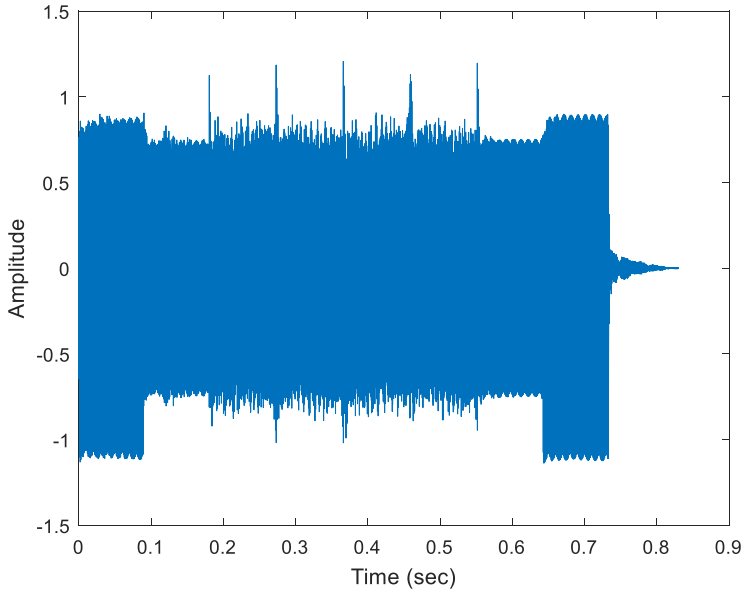

Figure 4.25: *FOSE* packet detection for Packet NS.1.

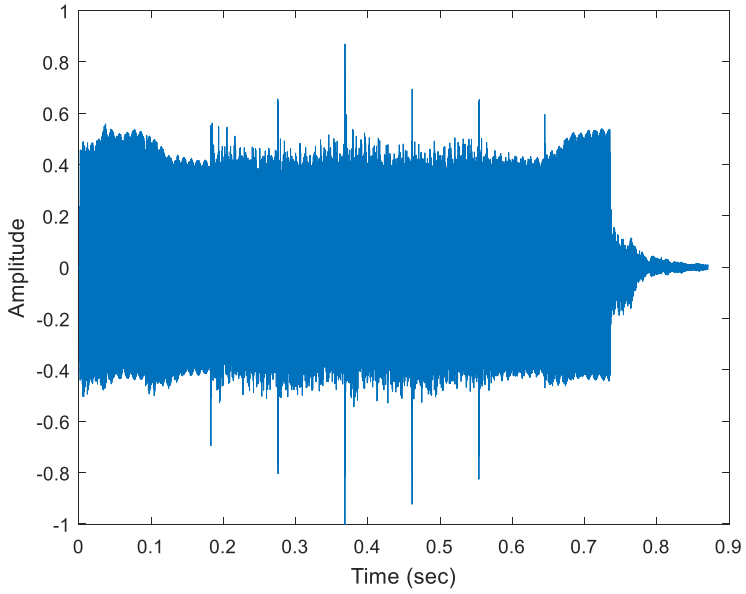

Figure 4.26: *FOSE* packet detection for Packet FS.1.

Observe in Figure 4.25 and Figure 4.26 that the *FOSE* based algorithm for packet detection sees the multipath at the trailing edge of the packet. This trailing edge multipath can cause problems for the frequency estimation process used to correct for the Doppler warp, as will be discussed in Chapter 5. Now that the packet has been extracted, the resultant symbol is demodulated.

4.5.3 Channel Estimation and Equalization

After receiving the burst and extracting the OFDM packets, symbol timing is determined. The operations performed are shown for the first packets of the received signals. To determine the correct symbol timing (which can vary based on the sample used for the timing estimate), the BER (bit error rate) is evaluated over the entire packet, using different synchronization points. This process will give an idea of where the OFDM symbol exists and how much the BER can change over the course of a packet as a result of the synchronization point.

Before showing the demodulation process for the OFDM bursts with multipath, the OFDM demodulation is illustrated for the ideal received signal. The first step in the demodulation process is to choose a synchronization point. The OFDM burst without any noise or sinusoids is shown in Figure 4.27 with a rectangle over the part of the symbol that will be demodulated. Though in practice the cyclic prefix is discarded prior to demodulation, for illustration purposes the first demodulation starts with the first half of the OFDM burst.

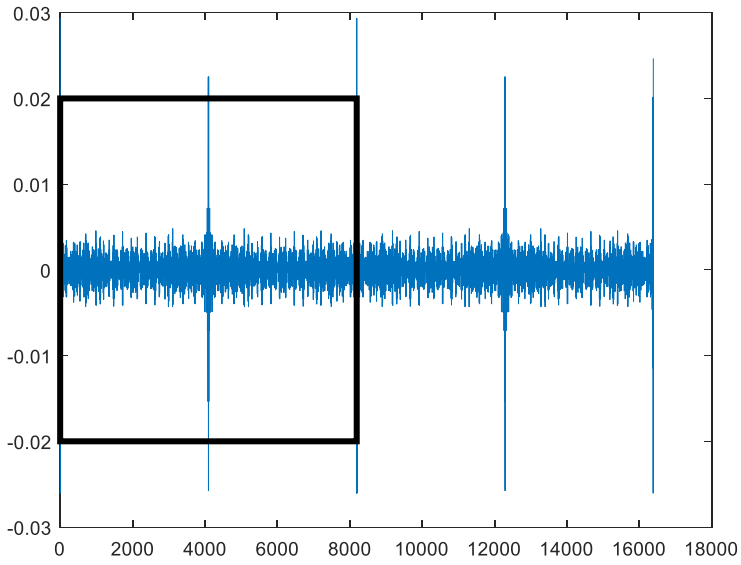

Figure 4.27: Ideal OFDM burst with rectangle showing part of burst to be demodulated.

Since each OFDM symbol generated at the transmitter consisted of 8192 samples, an 8192 FFT is performed on part of the OFDM symbol to convert the time domain OFDM symbol into the frequency domain. The first part of the OFDM burst is used at first to see how the estimation of the channel changes, as a function of the synchronization point. The pilot symbols were extracted from the FFT for channel estimation. The received content at the pilots is used to determine the channel magnitude and phase response estimates. X_p and Y_p refer to the transmitted

and received FFT samples at the p^{th} subcarrier. The channel impulse response (CIR) estimate corresponding to the p^{th} subcarrier is calculated as

$$\hat{H}_p = \frac{Y_p}{X_p} \tag{4.2}$$

The MATLAB function *interp* was used to perform interpolation of the CIR estimates at the pilot subcarriers to the data subcarriers, for magnitude and phase separately. Figure 4.28 and Figure 4.29 show the magnitude and phase estimates of the frequency response of the channel estimated from the symbol shown in Figure 4.27.

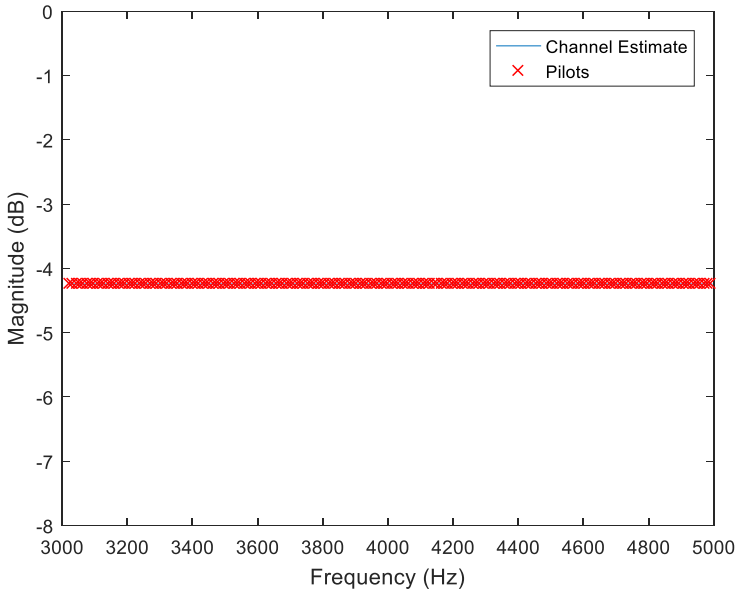

Figure 4.28: Magnitude of the Channel Response estimate.

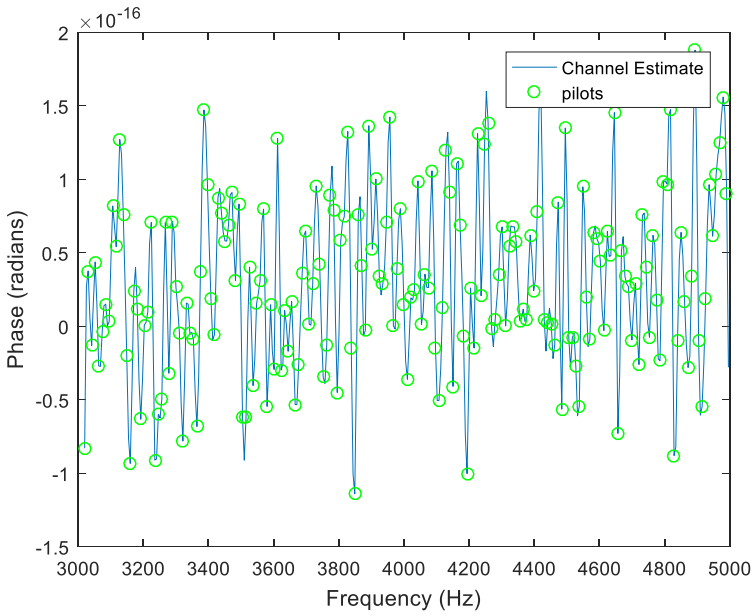

Figure 4.29: Phase of the Channel Response estimate.

Note that the channel response reflected in Figures 4.28 and 4.29 corresponds practically to distortion-less transmission, as is expected for the ideal received signal. Once the channel response estimate over the entire band of operation is obtained, frequency domain equalization is performed to negate the effect of the frequency selective channel. Let Y_k refer to the received OFDM symbol and $\hat{H}_k$ to the channel response estimate in the frequency domain. The equalized OFDM symbol in the frequency domain was obtained by:

$$X_{equalized} = \frac{Y_k}{\hat{H}_k} \quad k = 1, 2, \ldots K_{active} \tag{4.3}$$

The BPSK data symbols are extracted from the corresponding subcarriers of the equalized OFDM symbol by checking if the real part of $X_{equalized}$ at the subcarriers designated as data bits is greater than or less than zero. If the value was greater than 0, the data bit was classified as a 1, otherwise as a 0. The data bits extracted from the symbol in Figure 4.27 are shown in Figure 4.30.

Note how the imaginary part is near 0, while the real part matches with the transmitted bits, as expected in BPSK modulation and the ideal received signal.

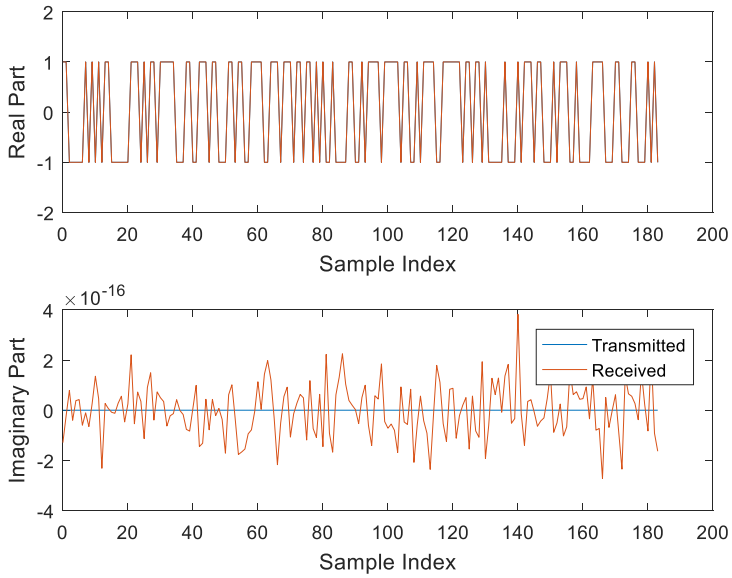

Figure 4.30: BPSK symbols extracted from OFDM symbol in Figure 4.27.

Figure 4.30 indicates that the received symbols overlap quite well with the transmitted symbols (BPSK bits) with zero errors taking place. To see how the equalization works with delay in the OFDM signal, a different part of the OFDM symbol is demodulated.

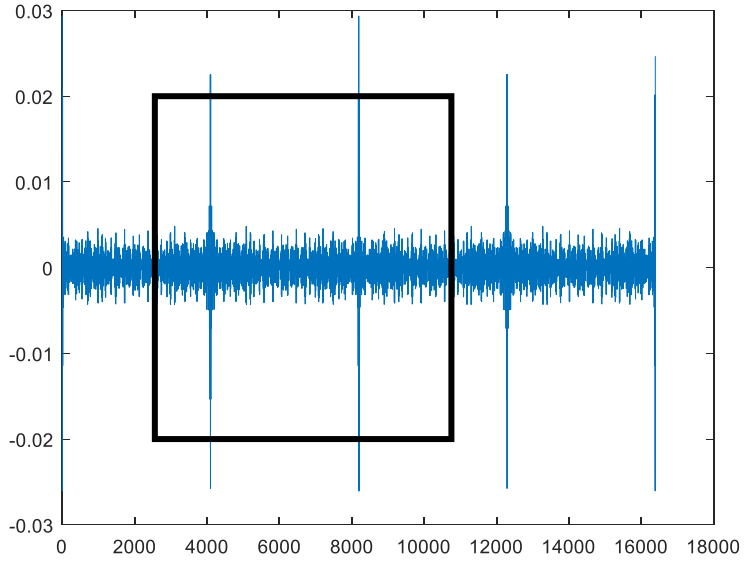

Figure 4.31: Ideal OFDM symbol with delay.

Figure 4.31 shows the different part of the OFDM symbol that is demodulated next with the channel response shown in Figure 4.32 and Figure 4.33. Similar to the example in Figure 4.27, the data symbols were extracted from the corresponding subcarriers of the equalized OFDM symbol by checking if the real part of $X_{equalized}$ at the subcarriers designated as data bits were greater than or less than zero. The resultant data symbols are shown in Figure 4.34.

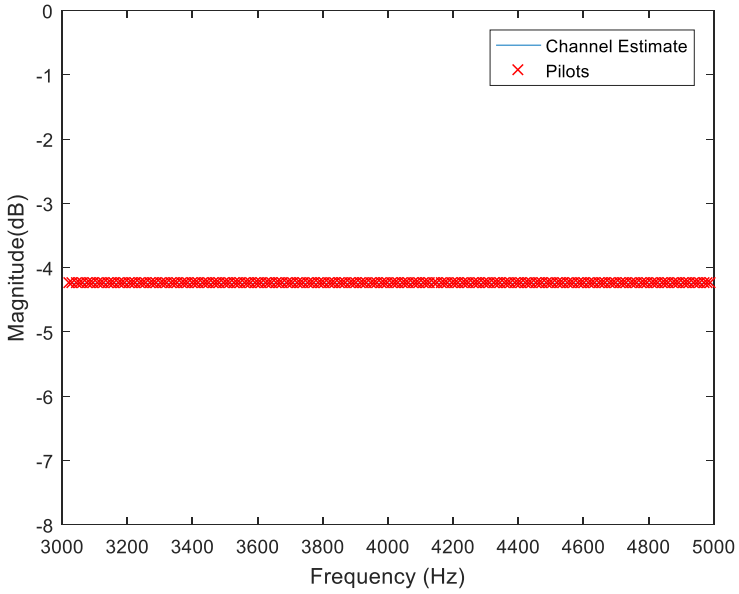

Figure 4.32: Magnitude of the Channel Response estimate.

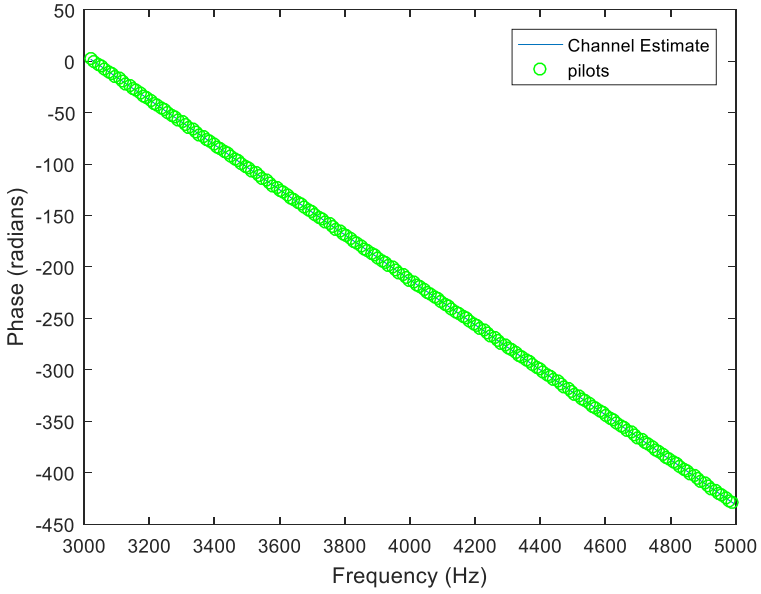

Figure 4.33: Phase of the Channel Response estimate.

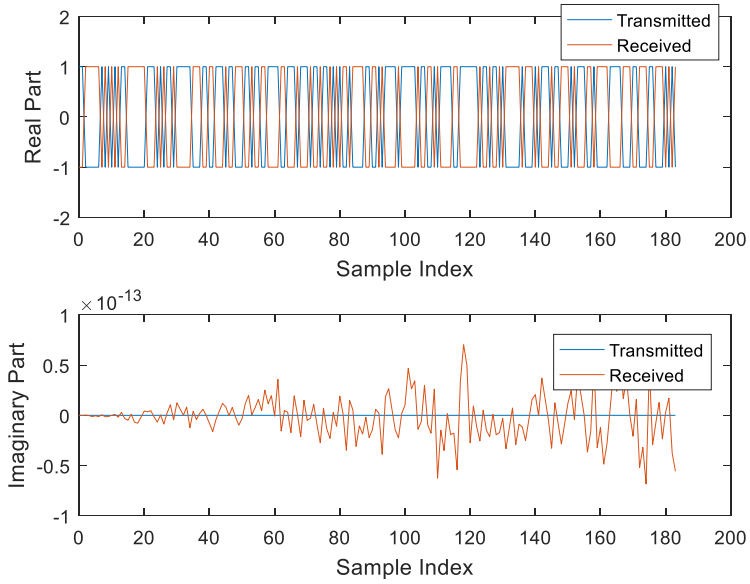

Figure 4.34: BPSK symbols extracted from time delayed symbol shown in Figure 4.31.

Figure 4.34 shows that given enough of a time delay, the equalization process is unable to correct for the phase, which leads to all of the bits being flipped. Observe in Figure 4.33 the steep rate of change in the phase estimate. Ultimately, the phase does not go through a multiple of 2π at zero frequency, causing a flip in sign of the equalized bits. To counter this, a window of the detected OFDM burst is used, usually in the second part of the OFDM burst. The reason that the second half of the OFDM symbol is used is because the cyclic prefix is discarded prior to decoding the OFDM.

The next step is analyzing the BER of the three received signals. To illustrate the effects of the phase delay or advance, the BER is calculated across the entire OFDM packet. Finding the BER over the entire packet will illustrate a region of the OFDM packet that can be selected for use as the synchronization point, or area. Figure 4.35, Figure 4.36, and Figure 4.37 show the BERs for the packets extracted in Figure 4.24, Figure 4.25, Figure 4.26.

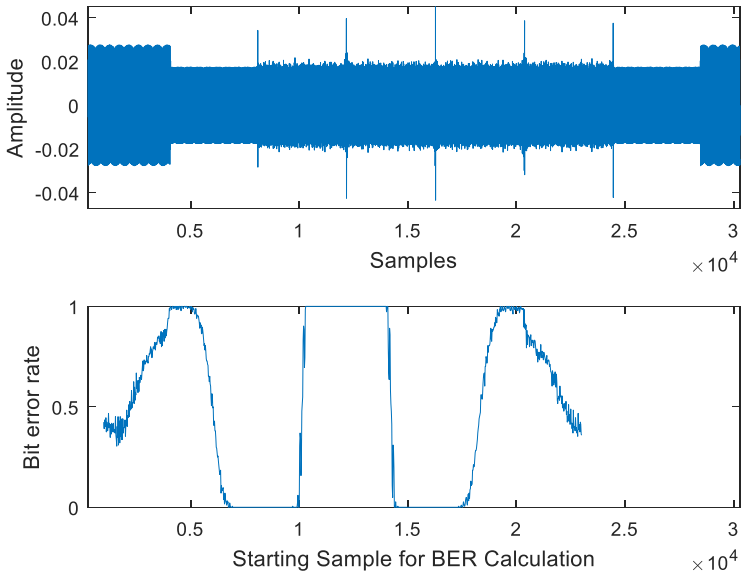

Figure 4.35: BER for packet #1 of the Ideal Received Burst.

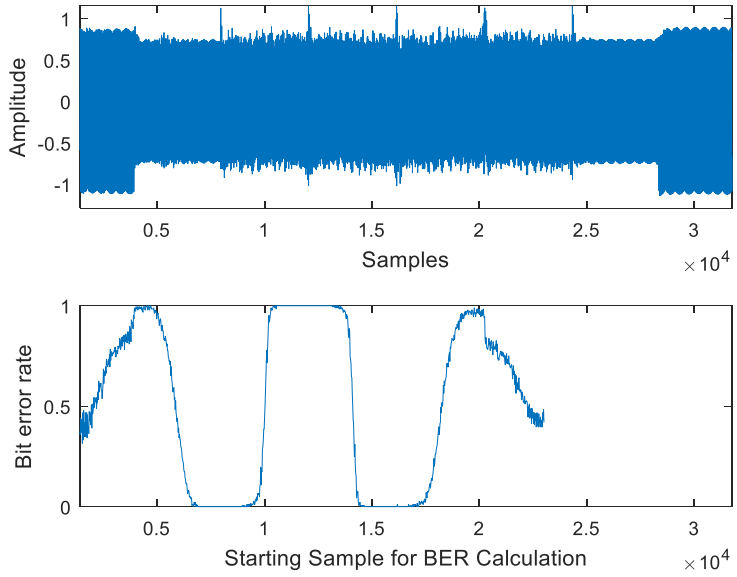

Figure 4.36: BER vs synchronization point for Packet NS.1.

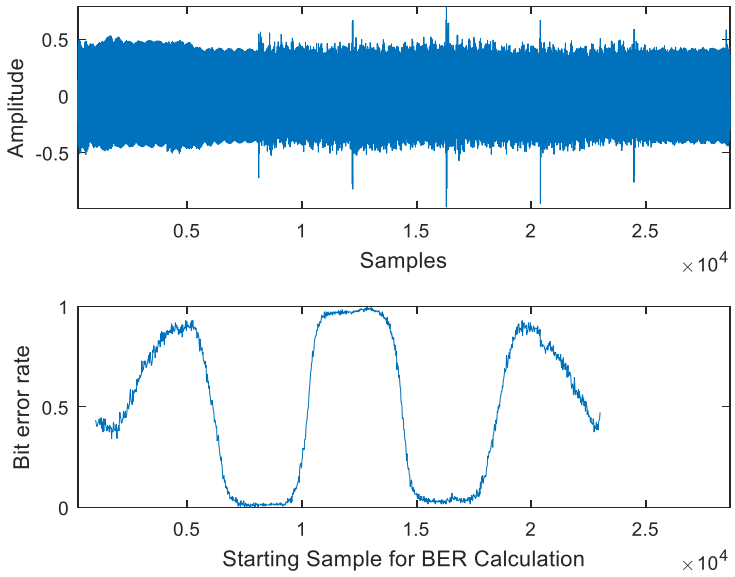

Figure 4.37: BER vs synchronization point for Packet FS.1.

The BER behavior for the received packets shows that as the microphone gets further from the transmitter, the BER gets worse, as expected due to increased multipath and lower signal to noise ratio. The BER behaviors also show that the lowest BER is usually found at around more than halfway into the packet. Notice from Figures 4.35, 4,36, and 4.37, that the lowest BER comes in a range between 1.50×10^4 and 1.70×10^4 samples into the CP+OFDM signal.

In practice, a synchronization point would be chosen for a given received OFDM burst. For these received signals, a synchronization point of 1.5792×10^4 samples (or the point used for the OFDM demodulation and BER calculation) was selected for use with the extracted packets. This time was used as an approximation for where the beginning of the OFDM burst was, since the length of the preamble was 8000 samples, the cyclic prefix was 8192, and the *FOSE* had a 400 sample window. In practice, this synchronization point would be used as opposed to calculating the BER for every sample in the received packet. The extracted symbols using the

sample point at 1.57×10^{4} samples for the ideal received signal, Packet NS.1, and Packet FS.1 are shown in Figure 4.40, Figure 4.43, and Figure 4.46, respectively.

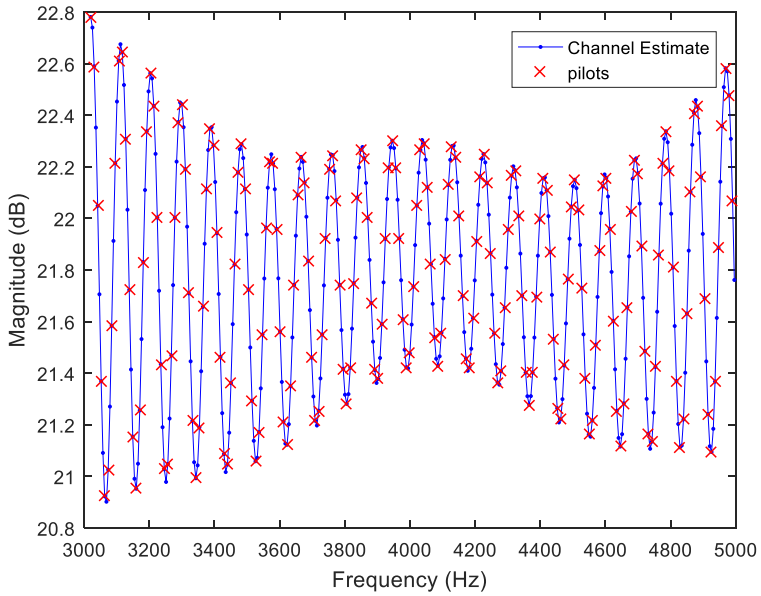

Figure 4.38: Channel magnitude response estimate for the Ideal Received Signal.

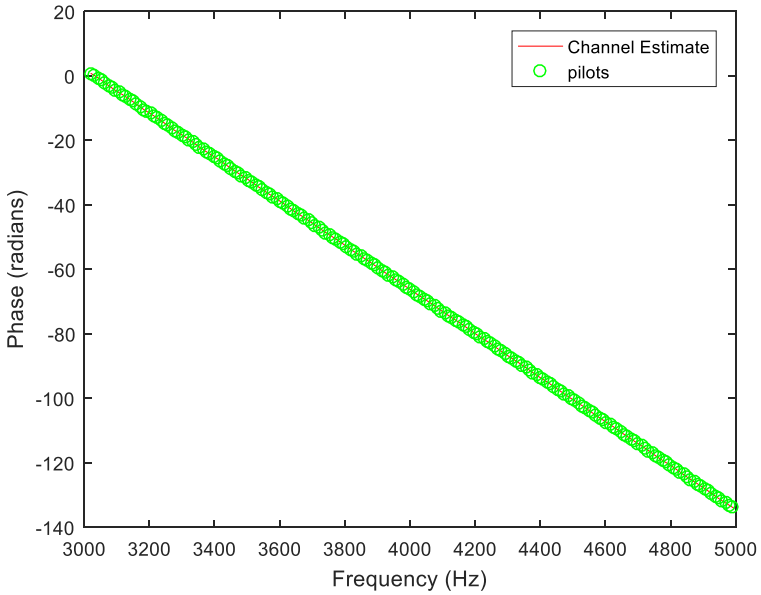

Figure 4.39: Channel phase response estimate for the Ideal Received Signal.

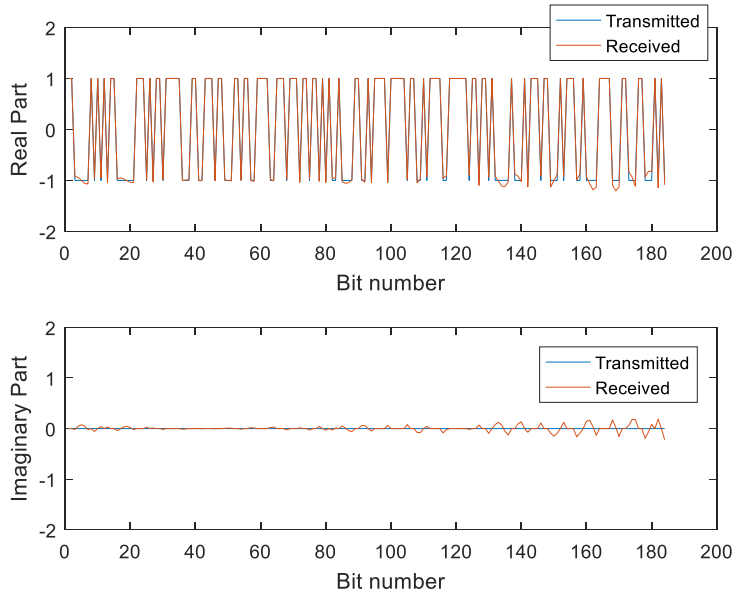

Figure 4.40: Symbols extracted from packet #1 of Ideal Received Signal.

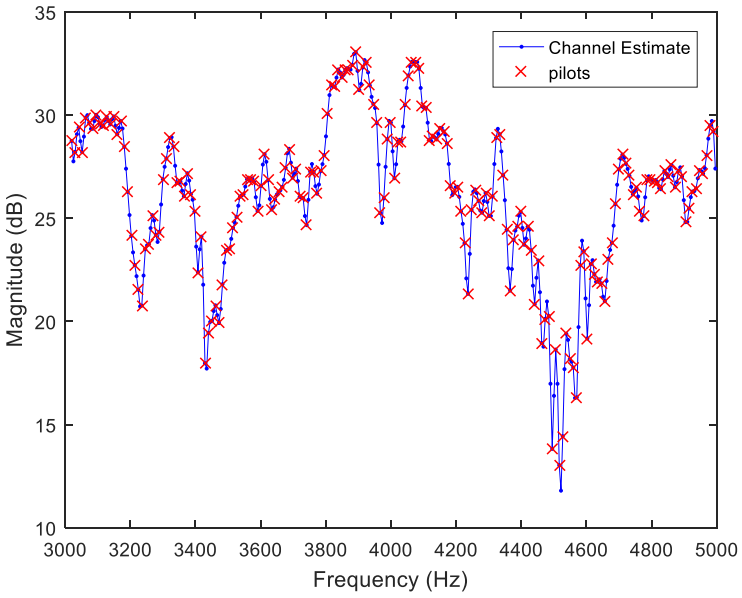

Figure 4.41: Channel magnitude response estimate for Packet NS.1.

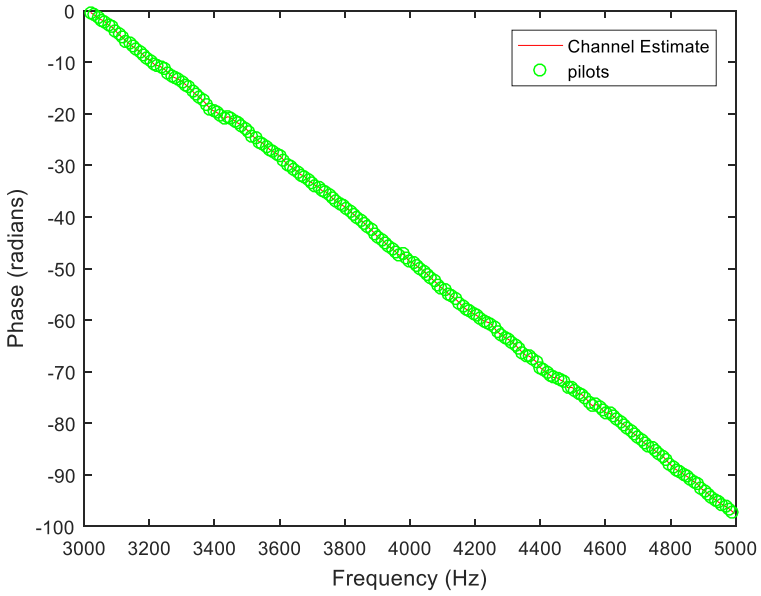

Figure 4.42: Channel phase response estimate for Packet NS.1.

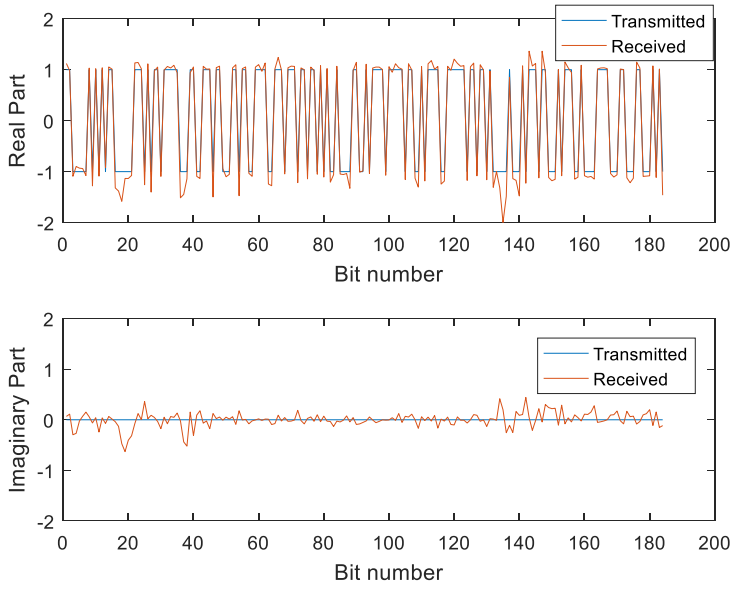

Figure 4.43: Symbols extracted from Packet NS.1.

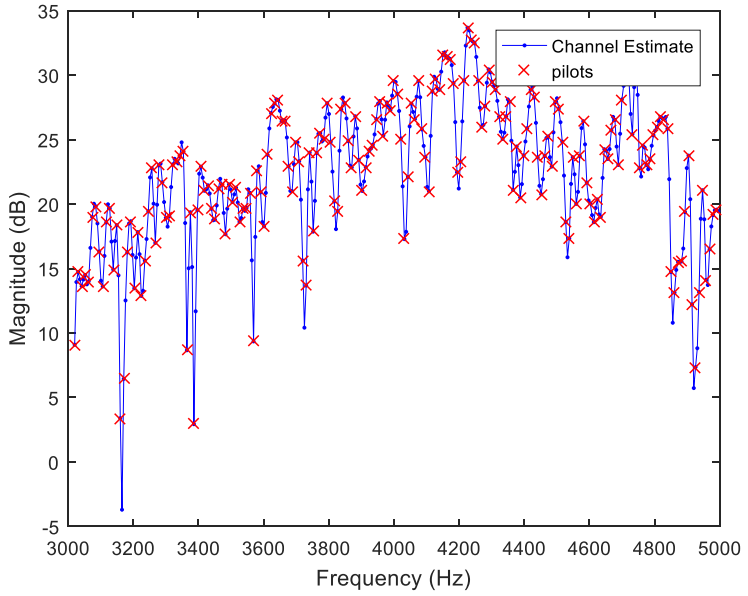

Figure 4.44: Channel magnitude response estimate for Packet FS.1.

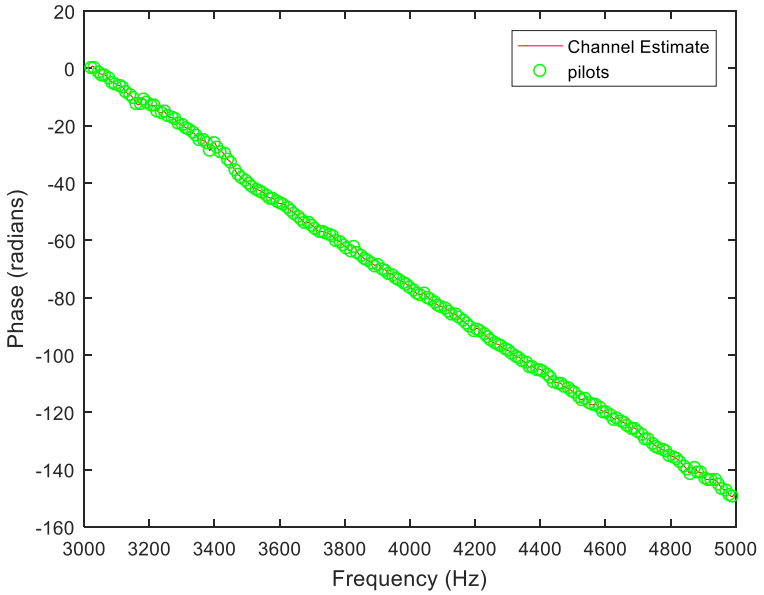

Figure 4.45: Channel phase response estimate for Packet FS.1.

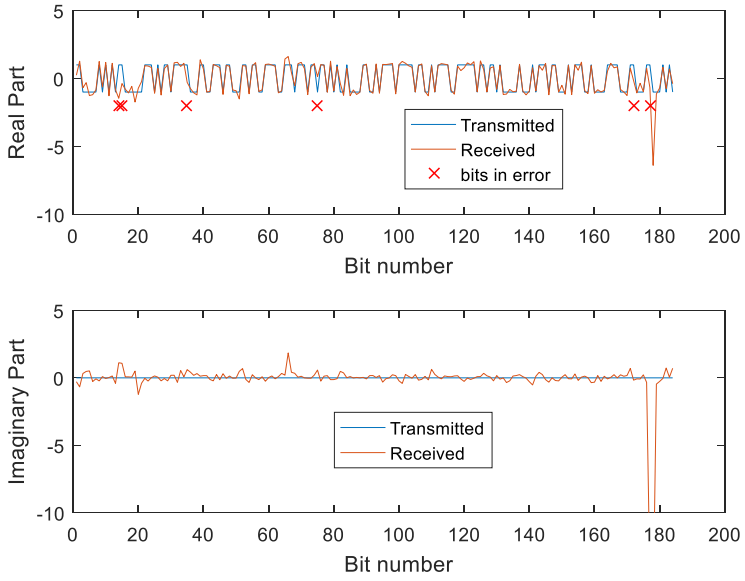

Figure 4.46: Symbols extracted for Packet FS.1.

In the case of the ideal received signal and the signal captured in the NS experiment, shown in Figures 4.40 and 4.43 respectively, the BER was 0, corresponding to 0 errors (out of 168 bits) in the received signal. In the case of the FS Experiment, shown in Figure 4.46, the BER was 0.0269, corresponding to 5 errors (out of 184 bits) in the received signal. From the channel frequency response estimate in Figs. 4.44 and 4.45, observe that the Frequency Response of the channel in the case of the FS experiment has larger and faster variation in comparison to the channel frequency response estimate in the case of the NS experiment, shown in Figure 4.41; the larger variation seems to be responsible for the larger BER. The signals received in the NS and FS experiments will be used as a benchmark for the signals in the NM and FM Experiments, where the latter will have a Doppler warp affecting the burst in addition to multipath.

In this chapter the OFDM transmitter design has been discussed. Several parameters for the OFDM transceiver were decided based on a signal composed of several sinusoids. This design is used in Chapter 5, which incorporates the added complexity of a Doppler warp affecting the

OFDM signal. To correct for the Doppler warp, estimates for the alpha and beta parameters of the Doppler warp model are used to then mitigate the Doppler effect. Several of the ideas discussed in this chapter, such as the *FOSE* measurement for detecting an OFDM packet and calculating the BER across an OFDM packet, are also used in Chapter 5.

5 Doppler Warp Correction of Acoustic OFDM

In Section 4.1 four experiments were described to test the Doppler warp model. The near stationary (NS) and far stationary (FS) experiments were conducted to generate a baseline of the OFDM received signal with just multipath. The near moving (NM) and far moving (FM) experiments involved the moving of a microphone through the point at which the stationary experiment was conducted. This chapter combines the estimation and correction of the Doppler warp model with the OFDM transceiver.

5.1 Doppler Warp Description

This section shows the simulation of the effects of a Doppler warp sinusoid. To start, the simulation model from Chapter 4 is described in more detail for the moving experiments. Recall that the experiments in which the microphone was moved at a constant rate in a semi-circle arc were labeled as NM and FM experiments. The diagram of the experiment is shown in Figure 4.1.

As discussed in Chapter 4, the transmitted signal is of a burst nature, with sinusoids at 2 and 6 kHz present before, after, and during an OFDM burst to estimate the Doppler warp that the OFDM symbol experiences. The estimation of the Doppler warp, using the sinusoids, facilitates the correction of the OFDM burst. The OFDM burst was generated in MATLAB with data modulated onto carriers between 3-5 kHz. The sinusoids included in the burst structure were placed at 2 kHz, 3kHz, 5 kHz, and 6 kHz. The resultant burst was transmitted using a speaker connected to the soundcard of a computer. A microphone moving at a varying speed relative to the speaker captured the acoustic transmission. The microphone was moved in a semicircle arc as illustrated in Figure 4.1. Since the microphone completed roughly one arc over the length of the transmitted burst, the microphone moved at roughly 1 ft/sec, though physically its speed could reach up to 3

ft/sec. In addition, the signal is simultaneously captured with a stationary microphone, so as to compare the received signal with multipath to the received signal with Doppler and multipath. The stationary microphone was close to the location where the microphone moving at varying speed came closest to the transmitter. A separate instance of MATLAB on the same computer acted as the OFDM receiver that captured the received signal.

As the packet takes longer to transmit due to the addition of more OFDM symbols, the nonlinear warp model (piecewise linear acceleration) shown in Chapter 3 may no longer apply. In this experiment, 4 successive packets are sent, with each packet containing the same data. The latter will show how the environment can change rapidly, over a short period of time.

5.2 Sinusoidal Doppler Estimation

In Chapter 4, a signal composed of four sinusoids, at 2, 3, 5 and 6 kHz, was used to determine several channel characteristics. The signal composed of four sinusoids is used to observe the distortion caused by the Doppler warp and multipath due to the channel. The transmitted signal is shown in Figure 5.1. The transmitted signal is 32384 samples in length, which at a sampling frequency of 44.1 kHz corresponds to 734 ms.

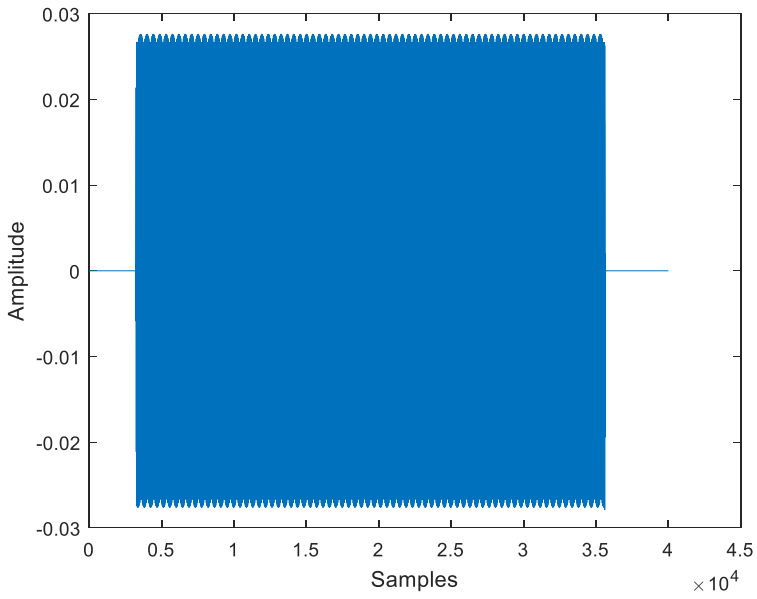

Figure 5.1: Transmitted signal used for delay spread estimation.

The signal shown in Figure 5.1 was transmitted from a speaker while a microphone was moved along the NM and FM experiment paths illustrated in Figure 4.1. The velocity of the microphone along the path was roughly 1 foot per second. 4 bandpass filters, with center frequencies at 2, 3, 5 and 6 kHz, were used to extract the 4 sinusoids from the received signal. The received signals and spectrograms from the NM experiment are shown in Figures 5.2 and 5.3, respectively.

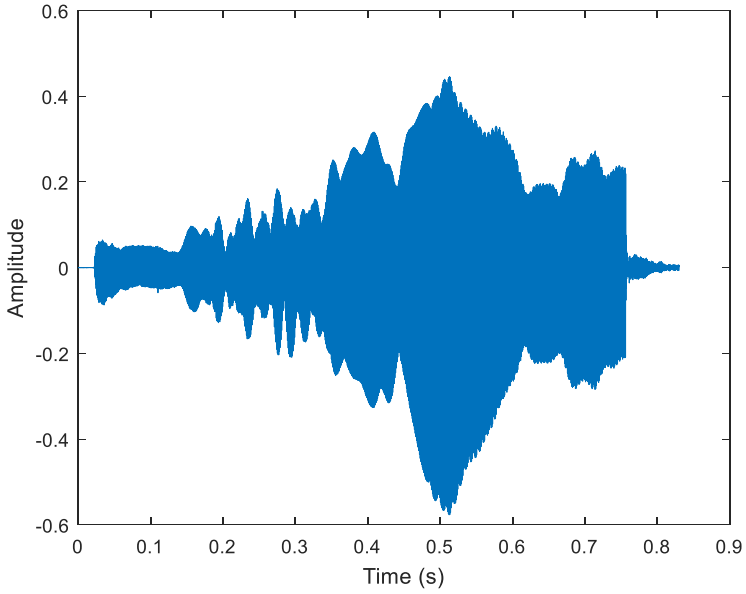

Figure 5.2: Received signal from NM Experiment.

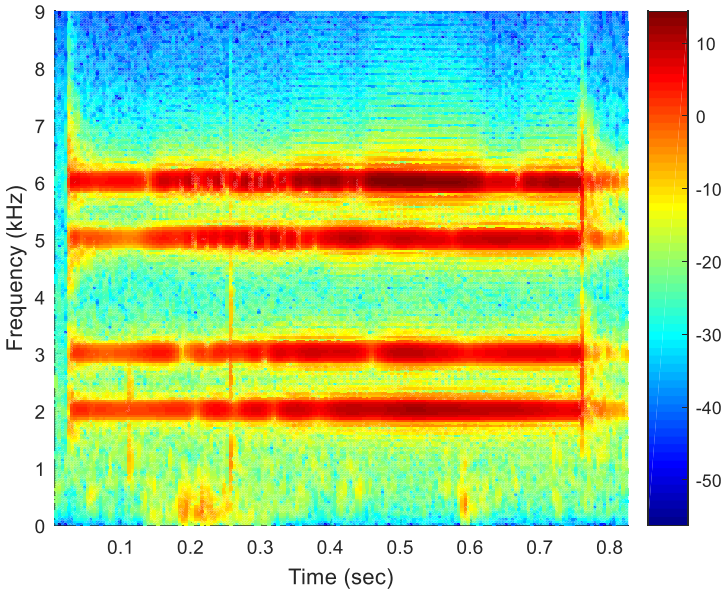

Figure 5.3: Spectrogram of received signal from NM Experiment.

Observe from Figure 5.2 and 5.3 that the movement of the microphone combined with the multipath in the room creates huge variations in the envelope (or nulls) of the received signal. The nulls in the signal are more noticeable in the first half of the signal, between 0.01 and 0.3 seconds,

and cause a reduction in the overall energy in the signal. It will be shown that overall distortion caused by the combination of Doppler and multipath can create uncertainty in the frequency measurements. Figures 5.4 and 5.5 show the received signal and spectrogram, respectively, obtained from the FM Experiment.

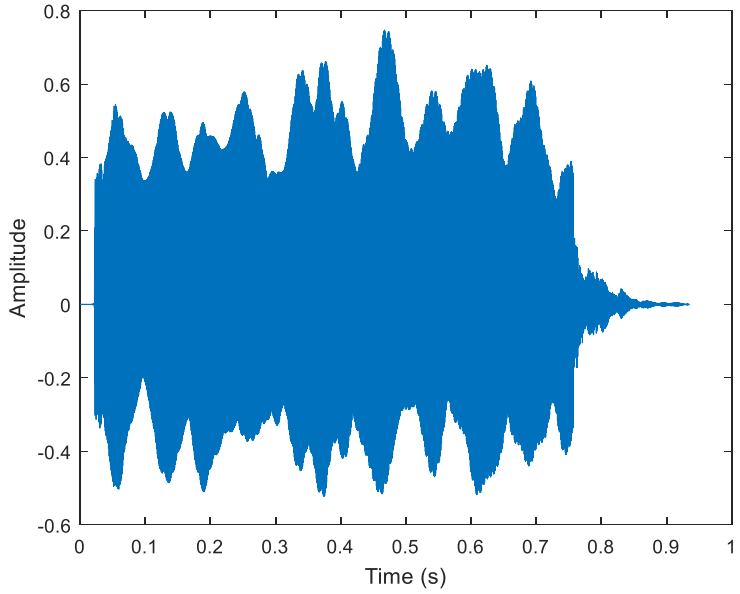

Figure 5.4: Received signal from FM Experiment.

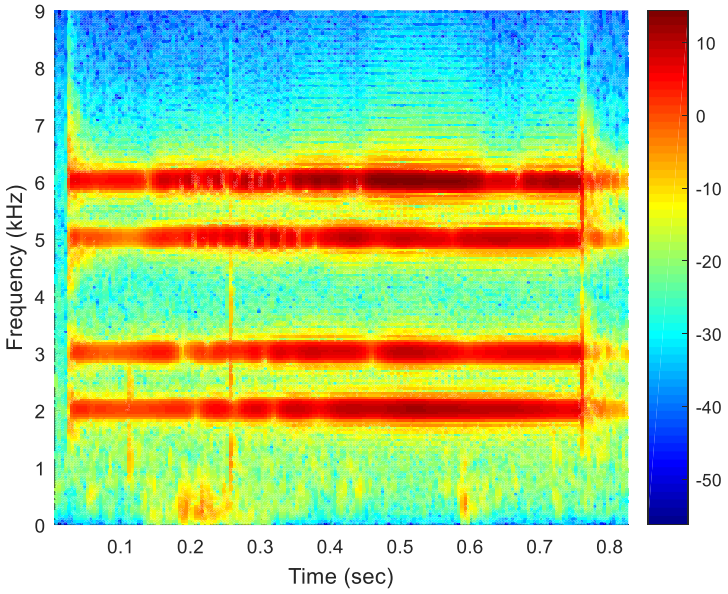

Figure 5.5: Spectrogram of received signal from FM Experiment.

Observe from Figure 5.4 and 5.5 that the movement of the microphone combined with the multipath in the room creates large variations in the envelope in the received signal.

Having used the signal composed of the 2, 3, 5, and 6 kHz sinusoids to determine the multipath present in the OFDM signal in Chapter 4, the signal can also be used to determine the effect of multipath and Doppler on the signal. To determine the Doppler and multipath that the received signal underwent, the frequencies of the sinusoids are tracked for all 4 frequencies.

All 4 frequencies are tracked over time by applying 4 narrowband filters to the received signal, each centered around the frequency being tracked. The frequency response of the filter used to extract the 5 kHz sinusoid is shown in Figure 5.6.

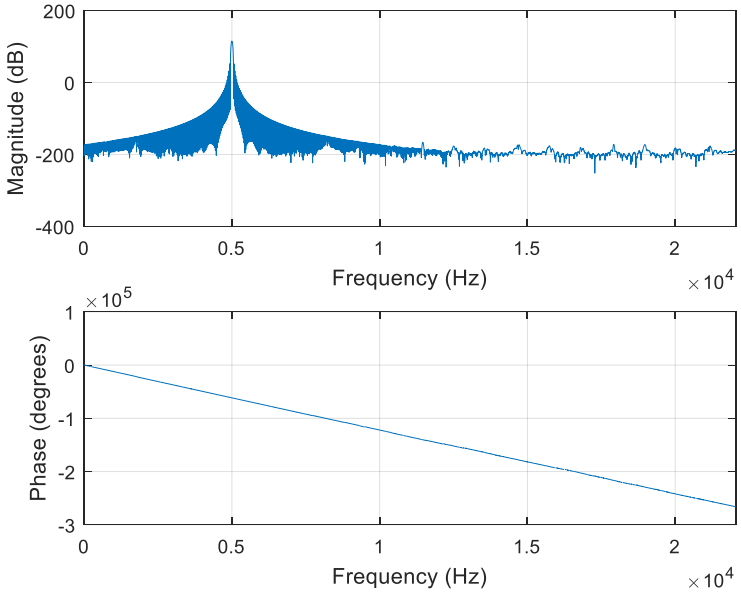

Figure 5.6: Frequency response of the 5kHz filter.

The filter was designed to be centered around 5 kHz with a 3 dB bandwidth of 30 Hz. The 3dB bandwidth is illustrated in Figure 5.7.

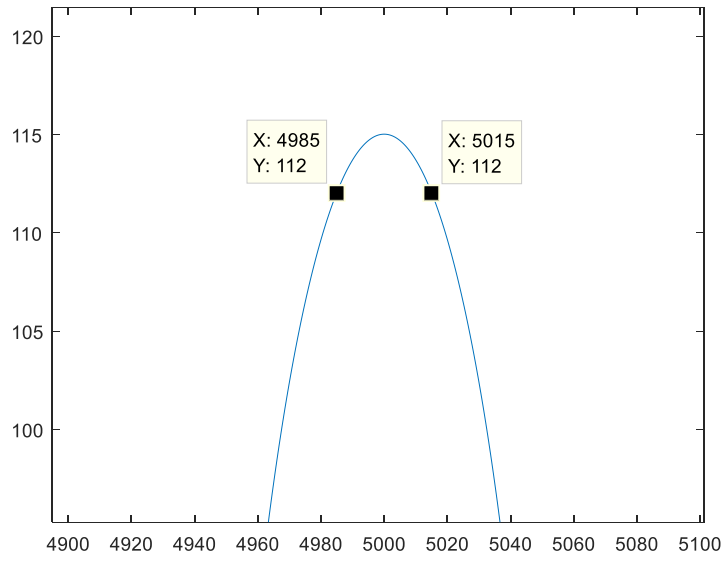

Figure 5.7: 3 dB Bandwidth of 5 kHz filter.

The reason for the 3 dB bandwidth is to facilitate capturing all of the possible frequency change resulting from the receiver moving at 1 ft/s. Since the receiver is moving at a relatively slow speed (1 foot/sec), the frequency will shift less than 100 Hz for even the highest frequency component at 6 kHz.

The extracted 5 kHz sinusoid after filtering is shown in Figure 5.8.

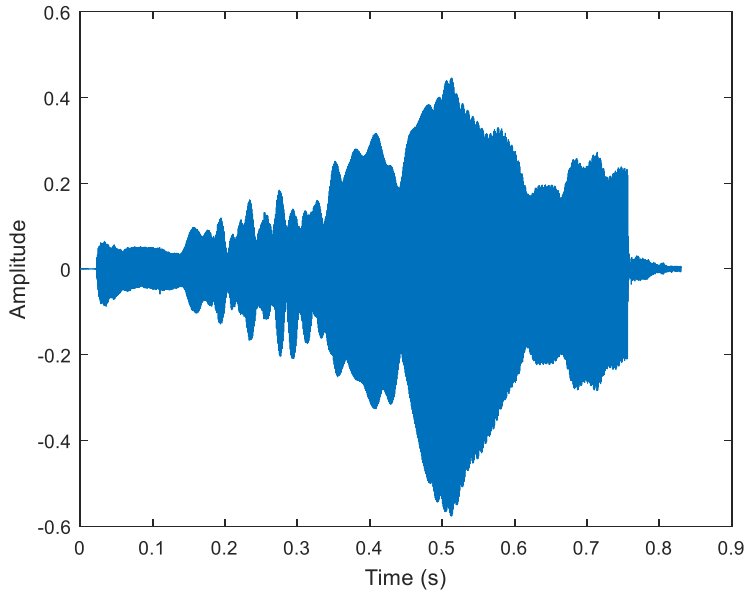

Figure 5.8: Extracted 5 kHz Sinusoid with Doppler and Multipath for NM Experiment.

FIR filters with a 3 dB bandwidth of 30 Hz are applied to extract the 2, 3, and 6 kHz sinusoids also, which are all shown in Figure 5.9. The reason that 30 Hz bandwidth was used was to capture as much of the frequency change arising from the Doppler movement. The frequency change could be as much as 15 Hz assuming a velocity change of 3 ft/s with a 6 kHz sinusoid. The speed of sound in air, of 1,126 ft/s, is used in this example.

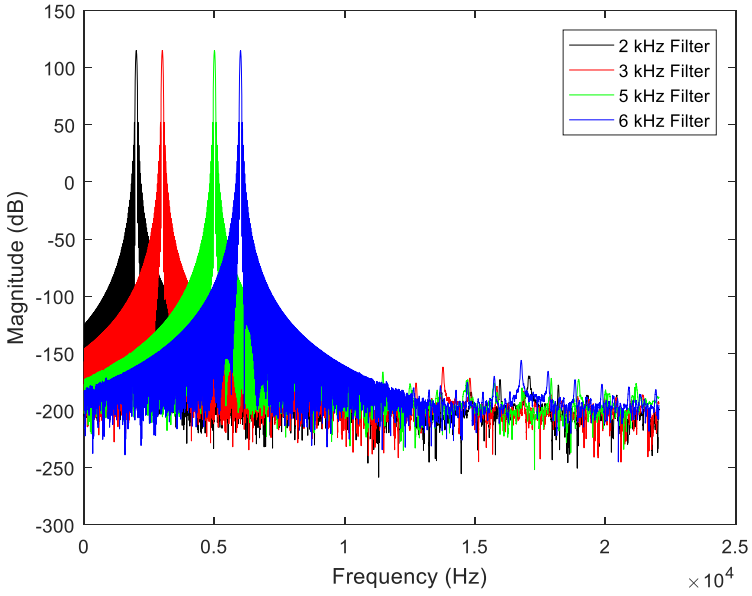

Figure 5.9: Magnitude Spectrum of 2, 3, 5, and 6 kHz Filters.

After extracting each sinusoid, its frequency as a function of time is estimated. The estimation is done by taking 400 sample windows every 500 samples over the entire signal and using AR parameter estimation (via the Burg method). The frequency estimation results for the 2, 3, 5, and 6 kHz sinusoid are shown in Figures 5.10, 5.11 5.12, and 5.13, respectively.

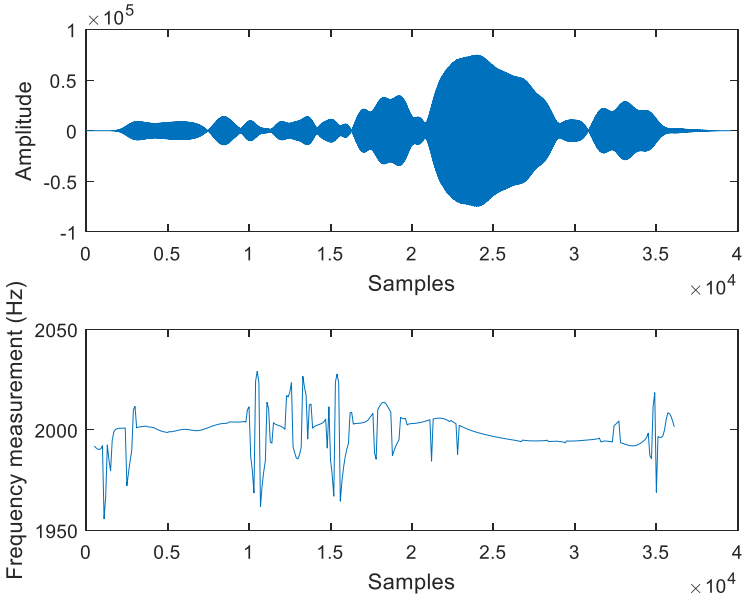

Figure 5.10: Extracted 2 kHz Sinusoid with Frequency Estimate from NM Experiment.

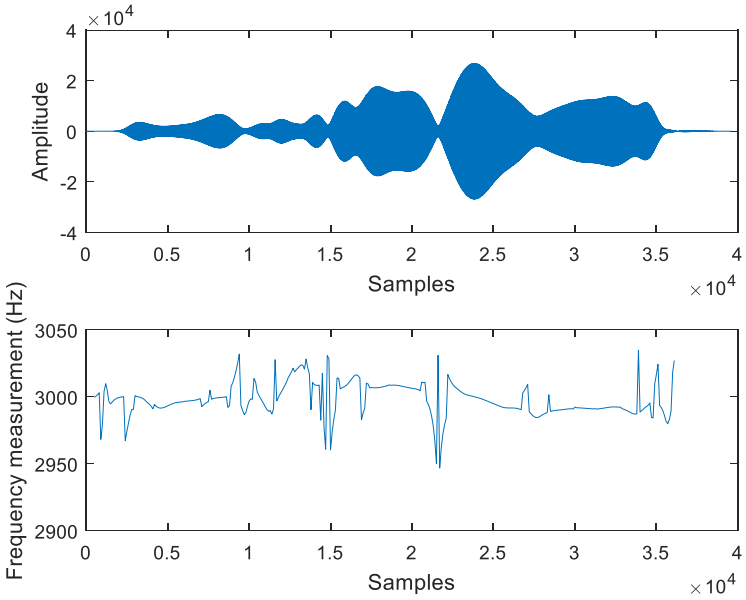

Figure 5.11: Extracted 3 kHz Sinusoid with Frequency Estimate from NM Experiment.

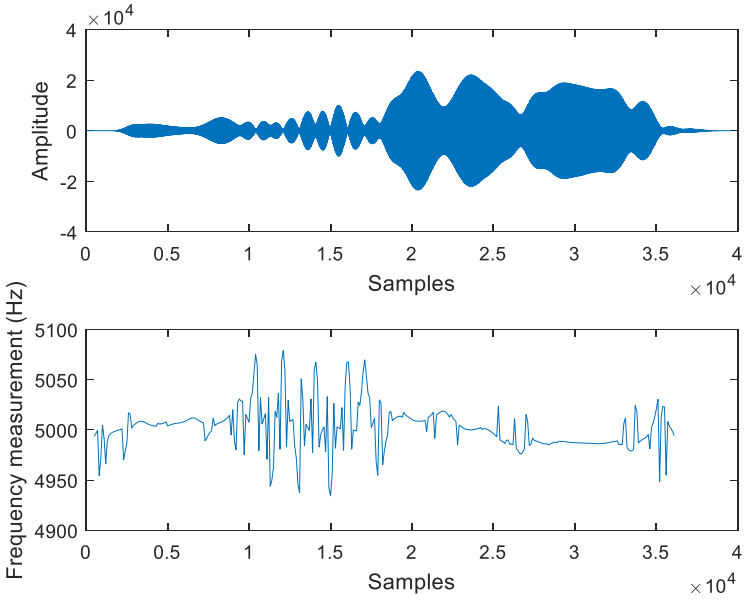

Figure 5.12: Extracted 5 kHz Sinusoid with Frequency Estimate from NM Experiment.

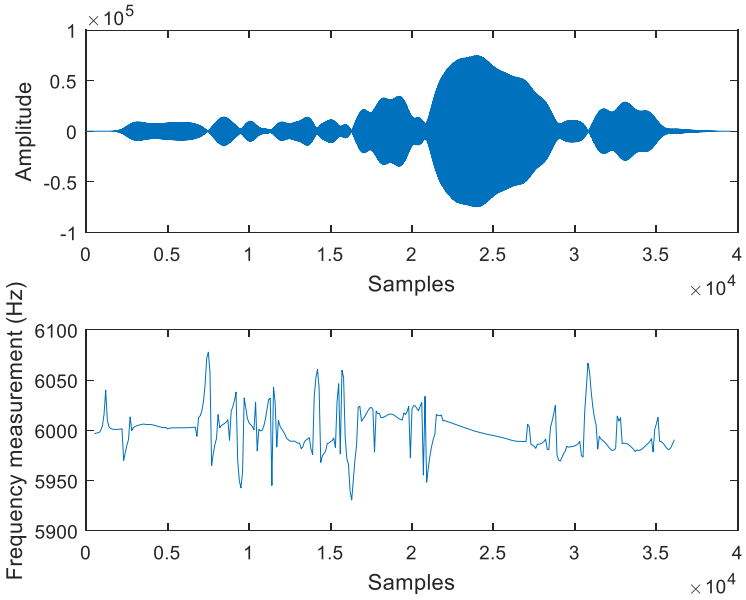

Figure 5.13: Extracted 6 kHz Sinusoid with Frequency Estimate from NM Experiment.

As observed from Figures 5.10 through 5.13, there is a lot of uncertainty in the frequency measurement where there are distinct amplitude nulls in the sinusoid, probably caused by the changing multipath in the room. These nulls correspond with large spikes in the frequency

measurement. For example, the deep nulls in the first half of the sinusoid in Figure 5.11 – between samples 10000 and 15000 – correspond to sudden spikes in the frequency measurements.

As seen in Figures 5.10 through 5.13, nulls due to multipath can lead to unreliable frequency measurements. However, in areas where the signal has more energy, such as in between samples 22000 and 27000 in Figure 5.13, the frequency estimates tend to be smooth and more reliable, as reflected by seeing fewer sudden spikes in the estimates. To use the most reliable frequency estimates possible, the time intervals where the energy is highest are used for frequency estimation; subsequently, these time instants and corresponding frequency estimates are used for estimating the alpha and beta parameters in the Doppler warp model. Time instants during the course of the sinusoid are used to update the alpha and beta parameters as new frequency estimates become available. In the next section the two different methods for estimating the alpha and beta parameters are described that parameterize the Doppler model in Section 3.3.

5.3 Over the Air Experiment with Doppler

In the previous section it was shown how a combination of Doppler warp and multipath can affect the frequency estimates obtained from such a signal. The frequency measurements used to estimate the Doppler warp model are critical to unwarping the Doppler affected signal. In this section the over the air experiment – associated with NM and FM Experiments with an OFDM signal transmitted to a moving receiver – is discussed. Using the Doppler warp estimation and correction model described in Section 3.3, sinusoids that are present before, during, and after the OFDM burst are used to estimate the possible Doppler warping that the signal underwent. Two different techniques are used to estimate the Doppler warp. The first technique uses the 3 and 5 kHz

sinusoids present in the preamble and postamble signals (signals described in Section 4.4) to estimate the Doppler warp and then demodulate the resultant OFDM symbol. Of the 3 and 5 kHz frequencies, the normalized absolute magnitudes of the extracted sinusoids were used to determine which frequency would be used for the determination of the warp parameters. The normalized absolute magnitude (NAM) was defined as:

$$NAM = \frac{1}{\max_i(|x_i|)} \sum_{i=0}^{n} |x_i| \tag{5.1}$$

x_i is the extracted sinusoid, and n is the length of the entire OFDM packet. The second technique used the sinusoids at 2 and 6 kHz to estimate the Doppler warp during the OFDM burst and then demodulate the resultant OFDM symbol. Similar to the 3 and 5 kHz frequencies, the sinusoid that had the larger energy over the sinusoid was used to estimate the Doppler warp.

5.3.1 Transmitter Packet Design

As discussed in Chapter 4, an OFDM burst with sinusoids at 2, 3, 5, and 6 kHz before, during, and after the OFDM burst is used as the transmitted Signal. Because multipath can distort the frequency estimates obtained from a received signal, the out of band frequencies at 2 and 6 kHz were added alongside the OFDM symbol. These out of band frequencies present during the OFDM burst are to obtain more accurate alpha and beta estimates more often and thus to better track the Doppler warping during the course of the OFDM burst. The structure of the transmitted OFDM burst is shown in Figure 5.14.

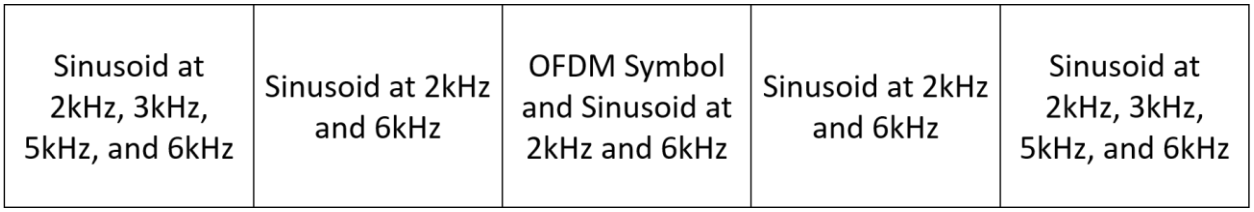

Figure 5.14: Transmitted OFDM structure used for Doppler Warp Correction.

The time domain representation and spectrogram of the transmitted OFDM packet are shown in Figure 5.15 and 5.16. respectively. This signal was transmitted using a sampling frequency of 44.1 kHz.

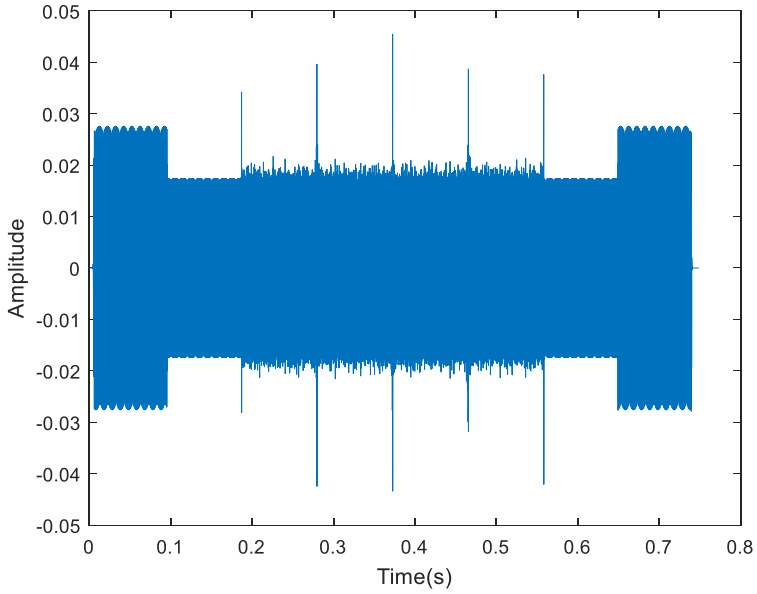

Figure 5.15: Transmitted signal in time domain.

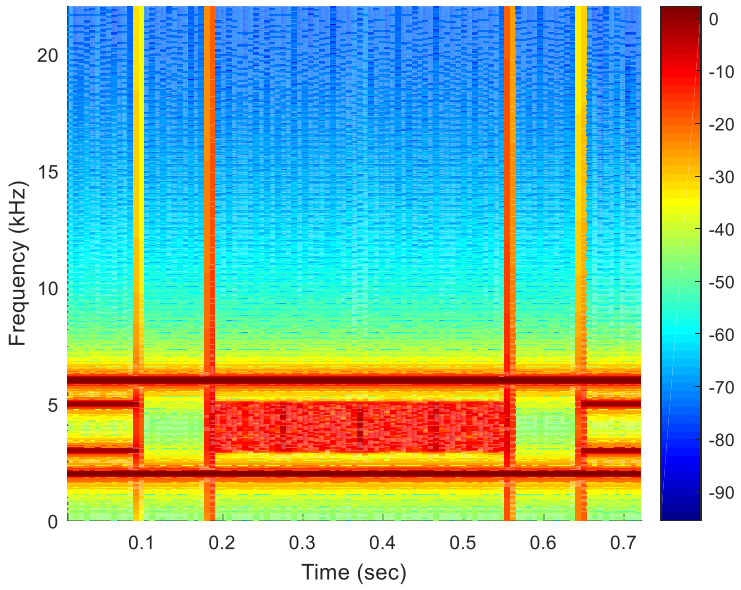

Figure 5.16: Spectrogram of Transmitted Signal.

In this section the results obtained by moving the microphone along the arc of a semicircle (as shown for the NM and FM Experiments in Figure 4.1) are described. In Subsections 5.3.2 and 5.3.3 the performance of the receiver is investigated when there is circular motion, in addition to the multipath. The 4 packets captured in the NM and FM Experiments are shown in Figures 5.17 and 5.18.

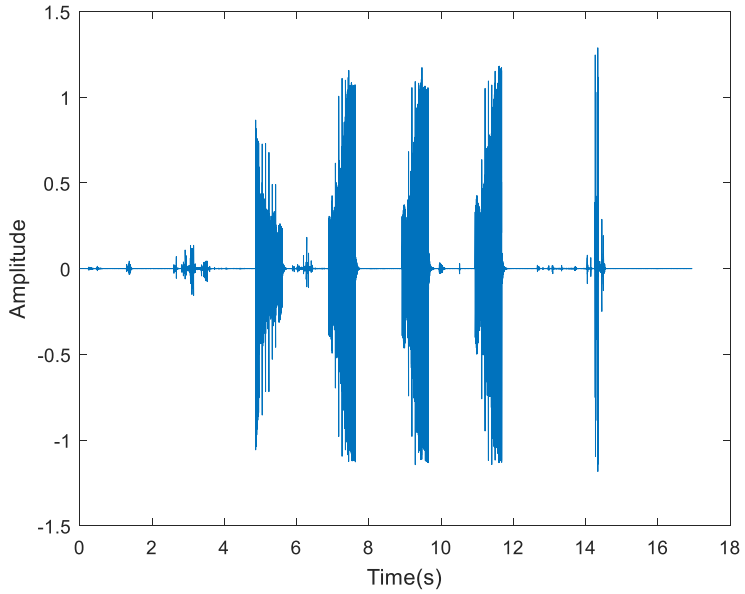

Figure 5.17: Received OFDM packets from NM experiment.

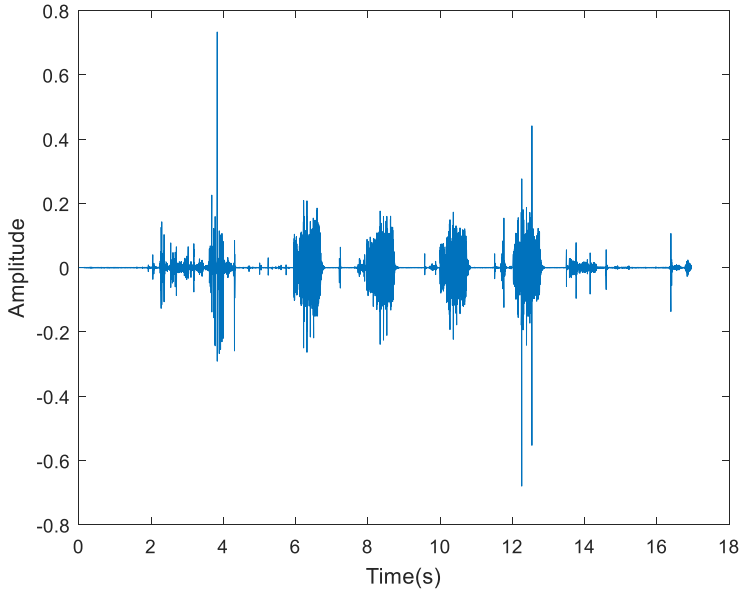

Figure 5.18: Received OFDM packets from FM Experiment.

Observe in Figure 5.17 the 4 packets from the NM Experiment that have undergone Doppler warping and multipath, roughly centered at 5, 7, 9, and 11 sec. Figure 5.18 shows the 4 packets from FM Experiment that have undergone Doppler warping and multipath at a greater distance between receiver and transmitter, roughly centered at just past 6, 8, 10, and 12 sec. Possibly because of the greater distance between receiver and transmitter, the amplitude, and subsequently overall energy of the packets from the FM Experiment is lower than those of the NM experiment. In order to correct for the Doppler and multipath distortions, the variations in frequency are used first to correct for the Doppler warp, followed by OFDM decoding and equalization (described in Section 4.5) to extract the bits from the Doppler corrected signal.

The first part of Doppler warp estimation was the extraction of the OFDM packet. The overall process is shown for the first packet of NM and FM experiments, with the parameters of the other packets discussed in Table 5.1. The *FOSE* measurement used in Subsection 4.4.2 was used to extract each packet. Figure 5.19 shows Packet NM.1 and Figure 5.20 shows Packet FM.1.

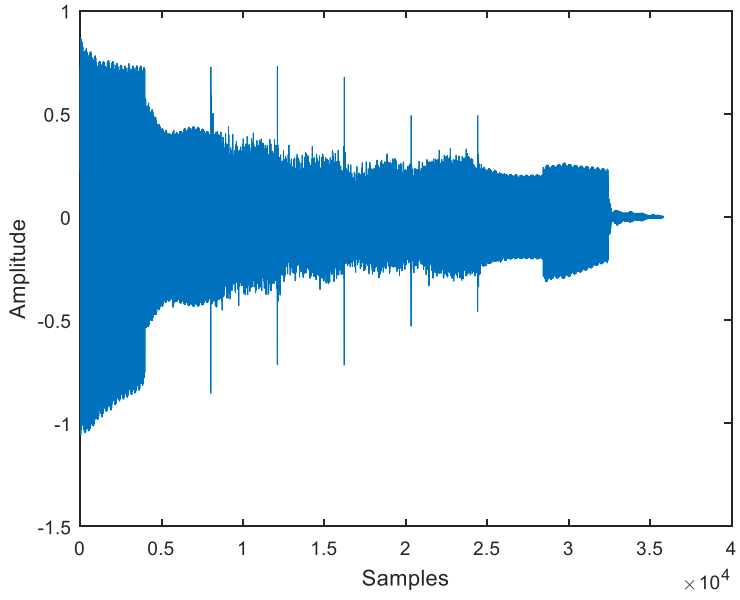

Figure 5.19: OFDM Packet NM.1.

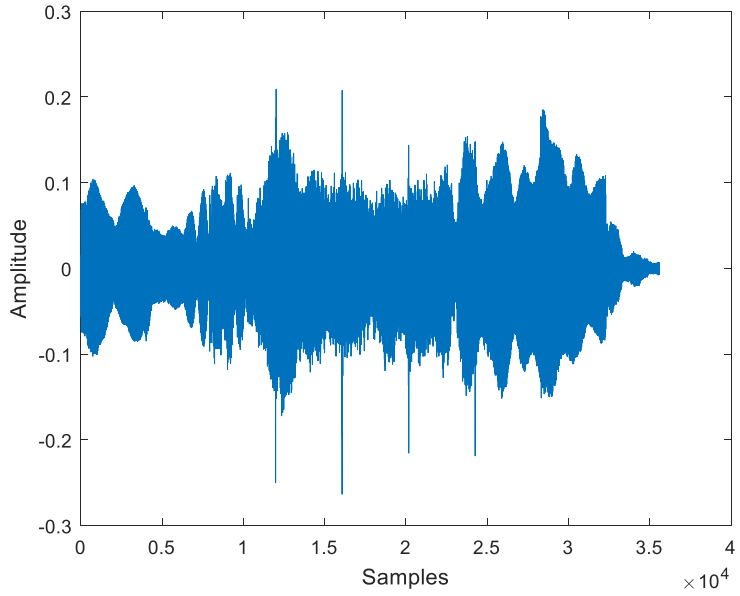

Figure 5.20: OFDM Packet FM.1.

Figure 5.20 shows the additional distortion that results from having the receiver at a further distance away. While the Packet NM.1 is clearly recognizable, Packet FM.1 was subject to more

multipath distortion. In the next section the process of Doppler warp Correction is shown, using the preamble and postamble sinusoids present in the packet.

5.3.2 Doppler Warp Correction using Preamble/Postamble

Once a packet was extracted from the signal, the sinusoids were used to estimate α and β using (3.22). In Chapter 3, frequency estimates taken at the beginning and end of a burst were used to estimate a nonlinear Doppler warp. Preamble/postamble frequency measurements – taken at specific times, denoted $\tilde{t}_0$ and $\tilde{t}_1$ for the preamble and postamble respectively – were used to determine the alpha/beta estimates for the Doppler warp.

The 5 kHz tone was used because the *NAM* was greater compared to the 3 kHz sinusoid overall in the measurements taken. $\tilde{t}_0$ and $\tilde{t}_1$ are found from finding the intervals over which the energy of the 5 kHz tone was the greatest in the first and second half of the packet. Figure 5.21 shows the absolute value of the extracted 5 kHz sinusoid, and the $\tilde{t}_0$ and $\tilde{t}_1$ points used.

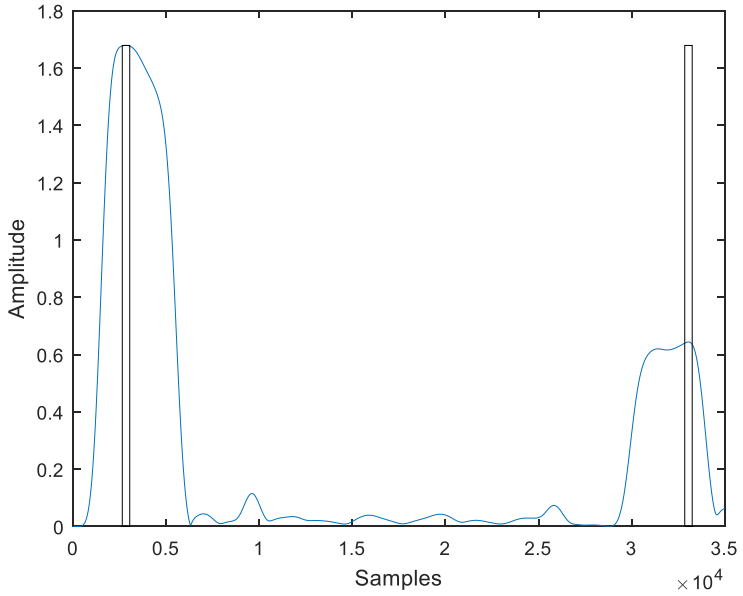

Figure 5.21: Absolute Value of Extracted 5 kHz Sinusoid from Packet NM.1.

$\tilde{t}_0$ and $\tilde{t}_1$ are found from finding the intervals over which the energy of the 5 kHz tone was the greatest in the first and second half of the packet. The centers of the intervals with the greatest sinusoidal energy found in the first and second half of the packet were taken to be $\tilde{t}_0$ and $\tilde{t}_1$, respectively. The time instant at which the frequency estimate of the pre-amble sinusoid was made, $\tilde{t}_0$, was determined to be 0.0319 seconds (or at sample 1407), while $\tilde{t}_1$ was determined to be 0.6942 seconds (or at sample 30614). The intervals around $\tilde{t}_0$ and $\tilde{t}_1$ are used to obtain frequency estimates are shown in Figures 5.21 and 5.22.

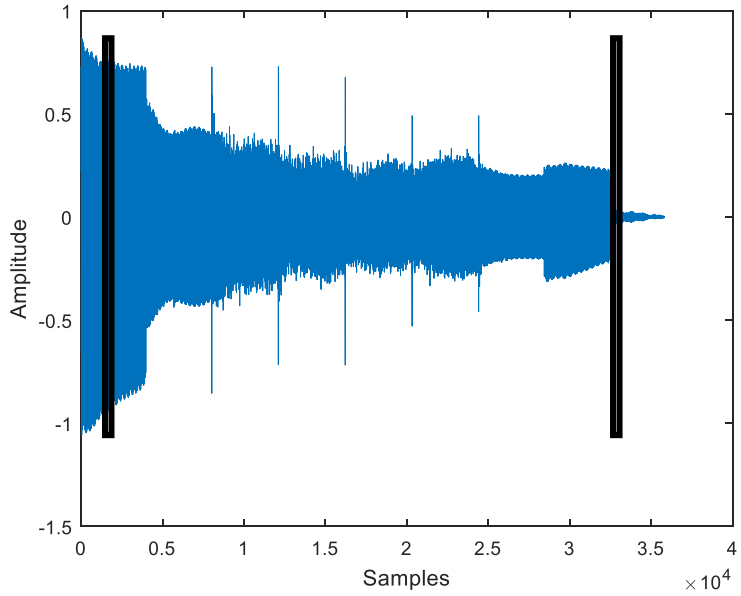

Figure 5.22: Packet NM.1 with black rectangles indicating the preamble and postamble time intervals used to obtain Frequency Estimates.

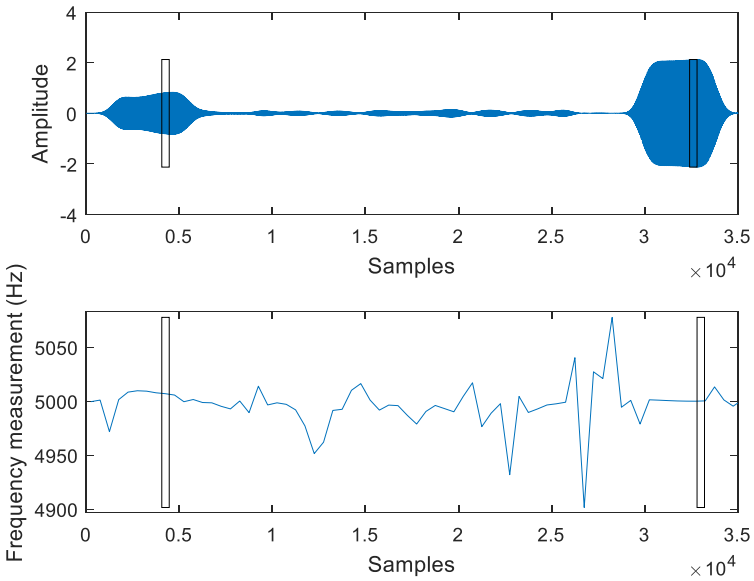

Figure 5.23: Extracted 5 kHz tone (top) and Frequency Estimate (bottom) from Packet NM.1.

Figure 5.23 shows the frequency estimates over time. The rectangles indicate the time intervals used to take the frequency estimates used in the alpha beta estimation. Figure 5.24 shows

the magnitude spectrum estimate of the pre-amble and post-amble sinusoids observed over the 400 sample window with Hanning shaping. The chirp-z transform was used to estimate the magnitude spectrum.

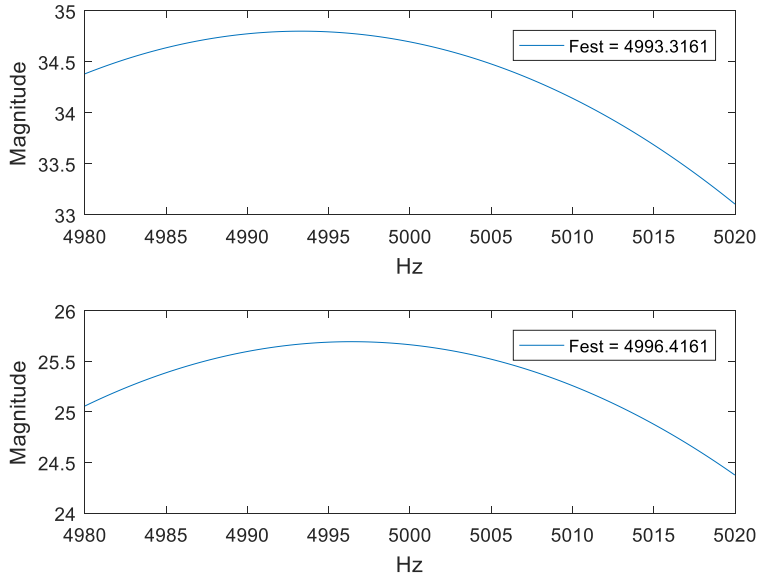

Figure 5.24: Magnitude spectrum of the preamble (top) and postamble (bottom).

The frequency of the pre-amble and post-amble sinusoids, estimated by looking for the peak in the magnitude spectrum in Figure 5.24, was equal to 4993.3 Hz and 4996.4 Hz respectively (Doppler shifts of about -7 and -4 Hz respectively). These frequency estimates (corresponding to $\frac{1}{\tilde{T}_0}$ and $\frac{1}{\tilde{T}_1}$ from Section 3.2) are used to generate alpha and beta parameters for use in the Doppler Warp Correction.

As mentioned in Section 5.2, areas where the sinusoidal energy tended to be large led to better frequency estimates. The 5 kHz tone was used because the energy was greater for that sinusoid overall in the measurements taken. Using the values for $\tilde{T}_0$, $\tilde{T}_1, \tilde{t}_0$, and $\tilde{t}_1$, α and β were

estimated to be -0.0059 and -4.6951$_{10}$-4 respectively. Figures 5.25 and 5.26 show the OFDM signal corresponding to the FM Experiment.

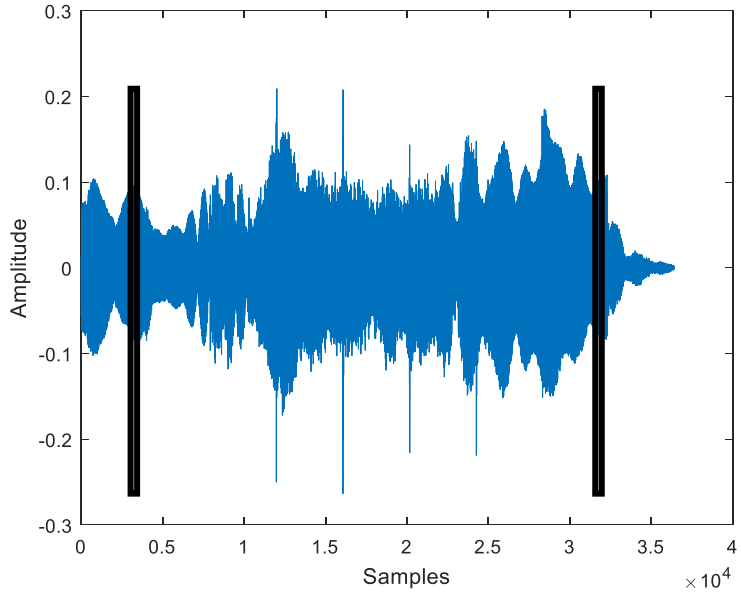

Figure 5.25: Packet FM.1 with black rectangles indicating the preamble and postamble time intervals used to obtain Frequency Estimates.

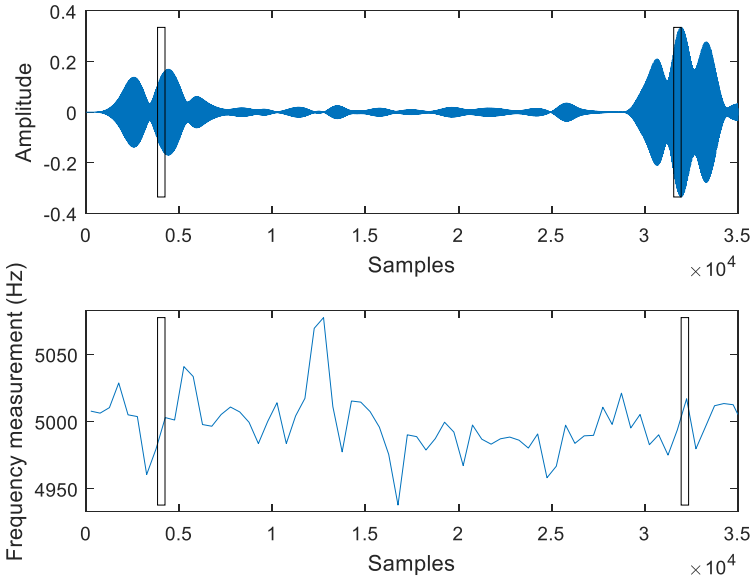

Figure 5.26: Extracted 5 kHz tone (top) and Frequency Estimate (bottom) from Packet FM.1.

Note in Fig. 5.26 that the frequency estimates vary wildly over the course of the 5 kHz sinusoid. Substantial multipath can cause the frequency estimates, and consequently, the Doppler estimate to be incorrect.

Figures 5.22 and 5.26 show how the frequency of the 5 kHz tone changes over the course of the OFDM burst. The information from the frequency estimates can be used to estimate the velocity of the OFDM burst. If f_{tx} is the (known) frequency of the sinusoid used and $\hat{f}_{rx}(t)$ the estimated frequency of the sinusoid, the relative velocity estimate can be calculated as:

$$\hat{v}(t) = \left(\frac{\hat{f}_{rx}(t) - f_{tx}}{f_{tx}} \right) c \tag{5.1}$$

where c is the speed of sound in the medium.

The change in frequency and relative velocity over the duration of the NM.1 Packet are shown in Figure 5.27.

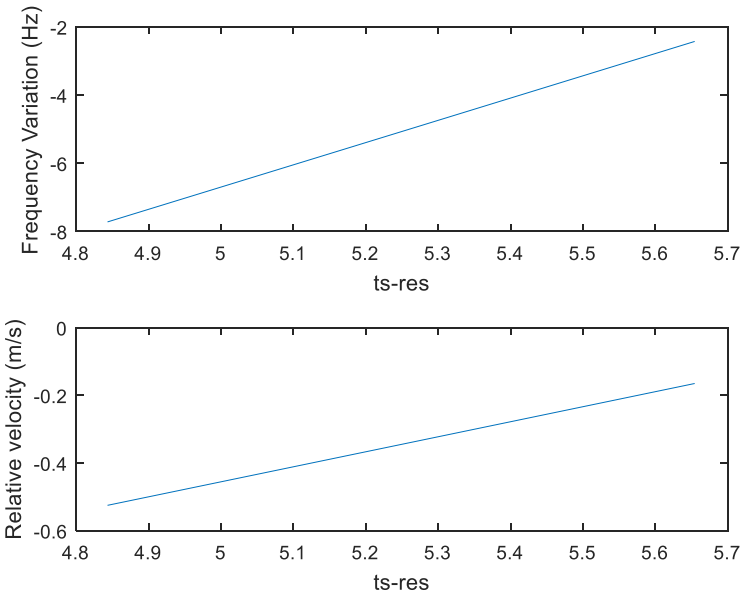

Figure 5.27: Frequency Variation (top) and Relative Velocity (bottom) of Packet NM.1.

The relative velocity is seen in Figure 5.27 to be on the order of 0.3 m/s, or roughly 1 foot/s. This matches well the relative speed of the arm moving across the receiver location. Ts-res stands for the resampled time instants found from alpha-beta estimates.

The change in frequency and relative velocity over the duration of the FM.1 Packet is shown in Figure 5.28.

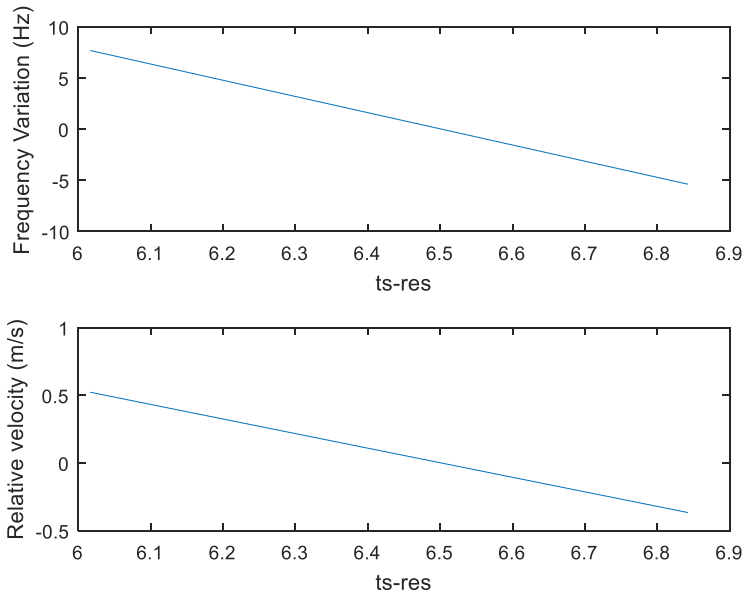

Figure 5.28: Frequency Variation (top) and Relative Velocity (bottom) of Packet FM.1.

The relative velocity is seen in Figure 5.28 to be on the order of 1 m/s, or roughly 3 foot/s. This is slightly faster than the relative speed of the arm moving across the receiver location. Ts-res stands for the resampled time instants found from alpha-beta estimates.

Having found an alpha and beta value from the preamble/postamble frequency estimates, (3.4) and (3.5) are used to undo the Doppler warp by creating a resampled signal. The inverse of the Doppler warp for the first packet is shown in Figure 5.29 compared to a uniform warp (represented as a straight line).

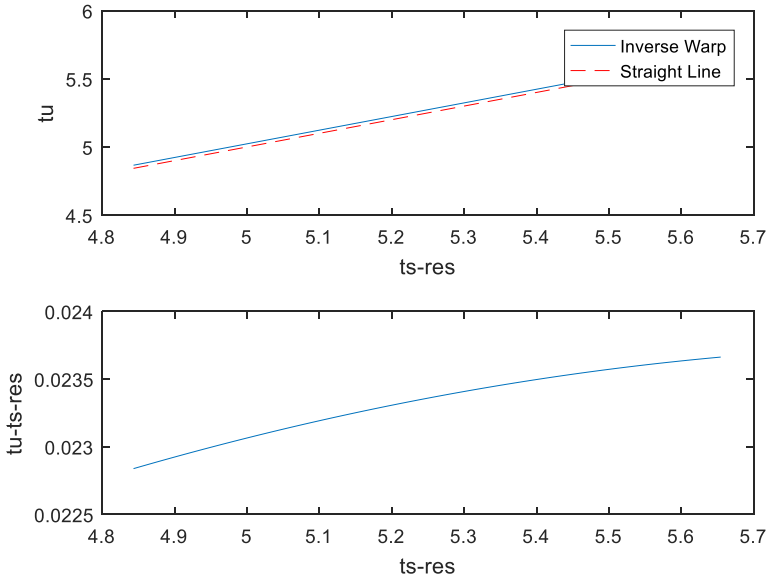

Figure 5.29: Packet NM.1 Inverse Nonlinear and Uniform Doppler warp (top) and Difference between Nonlinear and Uniform Doppler warps (bottom).

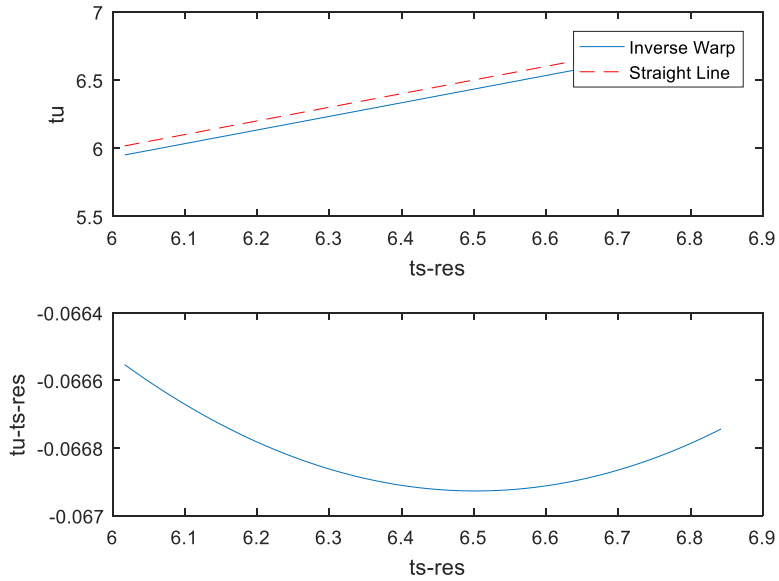

Figure 5.30: Packet FM.1 Inverse Nonlinear and Uniform Doppler warps (top) and Difference between Nonlinear and Uniform Doppler warps (bottom).

After the Doppler warp has been estimated and corrected for, the normal OFDM demodulation process shown in Section 4.4 is carried out on the resulting signal. In Chapter 4, to

determine the exact synchronization point corresponding to the lowest BER, the OFDM demodulation process was done for every 20th sample from sample 1000 to sample $23_{10}3$ of the extracted packet. The results of this demodulation from overlapping 8192 sample frames of Packet NM.1 are shown in Fig. 5.31.

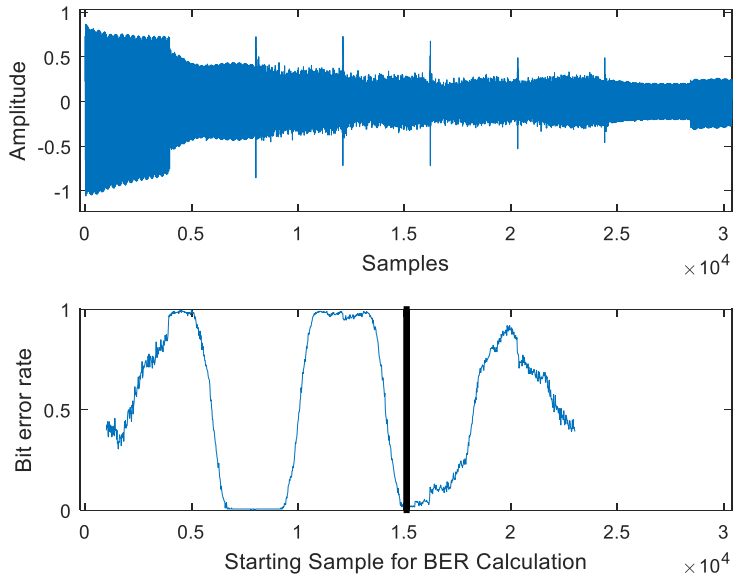

Figure 5.31: Packet NM.1 (top) and Packet NM.1 BER (bottom) using preamble/postamble for Doppler Warp Correction.

In Figure 5.31, the black line is used to indicate the synchronization point that generates the lowest BER. The synchronization point will be used as the point shown for the Channel Magnitude Estimate and the Channel Phase Estimate.

The BER calculation for several synchronization points across Packet FM.1 is shown in Figure 5.32.

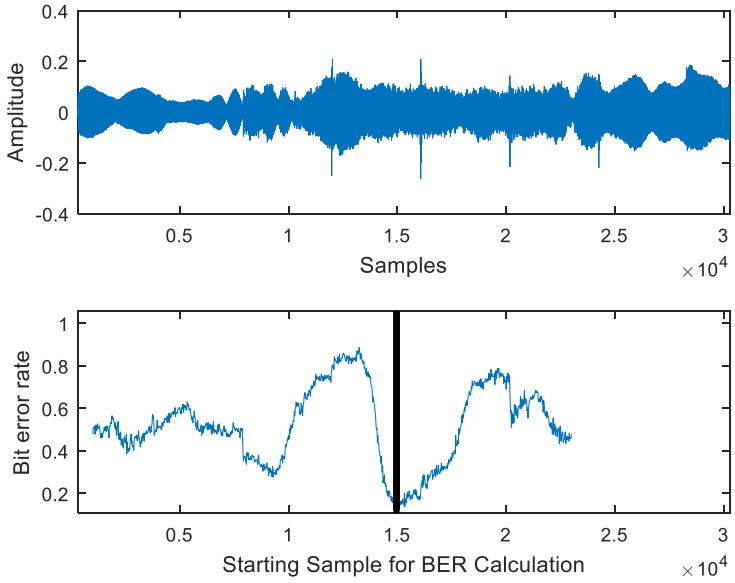

Figure 5.32: Packet FM.1 (top) and Packet FM.1 BER (bottom) using preamble/postamble for Doppler Warp Correction.

Figure 5.32 shows that the BER of the packets get worse as the distance between the receiver and transmitter is increased. A black line is again used to indicate the point of the lowest BER, and consequently, the synchronization point used to the show the Channel magnitude and phase estimates and the received symbols.

In the demodulation of the OFDM, first a channel estimate is taken and then used to equalize the OFDM, as explained in Subsection 4.4.2. The Channel magnitude and phase estimates are shown in Figures 5.33 and 5.34 for Packet NM.1.

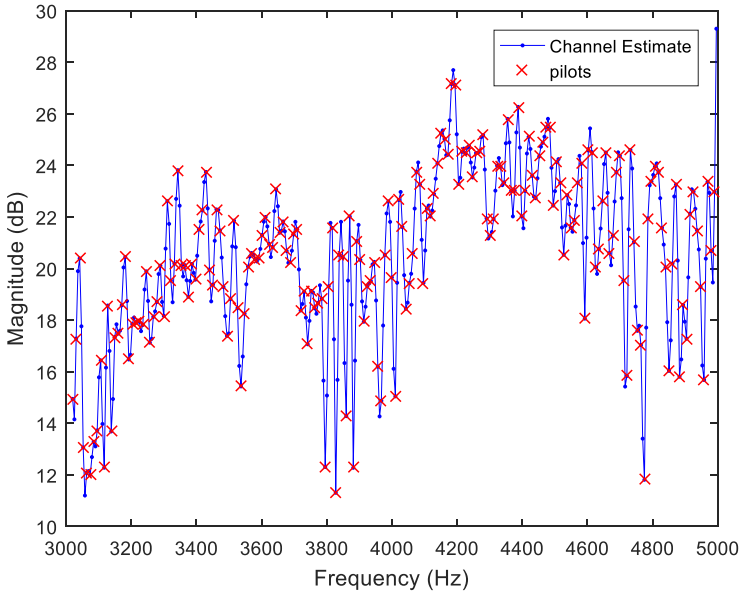

Figure 5.33: Channel magnitude response estimate for Packet NM.1.

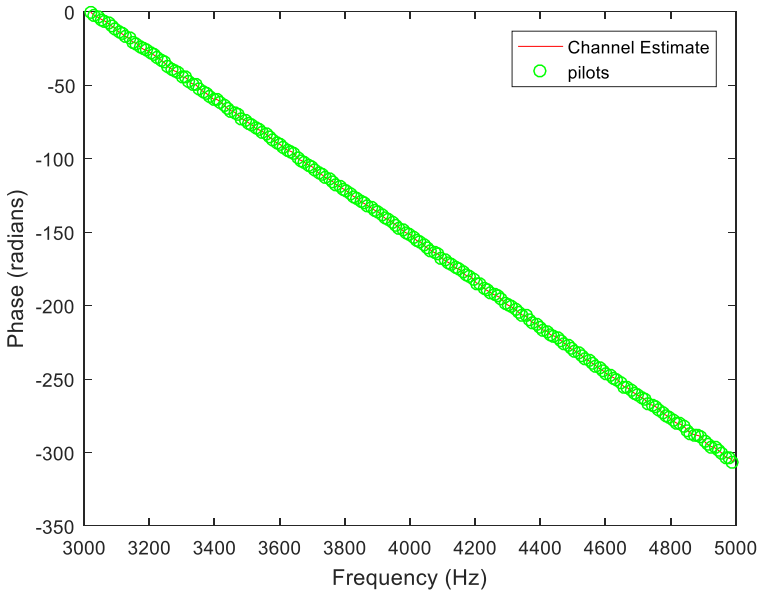

Figure 5.34: Channel phase response estimate for Packet NM.1.

Note the nearly linear phase in Fig. 5.34, indicating that the synchronization point chosen is a short distance away from the beginning of the symbol.

The Channel and Phase magnitude estimates are shown in Figures 5.35 and 5.36 for Packet FM.1.

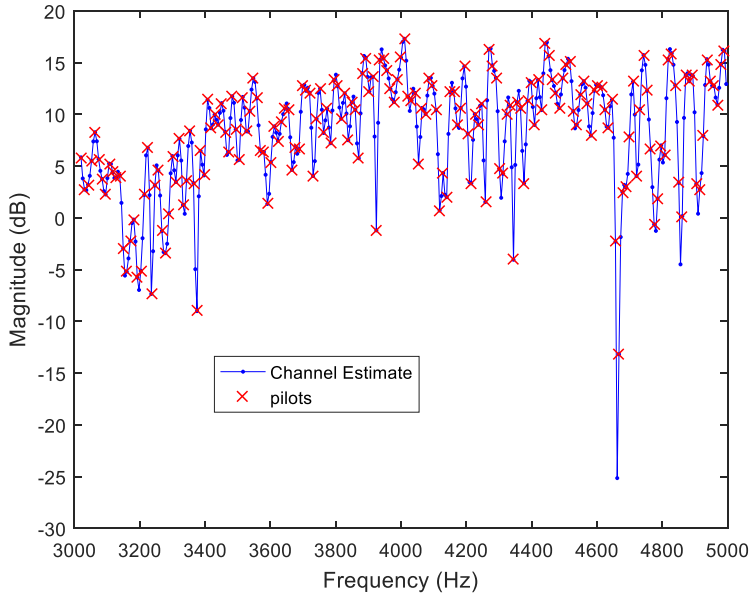

Figure 5.35: Channel magnitude response estimate for Packet FM.1.

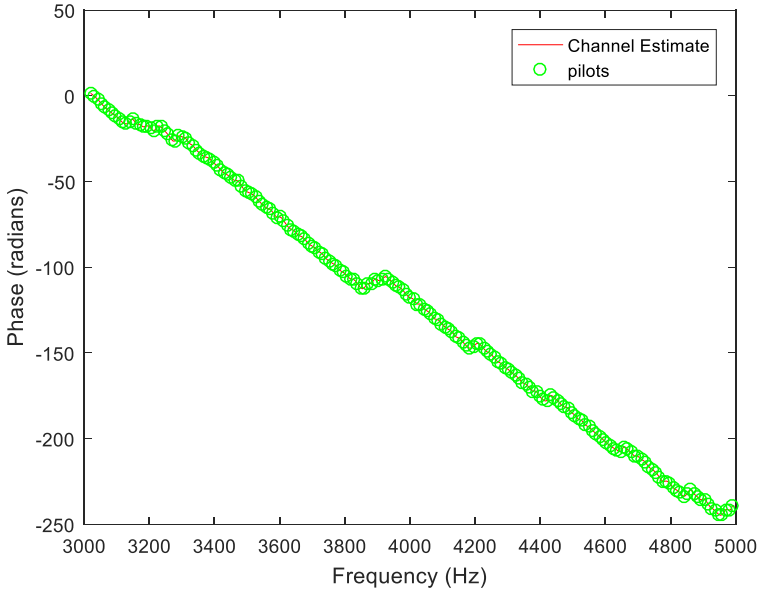

Figure 5.36: Channel phase response estimate for Packet FM.1.

These Channel and Phase magnitude estimates are in turn used to extract the bits from the OFDM. The synchronization point used is the point of the lowest BER seen in Figure 5.31.

The recovered bits for Packet NM.1 are shown in Figure 5.37.

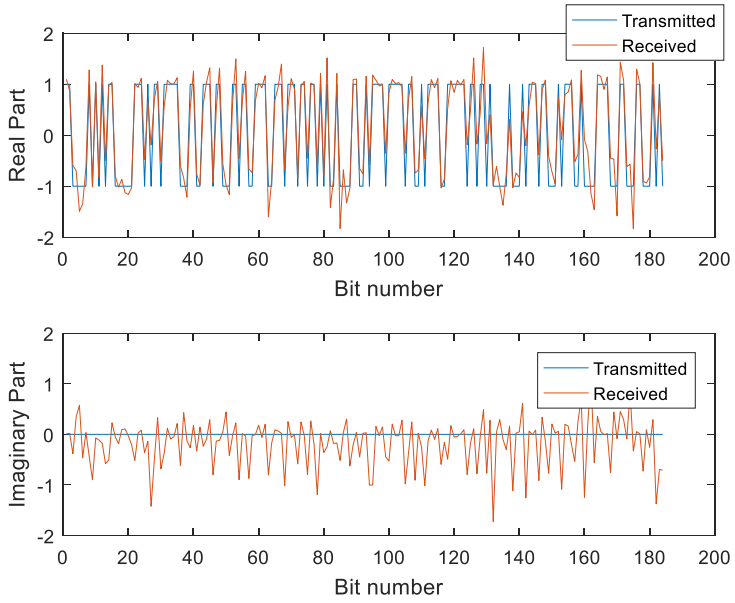

Figure 5.37: Extracted symbols from Packet NM.1.

As seen in Figure 5.37 the Doppler Warp Correction Model corrects for the Doppler warp, giving a 0 BER. However, this may not hold across all packets. Uncertainty in the frequency measurement can cause error. The recovered bits for Packet FM.1 are shown in Figure 5.38.

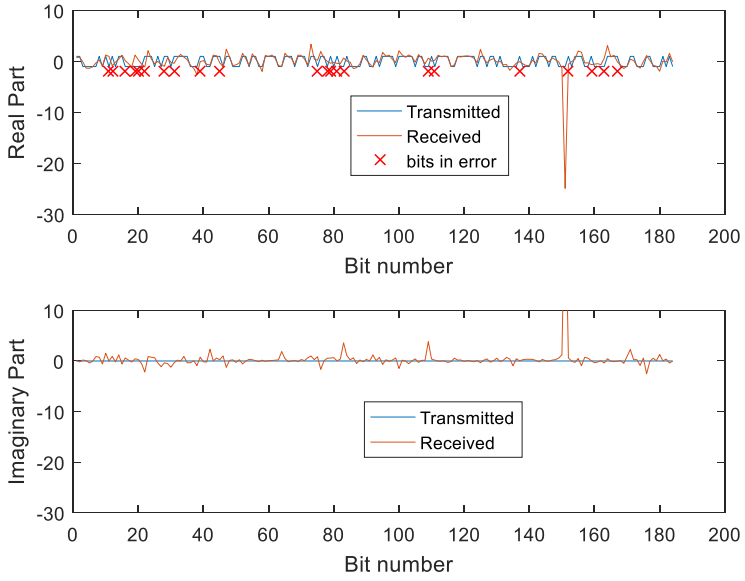

Figure 5.38: Extracted symbols from Packet FM.1.

The received bits for Packet FM.1 show that the additional distance between the transmitter and receiver affects the performance of the receiver. In the next section is investigated if using sinusoids that occur during the OFDM burst can improve the Doppler Warp Model and consequently the overall performance of the receiver.

The resultant alpha, beta, and BER values for all 4 packets in the NM and FM Experiments are summarized in Tables 5.1 and 5.2.

Table 5.1: Summary of Parameters for NM Experiment using 5 kHz Preamble/Postamble.

Packet #	T (msec)	$\hat{\alpha}$	$\hat{\beta}$	$\tilde{T}_0$ (msec)	$\tilde{T}_1$ (msec)	BER (based on 184 data bits)
1	0.2	0.0079	-0.00065	0.2003	0.2001	0
2	0.2	-0.0103	-0.00068	0.2008	0.2000	0.0761
3	0.2	-0.0118	0.00061	0.1999	0.2001	0.0163
4	0.2	-0.0191	0.00082	0.1999	0.2000	0.0815

Table 5.2: Summary of Parameters for FM Experiment using 5 kHz Preamble/Postamble.

Packet #	T (msec)	$\hat{\alpha}$	$\hat{\beta}$	$\tilde{T}_0$ (msec)	$\tilde{T}_1$ (msec)	BER (based on 184 data bits)
1	0.2	-0.0342	-0.0012	0.1997	0.2002	0.12
2	0.2	0.0382	-0.0020	0.2007	0.2008	0.36
3	0.2	-0.0447	-0.0019	0.2003	0.1992	0.35
4	0.2	-0.0143	0.0007	0.1998	0.1992	0.28

The alpha and beta values were calculated using the preamble and postamble measurements of the 5 kHz sinusoid. The 5 kHz sinusoid had more energy, and consequently was less distorted due to the multipath of the channel. As observed in Table 5.2, in the case of the FM Experiment, where the receiver is farther away from the transmitter and Doppler is affecting the signal, the BER results are quite a bit poorer than for the NM experiment. It is suspected that poorer frequency estimates, which are subsequently used to undo the Doppler warp, can be attributed to the added noise and multipath affecting the received signal. In the next section, the use of frequency estimates for the 2 and 6 kHz sinusoids taken before, after, and during the OFDM burst is investigated for generating the alpha and beta parameters for the Doppler Warp Model.

5.3.3 Doppler Warp Correction using Out of Band sinusoids

The previous section showed the BER performance resulting from Doppler warp correction using frequency estimates derived from the preamble and postamble signals. However, using the preamble/postamble frequency estimates can easily violate the validity of the assumed Doppler model since severe multipath affects the accuracy of the frequency estimates used to determine the Doppler warp model. An alternative is to use the out of band (OOB) sinusoids at 2 and 6 kHz that

exist during the preamble, postamble, and OFDM symbol to estimate the alpha and beta describing the warp characteristics. In the example of the NM.1 packet in Figure 5.19, using the 6 kHz frequency estimate gives a different $\tilde{t}_1$ that occurs during the OFDM burst. The estimates that are used are shown in Figure 5.39. Figure 5.40 shows the frequency estimates for the NM Experiment.

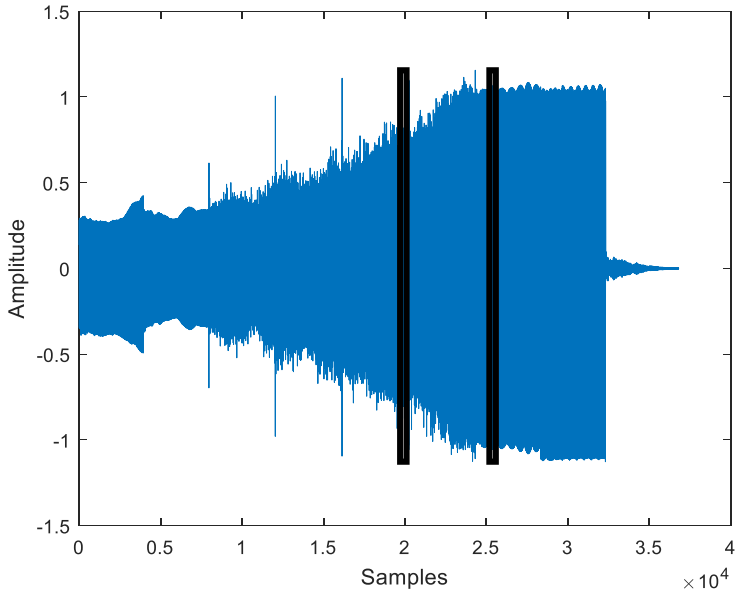

Figure 5.39: Packet NM.1 with black rectangles indicating the time intervals used to obtain Frequency Estimates.

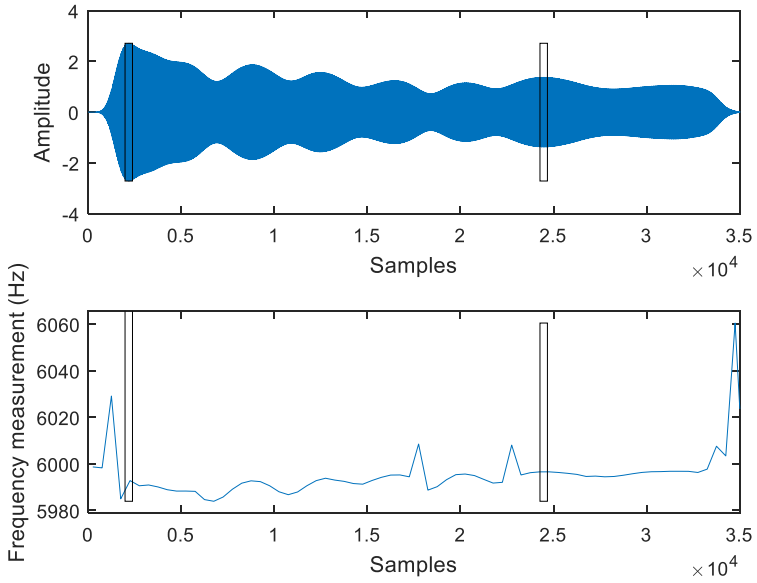

Figure 5.40: Extracted 6 kHz tone (top) and Frequency Estimate (bottom) from Packet NM.1.

Figure 5.39 and Figure 5.40 show that unlike with the preamble/postamble method, the frequency estimates are taken towards the middle of the burst, where the multipath has not affected the signal as much.

In the example of the FM.1 packet in Figure 5.20, using the 6 kHz frequency estimate gives a different $\tilde{t}_1$ that occurs during the OFDM burst. The estimates that are used are shown in Figure 5.41. Figure 5.42 shows the frequency estimates for the FM Experiment.

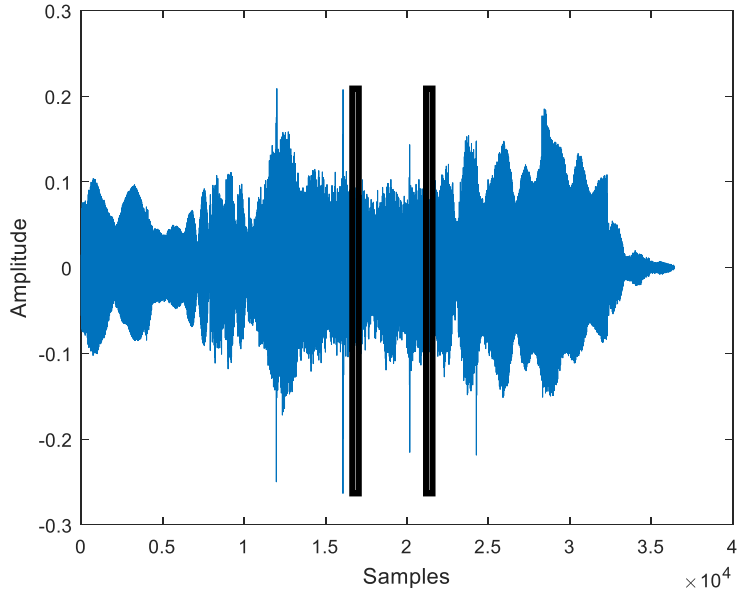

Figure 5.41: Packet FM.1 with black rectangles indicating the time intervals used to obtain Frequency Estimates.

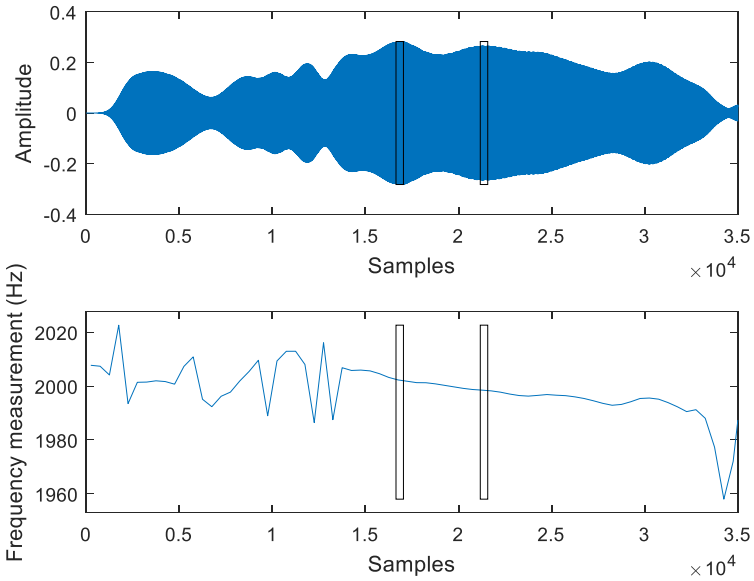

Figure 5.42: Extracted 2 kHz tone (top) and Frequency Estimate (bottom) from Packet FM.1.

Figure 5.41 and Figure 5.42 show that unlike with the preamble/postamble method, the frequency estimates are taken towards the middle of the burst, where the multipath has not affected the signal

as much. Note that in this case, the sinusoid extracted for frequency estimation was the 2 kHz sinusoid, a result of the determination that the 2 kHz component had the larger normalized absolute magnitude over the course of the packet.

The change in frequency and relative velocity over the duration of the burst for Packet NM.1 and FM.1 are shown in Figures 5.43 and 5.44, respectively.

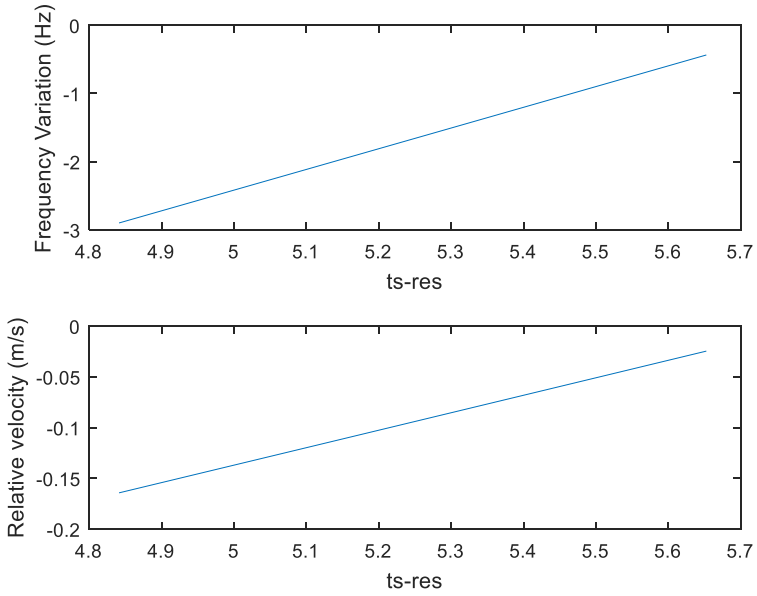

Figure 5.43: Packet NM.1 Frequency Variation (top) and Relative Velocity (bottom).

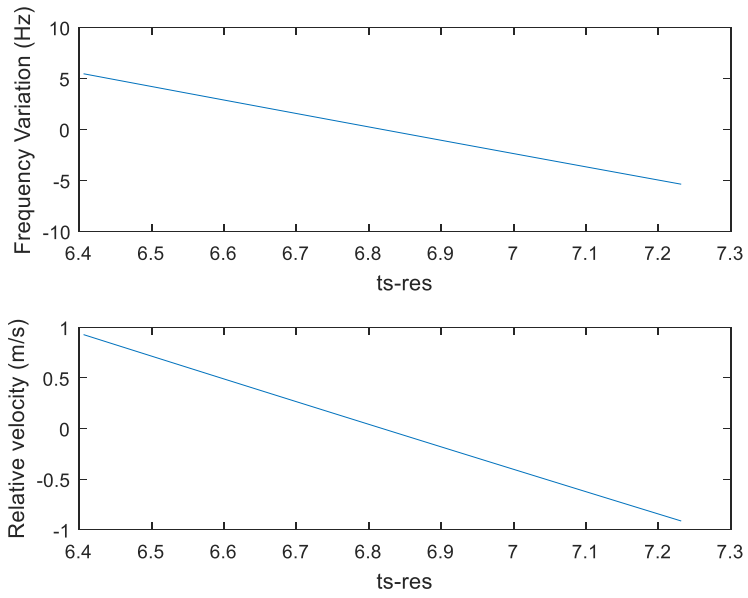

Figure 5.44: Packet FM.1 Frequency Variation (top) and Relative Velocity (bottom).

The relative velocity is seen in Figure 5.43 to be on the order of 0.15 m/s, or roughly 0.5 foot/s. Though this velocity measurement doesn't match up perfectly with the preamble /postamble velocity measurement in Figure 5.27, it is similar. The relative velocity is seen in Figure 5.44 to be on the order of 1 m/s, or roughly 3 feet/s. This velocity seems to be realistic compared to the movement of the arm and is close to the measurement from Figure 5.28. This would indicate that the frequency measurements Ts-res are the resampled time instants found from alpha-beta estimates.

Now that the frequency estimates are found using the OOB sinusoids, the inverse of the Doppler warps for Packets NM.1 and FM.1 are found and compared to a uniform warp (which is represented as a straight line). The inverse warps for Packets NM.1 and FM.1 are shown in Figures 5.45 and 5.46 respectively.

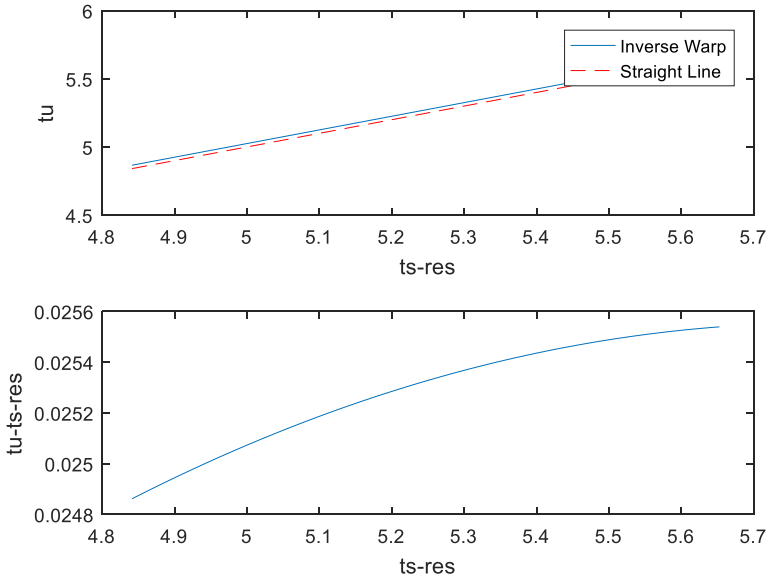

Figure 5.45: Packet NM.1 Inverse Nonlinear and Uniform Doppler warp (top) and Difference between Nonlinear Doppler warp and Uniform Doppler warp (bottom).

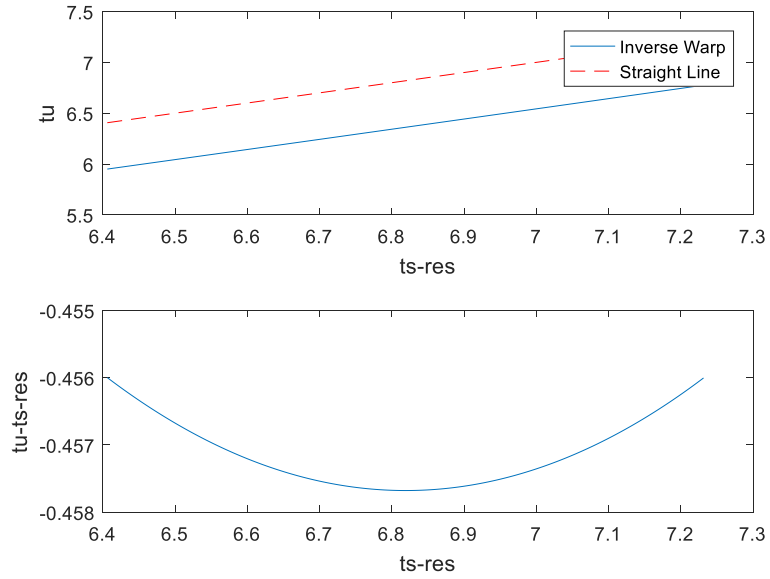

Figure 5.46: Packet FM.1 Inverse Nonlinear and Uniform Doppler warp (top) and Difference between Nonlinear Doppler warp and Uniform Doppler warp (bottom).

After using the inverse warps shown in Figures 5.45 and 5.46 to correct for Doppler warp, the BER is calculated over the entire Doppler Corrected packet for packets. The BER results over the

range of synchronization points, for Packets NM.1 and FM.1, are shown in Figures 5.47 and 5.48, respectively. The black line is used to indicate the synchronization point that yields the lowest BER.

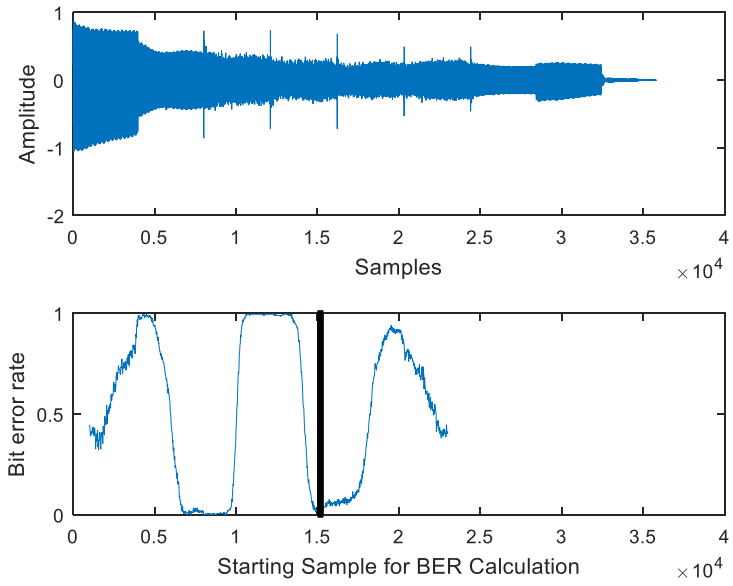

Figure 5.47: Packet NM.1 (top) and Packet NM.1 BER using OOB sinusoids for Doppler Warp Correction.

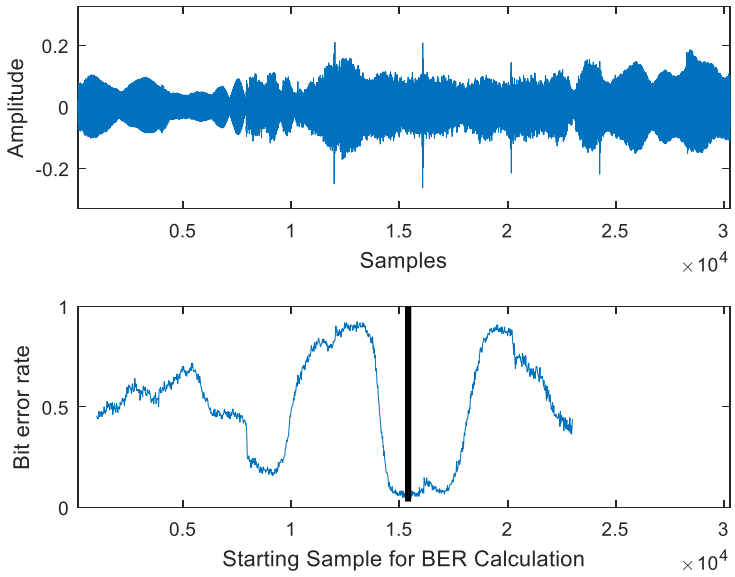

Figure 5.48: Packet FM.1 (top) and Packet FM.1 BER using OOB sinusoids for Doppler Warp Correction.

After calculating the BER over the course of all synchronization points the lowest BER for Packet NM.1 is found to be 0 (0 out of 184 bits), while the BER found for FM.1 is 0.03804 (or 7 bits out of 184). The extracted symbols for the two synchronization points are shown in Figures 5.49 and 5.50.

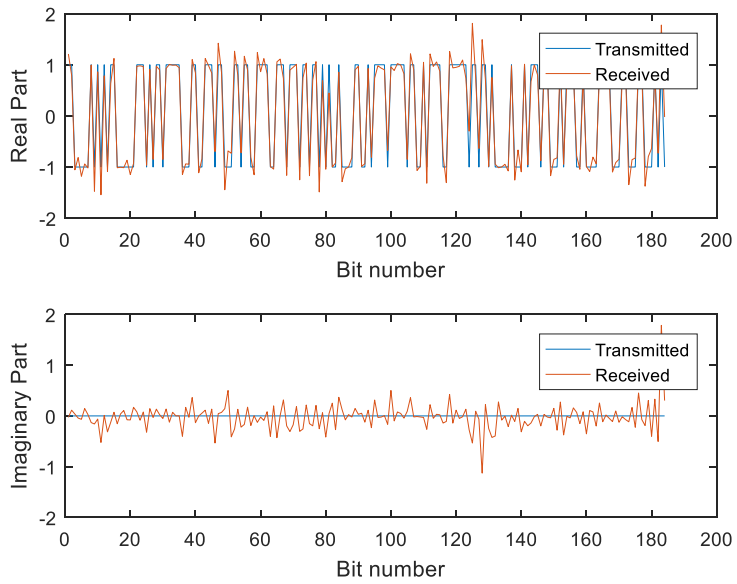

Figure 5.49: Extracted symbols from Packet NM.1 using OOB sinusoids to estimate the Doppler Warp Model.

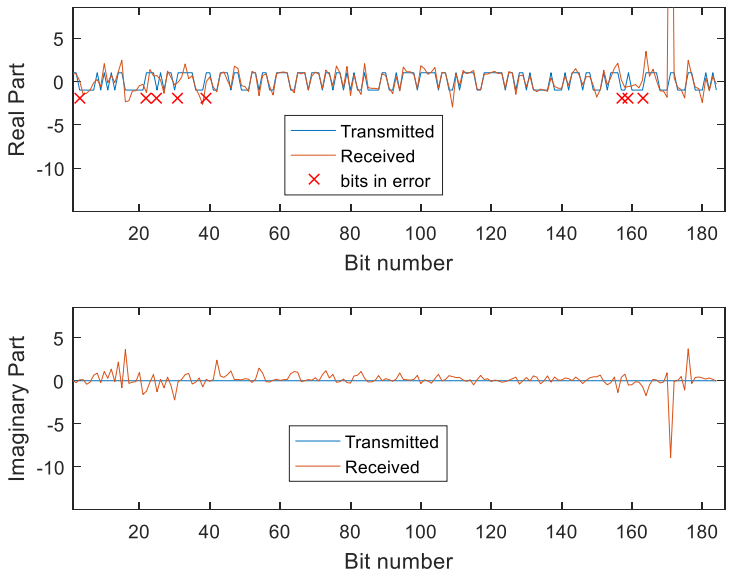

Figure 5.50: Extracted symbols from Packet FM.1 using OOB sinusoids to estimate the Doppler Warp Model.

Figures 5.49 and 5.50 show an improvement in BER (0/184 and 8/184) using the OOB sinusoids compared to the BER (0/184 and 22/184) using the preamble-postamble shown in Figure 5.37 and Figure 5.38 to estimate the Doppler Warp. Tables 5.3 and 5.4 summarize the results for all 4 packets using the OOB sinusoid to estimate and correct for the Doppler Warp.

Table 5.3: Summary of Results for NM Experiment using OOB Sinusoids.

Packet #	T (msec)	$\hat{\alpha}$	$\hat{\beta}$	$\tilde{T}_0$ (msec)	$\tilde{T}_1$ (msec)	BER (out of 184 data bits)
1	0.1667	0.0059	-0.0005	0.2003	0.2001	0
2	0.1667	0.1027	-0.0071	0.2008	0.2000	0
3	0.1667	-0.0191	0.0010	0.1999	0.2001	0
4	0.1667	-0.0118	0.0005	0.1999	0.2000	0

Table 5.4: Summary of Results for FM Experiment using OOB Sinusoids.

Packet #	T (msec)	$\hat{\alpha}$	$\hat{\beta}$	$\tilde{T}_0$ (msec)	$\tilde{T}_1$ (msec)	BER (out of 184 data bits)
1	0.5	-0.1342	0.0098	0.5006	0.4996	0.043
2	0.1667	-0.2895	0.0030	0.1664	0.1672	0.12
3	0.5	-0.1950	0.0085	0.4998	0.5004	0.060
4	0.1667	-0.0326	-0.0014	0.1664	0.1671	0.15

Note that in most cases, the 6 kHz sinusoid was used to estimate the Doppler warp except in the case of Packets FM.1 and FM.3. In the latter cases, the 2 kHz sinusoid had more energy over the packet interval and was therefore used instead.

The BER results in Tables 5.3 and 5.4, compared to Tables 5.1 and 5.2 respectively, show that there can be a significant advantage to using the sinusoids at 2 and 6 kHz that exist during the

course of the OFDM symbol in addition to (or instead of) the sinusoids at 2 and 6 kHz that are part of the preamble/postamble. In the FM Experiment, comparing Tables 5.2 and 5.4, the BER improved from 0.36 to 0.15 or less, which is a significant reduction. Even in the case of the NM Experiment, comparing Tables 5.1 and 5.3, the BER when using the OOB sinusoids produced a BER improvement over using the preamble/postamble sinusoids, rendering all BER to 0. Both methods yielded good results when Doppler was affecting the signal relatively more than the multipath.

A practical benefit of using the OOB sinusoids is that the temporal extent of the preamble and postamble signals can be drastically reduced, allowing packets to be sent more frequently, and thus increasing the overall data throughput. Note that this consideration reflects a tradeoff between bandwidth and the length of the signal (throughput).

6 Conclusion and Future Work

Several new techniques for Doppler correction and packet detection were presented, ultimately aimed at use in an underwater OFDM transceiver. The packet detection part of the work uses a Fraction of Sinusoidal Energy (*FOSE)* measure computed over the entire received signal to detect packets with a higher degree of certainty compared to a normal energy detector. The Doppler effect is modeled as a 2^{nd} order polynomial change in the time scale. Two different Doppler correction techniques are presented ultimately meant for use in underwater acoustic channels. The preamble/postamble approach appends a preamble and postamble – composed of multiple sinusoids – in time to each OFDM symbol in order to estimate the Doppler warp affecting the signal and thereby facilitate Doppler correction. The Out of Band sinusoid approach estimates the Doppler warp based on sinusoids that are present at the same time as the OFDM symbol but outside of the OFDM bandwidth in order to prevent interference.

Experiments were performed over an audio frequency acoustic channel in a reverberant room, as a convenient proxy to an underwater channel. Both methods of Doppler estimation and correction worked well for a receiver moving relatively fast (~1.5 ft/sec) with the receiver (microphone) near the transmitter (speaker). However, the second method – using sinusoids during the OFDM symbol – worked better in situations where the microphone was far from the transmitter and thus subject to relatively stronger multipath and noise. The better performance is hypothesized to be due to getting more accurate frequency estimates, as these form the basis for more accurate Doppler warp estimation and subsequent correction. In the case of the near experiment (~1 foot transmit-receive distance), the performance of both methods of Doppler warp correction approached the performance of the stationary experiment (both with a BER of 0 out of 184).

However, in the far experiment (~5 foot transmit-receive distance) the BER of the methods using the Doppler warp correction was at worst 0.163 (with 30 of 184 bits in error) while the performance with a stationary receiver produced a BER of at worst 0.0269 (with 5 out of 184 bits in error). This performance indicates that possibly improvements could be made to lower the BER.

Several assumptions underlie the Doppler model used here. One assumption is that the warp follows a second order polynomial, which needs only two frequency estimates. Another key assumption is that the Doppler rate is the same over each multipath component. Neither of these assumptions always holds, and the performance of the transceiver will be affected accordingly. However, note that the OOB Doppler estimation method can be readily modified to incorporate frequency estimates taken at additional time instants, making the second order polynomial warp assumption more valid over each (now shorter) time interval.

Future work for this research could include implementing the OFDM transceiver with the time warp estimation method on hardware. This setup with the hardware could be used to conduct experiments in an underwater environment. The use of specialized hardware would also help in relaxing constraints for the OFDM transceiver. These constraints include the 44.1 kHz sampling rate and consequently the 3-5 kHz bandwidth, choices made due to computer soundcard characteristics. Implementing the underwater setup would require two separate transducers, one at the transmit end and one at the receive end attached to the hardware that acts as the transceiver. Additionally, the implementation of a MIMO setup could be used to provide better performance. The setup could use several microphones placed together side by side moving along the path in the moving experiments, with MIMO based techniques potentially correcting for the different Doppler rates along different paths. The implementation of a MIMO setup could help remove one of the key assumptions made for this experiment.

Bibliography

[1] J. Preisig, Acoustic propagation considerations for underwater acoustic communications network development, ACM SIGMOBILE Mobile Computing and Communications Review, 11(4): p. 2-10, 2007.

[2] R. J. Urick, Principles of Underwater Sound. 1983, New York, NY: McGraw-Hill

[3] C. A. Balanis, Advanced Engineering Electromagnetics. 1989: John Wiley & Sons.

[4] M. Kerker, The Scattering of Light and other Electromagnetic Radiation. 3rd ed. 1973, New York, NY: Academic Press.

[5] C. P. Etter, Underwater Acoustic Modeling Principle, Techniques And Applications. 1991: Elsevier Science Publishers.

[6] M. Chitre, J. Potter, and H. Ong Sim. Underwater acoustic channel characterisation for medium-range shallow water communications, MTTS/IEEE TECHNO-OCEAN, pp. 40-45, 2004.

[7] R. Coates, Underwater Acoustic Systems. 1989, New York, NY: Wiley.

[8] L. Lanbo, Z. Shengli, and C. Jun-Hong, Prospects and problems of wireless communication for underwater sensor networks, Wireless Communications and Mobile Computing , 8(8): pp. 977-994, 2008.

[9] M. Stojanovic, Recent advances in high-speed underwater acoustic communications, IEEE Journal of Oceanic Engineering, 21(2): pp. 125-136, 1996.

[10] N. R. Chapman, and A. Price, Low frequency deep ocean ambient noise trend in the Northeast Pacific Ocean. The Journal of the Acoustical Society of America, 129(5): pp. EL161-EL165, 2011.

[11] D. B. Kilfoyle and A. B. Baggeroer, The state of the art in underwater acoustic telemetry. IEEE Journal of Oceanic Engineering, 25(1): pp. 4-27, 2000.

[12] S. Weinstein and P. Ebert, Data Transmission by Frequency-Division Multiplexing Using the Discrete Fourier Transform, IEEE Transactions on Communication Technology, 19(5): pp. 628-634, 1971.

[13] R. V. Nee and R. Prasad, OFDM for Wireless Multimedia Communications. 2000: Artech House, Inc. 280.

[14] T. M. Schmidl and D. C. Cox, Low-overhead, low-complexity [burst] synchronization for OFDM, 1996 IEEE International Conference on Converging Technologies for Tomorrow's Applications, pp. 1301-1306,1996.

[15] J. J. van de Beek, et al., Low-complex frame synchronization in OFDM systems, Fourth IEEE International Conference on Universal Personal Communications, pp. 982-986, 1995.

[16] K. Taura, et al., A digital audio broadcasting (DAB) receiver, IEEE Transactions on Consumer Electronics, 42(3): pp. 322-327, 1996.

[17] A. Peled, and A. Ruiz, Frequency domain data transmission using reduced computational complexity algorithms, Acoustics, Speech, and Signal Processing, IEEE International Conference on ICASSP, pp. 964-967, 1980.

[18] A. Thotappilly, "OFDM for Underwater Communication." M.S. Thesis, Virginia Polytechnic Institute and State University, Blacksburg, 2011.